FEMTOSECOND TIME-RESOLVED SPECTROSCOPY OF GAS-PHASE ANIONS: ELECTRON SOLVATION AND ISOLATED CHROMOPHORE DYNAMICS

Thesis by

I-Ren Lee

In Partial Fulfillment of the Requirements

for the Degree of

Doctor of Philosophy

California Institute of Technology

Pasadena, California

2011

(Defended November 22, 2010)

To My Parents

Acknowledgments

I would like to express my deepest gratitude to my advisor, Professor Ahmed Zewail for his guidance through my Ph.D. study at Caltech. It was an invaluable experience to work in *Femtoland*, where the state-of-the-art science and technology are developed and enriched with the perceptiveness, passion, and patience of Professor Zewail.

I gratefully acknowledge my colleagues, Dr. Daniel Paik, Dr. Ding-Shyue (Jerry) Yang, Dr. Spencer Baskin, Dr. Wonchul Lee, and Professor Luis Bañares, for the contributions in the works included in the thesis. It was such a wonderful experience to work together with these talented scientists. Without them, my research could not reach this point. I would like to especially mention Dr. Daniel Paik for his mentoring in my early years of Ph.D. study, which created a solid foundation that allows me to develop my own research ideas. In the past two years, it was my pleasure to work closely in a different lab (UED) with two brilliant scientists, Dr. Sang Tae Park and Mr. Andreas Gahlmann. I would like to offer my gratitude to all the Zewail group members and alumni for stimulating discussions.

Many thanks go to my committee members: Professor Peter Dervan, Professor Vincent McKoy, and Professor Mitchio Okumura, for the help and guidance.

My gratitude goes to my former advisor, Professor Po-Yuan Cheng for bringing me into the world of femtochemistry. His encouragement and support inspire me to come over to the United States to pursue my studies at Caltech. I would like to thank all my friends who accompanied me through the journey. Finally, I am very grateful to my parents for supporting me unconditionally.

Abstract

This thesis presents the studies of ultrafast dynamics of negatively charged molecules and clusters in the gas phase using femtosecond photoelectron spectroscopy. The core motifs of two distinct complex systems — solvated electrons and protein chromophores — were studied in the gas phase.

For the solvated electron systems — hydrated electrons and ammoniated electrons — were studied in finite-sized clusters in the gas phase. Interestingly, the results show a significant difference. In the hydrated electron, ground-state vibrational cooling is evident by the transient photoelectron spectra, while, in the ammoniated electron, a coherent motion with a 500-fs relaxation is observed. The difference is attributed to the cage rigidity, which results in different solvent motions for the electron's interaction with water (libration) or ammonia (phonon-like).

The photocycle of the photoactive yellow protein (PYP) has been studied extensively, but the dynamics of the isolated chromophore responsible for the transduction of phototacticity is less known. The anionic chromophore model molecule was investigated in the gas phase using femtosecond photoelectron spectroscopy and the results indicate that the protein function is in directing efficient conversion to the *cis*-structure and in impeding radical formation within the protein. Finally, a classic system of conformational twisting, stilbene, was studied in its anionic radical state. Ultrafast conversions from both *trans*- and *cis*- isomers are accompanied with coherent oscillation, in contrast to observations in the solution phase, and this suggests that a major solvent retardation take place. Dynamic studies of the photochemistry of gas-phase anions are very scarce due to the experimental difficulties. However, our results successfully resolve

the photophysics and photochemistry of the isolated species and, thereby, elucidate the effect of solution.

Table of Contents

CHAPTER 1.

Introduction

1.1. Femtochemistry

Real time observations of ultrafast changes in chemical reactions have been made possible since the introduction of femtosecond time-resolved methods in the 1980s.[1-3] Utilizing a femtosecond pump-probe methodology, molecules are coherently excited to their nonstationary state by a pump pulse and the evolution is then interrogated by a delayed probe pulse and recorded as a function of the delay time. The scope of this technique is not limited to resolving ultrafast kinetics of population flow between different states, but, more importantly, atomic motions can be revealed by following the wavepacket dynamics in real time. Femtochemistry has emerged in the past few decades and covers systems as small as a diatomic molecule through complex systems in the biological and material fields.

Gas-phase femtochemistry has the advantage of providing unperturbed physical pictures of reaction dynamics that are free of the interferences by solvent or bulk. Inherent physical properties of complex systems may be revealed by studying their core motif in the gas phase, although biochemists frequently criticize that studying biological chemicals in the isolated gas phase is completely irrelevant to the problems that they are facing. However, it is often necessary to first understand the structure and dynamic properties for the isolated system in the gas phase in order to understand those properties in their native environment.[4] In this thesis work, studies of ultrafast dynamics of negatively charged core motifs correlated to two distinct complex systems, protein and solvated electrons, are presented.

In this chapter, a general overview on gas-phase anion chemistry is given and classified into two categories — Section 1.2 covers the gas-phase monomer anion and

Section 1.3 gives an introduction to mesoscopic clusters and to solvated electron. In addition to those, a brief review of femtosecond photoelectron spectroscopy is given in Section 1.4. The content of this thesis is summarized in Section 1.5.

1.2. Gas-Phase Monomer Anion

Anions, negatively charged atoms or molecules, can also exist in the gas phase. Usually, anions can be prepared by electron impact on atoms or molecules in the gas phase. For instance, they can be generated by direct electron attachment or through electron transfer from neutrals and other anions.[5]

$$e^- + M \rightarrow M^-, \qquad \textbf{1.1a}$$

$$A + M \rightarrow A^+ + M^-, \qquad \textbf{1.1b}$$

$$A^- + M \rightarrow A + M^- \qquad \textbf{1.1c}$$

In addition, electrospray ionization has also been applied to prepare gas-phase anions, especially macromolecular and/or multicharged anions.[6] Many other methods such as plasma formation, secondary electron attachement, ion sputtering, laser ablation, matrix-assisted laser desorption/ionization (MALDI), etc. can also used in preparing isolated anions.

In practice, the preparation of gas-phase anions is nontrivial since their stabilities are usually an issue. The stability can be attributed to electronic and thermal parts. The electronic stability of anions is usually expressed by the *electron affinity* (EA), which is defined as the energy difference of the anions and their corresponding neutral atoms or molecules. The atoms and molecules with positive EA can form thermodynamically stable anions. The EA is an intrinsic property of atoms and molecules. A list of the

experimental and theoretical EAs of various atoms and molecules can be found in the review paper by the Schaefer group.[7] However, a great many molecules such as N_2, CO_2, CH_4, ethylene, benzene, etc., cannot form thermodynamically stable anions due to their negative EAs. Temporary negative ions (TNIs) can be formed only at a very short instant when they are capturing the free electrons.[5]

Thermal stability of anions is an important factor in generating gas-phase anions. The EA of most molecules ranges from fractions of eV to 3.5 eV.[7] The excess energy in the electron attachment processes can easily exceed the EAs and cause the instability of the anions. In addition, most anions have different structures from their source neutral molecules. Structural rearrangements are required to lower the vibrational excitation and to prevent the thermal instability. Autodetachment, the ejection of the excess electron, may occur to release the excess energy. In some cases, dissociation can occur, when the excess energy is higher than the dissociation barrier. To prevent these unwanted processes from happening, efficient quenching of vibrational energy is essential to the preparation of gas-phase anions. A supersonic-expansion molecular beam, which can provide efficient cooling, is ideal in gas-phase anion preparation.

Most anions can be classified into two types —the dipole bound anions and the conventional (valence) anions— by how the excess electron attaches to the molecules. Removed from these two categories, quadrupole bound anions and double Rydberg dianions are also found experimentally in some extremely rare cases and will not be discussed in this thesis.[8,9]

In some neutral molecules with very a strong dipole (dipole moment > 1.625 debyes or 0.6993 a. u.), the excess electron can be held by the dipole moment and form

dipole bound anions. However, the dipole bound electron is usually very loosely bound to the molecules and is very diffusive. The structures of the anions are usually very similar to their corresponding neutral molecules, since the molecular orbitals are unperturbed and result in narrow peaks in photoelectron spectra due to the dominant 0–0 transition. It is worth mentioning that the anion radicals of some nucleic acid bases, such as uracil and thymine, were prepared in the molecular beam machine and their photoelectron spectra were recorded and assigned to dipole bound anions.[10,11] These anion radicals have drawn much attention, because it is relevant to the genetic damage due to the electron attachment to the nucleic acids, which can be induced by radiation.[12]

In contrast, the excess electron in a valence anion occupies the empty orbital. Due to the perturbation of the electronic structure, the equilibrium structures of anions are usually different from those of the corresponding neutral molecules and broadened peaks can usually be found in the photoelectron spectra of these anions.

Photoisomerization is one of the key reactions that trigger many biological functions such as vision and phototacticity. In the photoactive yellow protein (PYP), the primary step of the photocycle is triggered by the *tran-cis* isomerization of its anionic *p*-coumaric acid chromophore.[13-15] It has been shown that in the denatured protein or the model molecules in solution the dynamics shows a significant difference from the native protein environment.[16-19] An anionic model molecule is prepared in the gas-phase with the dissociative electron attachment; the gas-phase deprotonated anion is then investigated by femtosecond spectroscopy. The result of this work was reported in *Proceedings of the National Academy of Sciences of the United States of America* in 2006 and the function of protein environment has been resolved by comparing the result of the

gas-phase and condensed-phase studies.[20] The manuscript of this work is included in Chapter 5. Finally, a similar model molecule with the central double bond twisting, stilbene, is studied in its gas-phase radical anion form. The result was published on *Journal of the American Chemical Society* in 2008 and the manuscript is included in Chapter 6.

1.3. Mesoscopic Clusters and Solvated Electron

Clusters are defined as aggregates of atoms, ions, or molecules formed by interactions ranging from weak van der Waals forces to strong ionic bonds. Although the earliest report of the formation of aggregates and related nucleation phenomena can be traced back to the 1930s or earlier, the field of cluster studies using mass spectrometers and ion sources began to emerge in the 1950s and grew rapidly in the 1970s and 1980s to become a subject of considerable interests.[21-23]

The major goal of cluster studies is to bridge the gap between microscopic (isolated atoms and molecules) and macroscopic (bulk) states, and contributions have been made to benefit diverse disciplines including atomic, molecular, nuclear, and condensed-matter physics.[21-23] Fundamental physical properties can be obtained systematically with size-dependent studies using current mass spectrometry technologies. Those properties can be classified into two regimes: (1) those with a size dependence, described by a smooth power-law, that extrapolates to the corresponding bulk limit, and (2) those that show a highly nonmonotonic size dependence (nonscalable regime).[23] The latter region is attributed to the unique cluster structures and the quantum confinement effect, while the energy gap is discrete in those clusters.

Steady-state physical properties of clusters such as structural, thermodynamic, and energetic information have been widely studied experimentally using mass and optical spectrometry. These properties are of importance toward the understanding of the transition from the microscopic to the macroscopic regime. Recent developments of chemical dynamics have also been introduced to cluster studies: In the past two decades, femtosecond time-resolved spectroscopic techniques have been integrated into the studies of cluster dynamics and successfully tackled many fundamental problems. Those studies are not limited to the sizeable systems that aim to find the trend or mimic the dynamics of bulk systems. Some reaction intermediates of bimolecular reactions can also be prepared in vacuum. With the pump-probe scheme, the transition-state dynamics of bimolecular reaction can be resolved. A recent review paper summarized the relevant works that have been done in this group.[24] These studies can be summarized into five categories: (1) vibrational energy redistribution, (2) bimolecular reaction, (3) microscopic solvation, (4) caging and recombination, and (5) biological complexes.

Clusters can be either neutral or ionic (both positively and negatively charged). However, separating neutral clusters by their sizes is not straightforward. Although their size information can be carried over with the post-ionization method, evaporation (loss of some composite elements) of the clusters during the ionization and detection processes may lead to complexities. In contrast, charged clusters can be separated by their mass-to-charge ratio (m/e) in a mass spectrometer. Clusters with well-defined sizes can then be interrogated by various laser spectroscopic methods. Photoelectron spectroscopy is one of those methods, which is widely applied in the field of cluster studies mainly because of its high sensitivity. Especially when the clusters are negatively charged, the photon

energy requirement in photoelectron spectroscopy is as low as a few electron volts (eV) or even lower, which makes the availability of the laser much more permissive compared to the need of VUV or multiphoton ionization.

Solvation, by the International Union of Pure and Applied Chemistry (IUPAC) definition, is an interaction of a solute with the solvent, which leads to stabilization of the solute species in the solution.[25] Solvation dynamics, one of the most popular topics in chemistry, has attracted great attention, because of its importance in chemical and biological systems, especially when the solvent is water.[26,27] The solvation problem was first treated with a dielectric continuum model. However, it has been well known that the hydration layer adjacent to a protein surface exhibits a more rigid and denser structure compared to that of bulk and has crucial influences on protein structure, folding, dynamics, and function.[28-30] The solvation dynamics of its core motif becomes very important, and clusters can be a good candidate to approach this problem in an isolated environment. The microscopic solvation dynamics studies with gas-phase clusters was pioneered by the Lineburger group using $I_2^-(CO_2)_n$ and $I_2^-(Ar)_n$ clusters and the solvent dependence of the photodissociation of I_2^- has been observed.[31-35] In addition, size-dependent cluster studies can also answer the question of how many molecules are needed for the solvation behaviors to reach their bulk properties. Moreover, the finite-size experimental data are very useful for the benchmark of models using the molecular dynamics (MD) simulations.[36]

When an excess electron is attached to a cluster, the excess electron can be held in two different ways. In some cases, for example $(O_2)_n^-$ clusters, the excess electron occupies an empty orbital of one composite molecule and forms a stable anion and the

anion is further stabilized by surrounding *solvent* molecules. In contrast, some molecules, such as water, ammonia, and benzene, cannot form stable anions due to their highly negative EA. The excess electron is collectively held by a group of atoms or molecules. The latter case is known as the "*solvated electron.*"

Solvated electrons have drawn considerable attention since the observation of blue color change when sodium was dissolved in liquid ammonia in 1808 by Humphry Davy.[37] After the first publication by Weyl in 1863,[38] it was later hypothesized that the change of color is due to the absorption of electrons that are trapped in cavities created by solvent molecules.[39] Theoretical work by Ogg supported this hypothesis and suggested that the individual electron is self-trapped, or caged, in the solvent cavity, hence, the "*solvated electron.*"[40] Much later, in 1962, solvated electrons in water, *hydrated electrons*, were discovered with ionizing radiation.[41] Hydrated electrons are especially important not only owing to the abundance of water, but also due to their importance in the radiation/electron damage of biological systems such as DNA damage.[42]

In a simple picture of an electron in a cavity, the structure of the solvated electron states is analogous to those of a hydrogen atom, with an *s*-type ground state and a *p*-type excited state.[43] The absorption of an infrared (IR) photon promotes the solvated electron to the *p*-type excited state and is followed by the relaxation to the ground state at a non-stationary presolvated geometry. The ground-state solvation then takes place to release excess energy. The solvation dynamics in the bulk (solution phase) have been studied extensively; see the introduction section in Chapter 3 and 4 for detail.

Preparations of the hydrated electron and the ammoniate electron clusters were first reported by the Haberland group.[44] Steady-state properties have been investigated

intensively especially in the case of the hydrated electron; see chapters 3 and 4 for detail. In 2004, the first femtosecond time-resolved spectroscopy studies of the hydrated electron clusters were reported by this group and the Neumark group in the same issue of *Science Magazine*.[45,46] Both works show a virtually identical excited-state relaxation on the few-hundred fs timescale, while a several-hundred fs ground-state solvation is observed by this group. The manuscript of the work by this group is included in Chapter 3 in this thesis. The Neumark group has continued with a few similar works on different conditions of cluster formations, and also with different solvents; see their reviews for detail.[47,48] In 2008, the historical problem, the solvation dynamics of the ammoniated electron, was resolved and reported by this group in *ChemPhysChem*.[49] The manuscript of this work is included in Chapter 4.

1.4. Femtosecond Photoelectron Spectroscopy

Photoelectron spectroscopy (PES) is one of the most popular methods used in gas-phase molecular and cluster studies. By absorption of photon energy, molecules or anions undergo photoionization or photodetachment, respectively, and yield photoelectrons that are then collected and analyzed by their kinetic energy.

The electron kinetic energy, *eKE*, of the photodetachment of anions can be described using the following equation:

$$eKE = E(anion) + h\nu - E(neutral) \qquad \textbf{1.2}$$

where *E(anion)* and *E(neutral)* are the energies of the initial anion state and the final neutral state in the photodetachement process, respectively, h is the Planck constant, and ν is the wavelength of the photon used in this process.

Peak intensity and shape in PES are determined by the Franck-Condon overlap between the initial state and the final state. In PES of anionic species, the adiabatic electron affinity (AEA) can be obtained from the onset of the peak, while the vertical detachment energy (VDE) can be extracted from the peak position. The difference in VDE and AEA reflects the degree of structural difference between the initial anion state and the final neutral state. In a dynamic system, the peak shape changes as a function of the vibrational excitation. Following the vibrational relaxation processes can be made possible by carefully monitoring the change of the peak shape.

Unlike other popular methods such as laser induced fluorescence (LIF) and resonance multiphoton ionization (MPI), PES does not require the laser wavelength to be on a resonance of the probed species. It is especially beneficial in time-resolved studies because the probed species may change over time. While other methods may be limited by a small probing window due to the excitation wavelength, PES has the advantage of globally monitoring those species that are involved in a chemical reaction.

Time-resolved PES, also known as TRPES, has been developed in concert with the improvement of laser technology, with time resolution from nanosecond through femtosecond and even attosecond timescale. Femtosecond TRPES was first introduced to the field of gas-phase anion studies by the Neumark group.[50] In the past few decades, femtosecond TRPES has been heavily involved in the gas-phase anion and cluster studies. See the review by Stolow *et. al*. for detail.[51]

1.5. Contents of the Thesis

Femtosecond time-resolved photoelectron spectroscopy has been applied in

different systems in this group. A brief review of the experimental details that were used in this thesis work is given in Chapter 2. Chapters 3 and 4 cover the solvated electron dynamics problems. The hydrated electron, an important system with biological significance, has been experimentally studied and the results were published in *Science* in 2004 and the manuscript of this publication is included in Chapter 3.[45] The ammoniated electron, a historical system for more than two centuries, and its cluster dynamics has been resolved and shows a significant difference from the hydrated electron case. The result was published in *ChemPhysChem* in 2008 and the manuscript is included in Chapter 4.[49]

Chapters 5 and 6 cover the works on the dynamics of gas-phase anions and anion radicals. A biological mimic system in persuading the dynamics of the photoactive yellow protein (PYP) was investigated using the femtosecond TRPES with the isolated anionic model molecules. The result was published in *Proceedings of the National Academy of Sciences of the United States of America* in 2006 and, by comparison to the results obtained from the native protein environment and those in the solutions, the role of the protein environment of this system has been answered.[52] The manuscript of this work is included in Chapter 5. Finally, the most popular model molecule with central double bond twisting, stilbene, is studied in the gas-phase radical anion form.[52] The result was published in *Journal of the American Chemical Society* in 2008 and the manuscript is included in Chapter 6.

References

(1) Zewail, A. H. *Angew. Chem.-Int. Edit.* **2000**, *39*, 2587.

(2) Zewail, A. H. *Femtochemistry: Ultrafast Dynamics of the Chemical Bond.*; World Scientific: Singapore, 1994.

(3) Manz, J.; Wöste, L. *Femtosecond Chemistry*; VCH: Weinheim, 1995.

(4) Bonačić-Koutecký, V.; Brauer, B.; Burmeister, F.; Eberhardt, W.; Gerber, R. B.; González, L.; von Helden, G.; Kammrath, A.; Kim, S. K.; Manz, J.; Meijer, G.; Mitrić, R.; Neeb, M.; Neumark, D. M.; Schultz, T.; Stanzel, J. In *Analysis and Control of Ultrafast Photoinduced Reactions*; Kühn, O., Wöste, L., Eds.; Springer: New York, 2007.

(5) Illenberger, E. In *Gaseous Molecular Ions*; Illenberger, E., Momigny, J., Eds.; Springer-Verlag: New York, 1992, p 241.

(6) Waters, T.; Wang, X. B.; Wang, L. S. *Coord. Chem. Rev.* **2007**, *251*, 474.

(7) Rienstra-Kiracofe, J. C.; Tschumper, G. S.; Schaefer, H. F.; Nandi, S.; Ellison, G. B. *Chem. Rev.* **2002**, *102*, 231.

(8) Gutowski, M.; Skurski, P.; Li, X.; Wang, L. S. *Phys. Rev. Lett.* **2000**, *85*, 3145.

(9) Xu, S. J.; Nilles, J. M.; Hendricks, J. H.; Lyapustina, S. A.; Bowen, K. H. *J. Chem. Phys.* **2002**, *117*, 5742.

(10) Hendricks, J. H.; Lyapustina, S. A.; deClercq, H. L.; Snodgrass, J. T.; Bowen, K. H. *J. Chem. Phys.* **1996**, *104*, 7788.

(11) Hendricks, J. H.; Lyapustina, S. A.; deClercq, H. L.; Snodgrass, J. T.; Bowen, K. H. *Biophys. J.* **1996**, *70*, SU495.

(12) Steenken, S. *Chem. Rev.* **1989**, *89*, 503.

(13) Larsen, D. S.; van Grondelle, R. *ChemPhysChem* **2005**, *6*, 828.

(14) Cusanovich, M. A.; Meyer, T. E. *Biochemistry* **2003**, *42*, 4759.

(15) Borgstahl, G. E. O.; Williams, D. R.; Getzoff, E. D. *Biochemistry* **1995**, *34*, 6278.

(16) Usman, A.; Mohammed, O. F.; Heyne, K.; Dreyer, J.; Nibbering, E. T. J. *Chem. Phys. Lett.* **2005**, *401*, 157.

(17) Changenet-Barret, P.; Espagne, A.; Charier, S.; Baudin, J. B.; Jullien, L.; Plaza, P.; Hellingwerf, K. J.; Martin, M. M. *Photochem. Photobiol. Sci.* **2004**, *3*, 823.

(18) Changenet-Barret, P.; Espagne, A.; Plaza, P.; Hellingwerf, K. J.; Martin, M. M. *New J. Chem.* **2005**, *29*, 527.

(19) Larsen, D. S.; Vengris, M.; van Stokkum, I. H. M.; van der Horst, M. A.; Cordfunke, R. A.; Hellingwerf, K. J.; van Grondelle, R. *Chem. Phys. Lett.* **2003**, *369*, 563.

(20) Lee, I. R.; Lee, W.; Zewail, A. H. *Proc. Natl. Acad. Sci. U.S.A.***2006**, *103*, 258.

(21) Castleman, A. W.; Jena, P. *Proc. Natl. Acad. Sci. U.S.A.***2006**, *103*, 10552.

(22) Castleman, A. W.; Jena, P. *Proc. Natl. Acad. Sci. U.S.A.***2006**, *103*, 10554.

(23) Jena, P.; Castleman, A. W. *Proc. Natl. Acad. Sci. U.S.A.***2006**, *103*, 10560.

(24) Cheng, P. Y.; Baskin, J. S.; Zewail, A. H. *Proc. Natl. Acad. Sci. U.S.A.***2006**, *103*, 10570.

(25) *IUPAC. Compendium of Chemical Terminology*; McNaught, A. D.; Wilkinson, A., Eds.; Blackwell Scientific Publications: Oxford, 1997.

(26) Jimenez, R.; Fleming, G. R.; Kumar, P. V.; Maroncelli, M. *Nature* **1994**, *369*, 471.

(27) Simon, J. D. *Accounts Chem. Res.* **1988**, *21*, 128.

(28) Merzel, F.; Smith, J. C. *Proc. Natl. Acad. Sci. U.S.A.***2002**, *99*, 5378.

(29) Pal, S. K.; Zewail, A. H. *Chem. Rev.* **2004**, *104*, 2099.

(30) Levy, Y.; Onuchic, J. N. *Annu. Rev. Biophys. Biomolec. Struct.* **2006**, *35*, 389.

(31) Ray, D.; Levinger, N. E.; Papanikolas, J. M.; Lineberger, W. C. *J. Chem. Phys.* **1989**, *91*, 6533.

(32) Papanikolas, J. M.; Vorsa, V.; Nadal, M. E.; Campagnola, P. J.; Buchenau, H. K.; Lineberger, W. C. *J. Chem. Phys.* **1993**, *99*, 8733.

(33) Papanikolas, J. M.; Vorsa, V.; Nadal, M. E.; Campagnola, P. J.; Gord, J. R.; Lineberger, W. C. *J. Chem. Phys.* **1992**, *97*, 7002.

(34) Vorsa, V.; Nandi, S.; Campagnola, P. J.; Larsson, M.; Lineberger, W. C. *J. Chem. Phys.* **1997**, *106*, 1402.

(35) Vorsa, V.; Campagnola, P. J.; Nandi, S.; Larsson, M.; Lineberger, W. C. *J. Chem. Phys.* **1996**, *105*, 2298.

(36) Berry, R. S. *J. Phys. Chem.* **1994**, *98*, 6910.

(37) Edwards, P. P. *Adv. Inorg. Chem.* **1982**, *25*, 135.

(38) Weyl, W. *Ann. Phys.* **1863**, *197*, 601.

(39) Kraus, C. A. *J. Am. Chem. Soc.* **1908**, *30*, 1323.

(40) Ogg, R. A. *Phys. Rev.* **1946**, *69*, 668.

(41) Hart, E. J.; Boag, J. W. *J. Am. Chem. Soc.* **1962**, *84*, 4090.

(42) Simons, J. *Accounts Chem. Res.* **2006**, *39*, 772.

(43) Coe, J. V. *Int. Rev. Phys. Chem.* **2001**, *20*, 33.

(44) Armbruster, M.; Haberland, H.; Schindler, H. G. *Phys. Rev. Lett.* **1981**, *47*, 323.

(45) Paik, D. H.; Lee, I. R.; Yang, D. S.; Baskin, J. S.; Zewail, A. H. *Science* **2004**, *306*, 672.

(46) Bragg, A. E.; Verlet, J. R. R.; Kammrath, A.; Cheshnovsky, O.; Neumark, D. M. *Science* **2004**, *306*, 669.

(47) Ehrler, O. T.; Neumark, D. M. *Accounts Chem. Res.* **2009**, *42*, 769.

(48) Neumark, D. M. *Mol. Phys.* **2008**, *106*, 2183.

(49) Lee, I. R.; Lee, W.; Zewail, A. H. *ChemPhysChem* **2008**, *9*, 83.

(50) Greenblatt, B. J.; Zanni, M. T.; Neumark, D. M. *Chem. Phys. Lett.* **1996**, *258*, 523.

(51) Stolow, A.; Bragg, A. E.; Neumark, D. M. *Chem. Rev.* **2004**, *104*, 1719.

(52) Lee, I. R.; Bañares, L.; Zewail, A. H. *J. Am. Chem. Soc.* **2008**, *130*, 6708.

CHAPTER 2.

Experimental

2.1. Overview

The apparatus used in this thesis work is composed of three major components: the molecular beam machine, the femtosecond laser system, and the data acquisition system. The molecular beam machine is used to prepare, purify, and identify the anion and to analyze the transient species produced by the laser pulses provided by the femtosecond laser system.

In this thesis, we have used the molecular apparatus that was built by Dr. Daniel H. Paik and coworkers during his Ph.D. study and the details of this apparatus are described in his thesis (Caltech 2004).[1] Some modifications and add-ons were made afterwards. In this section, a summary will be given for the shared parts while detail will be given for the newly added-on and modified parts.

2.2. Molecular Beam Machine

The molecular beam machine includes the vacuum system, the ion source, the primary time-of-flight mass spectrometer (TOF/MS), the reflectron TOF/MS, and the magnetic-bottle photoelectron spectrometer, as shown in Fig. 2.1. Each element is described in a separated subsection below.

2.2.1. Vacuum System

The molecular beam apparatus employs differential pumping to ensure a satisfactory vacuum level in each section. The molecular beam machine can be divided into three major chambers according to the different vacuum requirements, as shown in Fig. 2.2.

The first chamber, where the gas jet of sample mixtures is introduced into the vacuum chamber, requires significant pumping power since the high throughput of the gas jet is directly released into this chamber through a pulsed nozzle. This chamber is pumped by a diffusion pump (Varian, VHS-6), which is backed up by a roots blower (Leybold, RUVAC WAU251) and a mechanical pump (Leybold, TRIVAC D65BCS). Pressure of the chamber is checked by a thermal gauge. The normal operation pressures of this chamber are lower than 1×10^{-3} torr and $1\text{-}2\times10^{-2}$ torr with and without loading (gas jet), respectively.

The second chamber is separated from the first chamber by a small hole or a skimmer both with an ~1 cm opening, allowing the dense gas pack from the pulsed nozzle to be drifted to the repeller of the liner time-of-flight spectrometer. This chamber is pumped by a diffusion pump (Varian VHS-6), which is backed up by a mechanical pump (Leybold, TRIVAC D65BCS). The normal operating pressure of this chamber is low 10^{-6} torr (with and without loading).

The third chamber is directly attached to the second chamber. High vacuum is required in this chamber since the detectors of mass and photoelectron spectrometers are located in this chamber. This chamber is operated at a range of high 10^{-7} to low 10^{-6} torr. Pumping of this chamber is achieved by a diffusion pump (Varian, VHS-4), which is backed up by the shared roughing mechanical pump with the second chamber. Additional pumping is provided by a turbo molecular pump (Preiffer, Balzers TPU510) while loading is on to ensure the high vacuum level.

All three diffusion pumps are attached to the chambers through pneumatic gate valves (MDC, GV-6000-V-ASA-P and GV-4000-V-ASA-P). The block diagram of the

vacuum system is illustrated in Fig. 2.3. This system is protected by a home-built interlock system to protect the system against the damage caused by accidents such as electricity loss or misoperation.

2.2.2. Ion Sources

Ion sources are used to prepare the anion mixture samples for later purification and investigation. The ion source is composed of three major components: the gas inlet system, the pulsed nozzle, and the electron attachment source.

In this thesis, three configurations with two types of nozzles have been described. First, in the work of solvated electrons in the water clusters (Chapter 3), the carrier gas, nitrogen, blows through the top surface of water (or deuterium oxide) in the sample reservoir and picks up the vapor. The gas mixture is then released into vacuum by a pulsed General Valve. The General Valve is an electric-magnetic driven nozzle with a puppet and a small orifice and is controlled by its controller (Parker Hannifin, IOTA1). The typical opening time of the nozzle is ~150–200 μs at a repetition rate of 20 Hz. The assembly is shown in Fig. 2.4.

Once the gas mixture is released into the vacuum, collisional cooling induced by supersonic expansion takes place and aggregation of molecules is favorable in the region of the supersonic expansion. A home-built continuous thermal electron gun, illustrated in Fig. 2.5, is used to provide an electron beam with a kinetic energy of 1 KeV that intercepts the gas packet in this region. A mixture of clusters, including the desired anion clusters, is prepared here and drifted into the linear tandem time-of-flight mass spectrometer for further purification and interrogation.

The second configuration is used for the work described in Chapter 5, since the heating of a solid sample is needed to provide sufficient vapor pressure in this experiment. A modification on the source assembly was made in order to provide better sample delivery. In the previous configuration, the nozzle is far away (~50 cm) from the sample reservoir. In order to prevent the sample from condensation in the line, it is necessary to keep this line at a temperature slightly higher than the sample reservoir. However, this cannot prevent the condensation completely and it also takes a very long time to reach equilibrium. In the new design, the sample reservoir is moved very close to the nozzle to solve this problem. This newly designed sample delivery system is shown in Fig. 2.6.

The electron attachment source used in this experiment is also different. A pulsed electron bombardment source is attached right next to the exit of the nozzle. The drawing of the source and the simulated electron trajectory are shown in Fig. 2.7.

Finally, the third configuration, which was used in the works described in chapters 4 and 6, is the Even-Lavie high-pressure nozzle with the thermal electron gun that comes with the nozzle.[2] The specialty of this nozzle is that it can operate at an extremely high backing pressure (up to 100 bar). Under such high backing pressure, the collisional cooling in the supersonic jet is more efficient and has more success in preparing weakly bound clusters. This nozzle is controlled by a higher current driver. Up to 100 A of peak current from the discharge of a capacitor is used for driving the solenoid and pulling the pin back against tremendous resistant force because of the high pressure. A sample reservoir and heater are also integrated in this nozzle assembly.

A miniature thermal electron gun that comes with the Even-Lavie nozzle is attached right at the exit of the nozzle. The electron gun can be operated in pulsed or

continuous mode. A continuous mode is used in our setup with a ~200 V DC floating voltage on the tungsten filament and repeller. The tungsten filament is heated up by a DC voltage at ~9 V to provide thermal emission of electrons.

2.2.3. Primary Time-of-Flight Mass Spectrometer

The primary TOF/MS is mainly used to separate anions according to the flight time in the spectrometer and to record the mass spectrum of the anions. It includes five major components: the accelerator, the deflectors, the Einzel lens, the mass gate, and the detector assembly, as illustrated in Fig. 2.8.

The accelerator in this apparatus is adapted from the design of Wiley and McLaren.[3,4] The design of two-stage acceleration compensates for the initial spread of velocity along the time-of-flight axis (z-axis). The flight time in the mass spectrometer has the following relationship to the mass, charge, and other instrument parameters such as acceleration potential and distance of travel. The flight time is virtually proportional to the square root of m/e but with a small uncertainty that is caused by the initial energy spread of the ions.

Since anions are prepared outside the accelerator, the accelerator has to be operated in pulsed mode, in order to provide a sharp starting time for the anions flying through the TOF/MS. This is achieved by applying a fast-rise high-voltage pulse onto the accelerators. The high-voltage pulses with a 1 KV/20 ns rise time are achieved by applying a high-speed high-voltage switch (Behkle, HTS51-06), which takes a TTL control pulse and is powered by a high-voltage DC power supply (Bertan, 205B-03R) at ~2–3KV. The falling time of the high-voltage pulse is not very important since most

anions depart from the accelerator within a few microseconds.

The accelerated anions then pass through two sets of deflectors. Each deflector consists of a pair of two parallel plates. One of the plates is floated with DC voltage and the other one is grounded. Two sets of deflectors are used in the apparatus to correct the anion trajectory on the x- and y- axis by adjusting the floating DC voltage.

Following the deflectors is the Einzel lens. The Einzel lens used in this apparatus consists of three hollow cylinders in a row along the z axis with the central one floated with high-voltage DC while the other two cylinders are grounded. The purpose of Einzel lens is to focus the anion beam spatially on the desired position alone the z-axis to ensure the maximum overlap between the anion beam and the laser beams to optimize the signal intensity.

The mass gate is placed near the laser interaction region and is only used in fragment studies. The purpose of the mass gate is to select the parent anion by allowing only a single anion species to pass through the mass gate and rejecting the rest of the species with different *m/e*. The mass gate used in this work adapted the design by Euke and colleagues and is composed of two interleaved combs that are floating at positive and negative high voltage (~ ±500 V). While the high voltages are on, anion species experience the potential in between positive and negative electrodes then collide onto the positive electrodes and cannot pass through the mass gate. The selection of desired anions is achieved by temporarily turning off the voltages using an inverted short square pulse. The voltage and switching is provided by a pair of high-voltage pulsers (DEI, PVM-4201) which can provide a maximum voltage of ±950 V with a 15-ns rise and fall time and is controlled by a TTL control pulse. The mass gate is only operated during the

fragmentation studies, which are described in the Section 2.2.4, and both comb electrodes are otherwise grounded.

Anions pass through the laser interaction region and then arrive at the detector. As illustrated in the onset of Fig. 2.8, the detector is constructed of stacks of two multichannel plates (MCP) in the chevron configuration and operated at ~2 KV. The signal is connected to the digital oscilloscope (LeCroy, 9361) and the mass spectra are recorded as a function of flight time. In practice, this mass spectrometer is usually calibrated before the experiment by known clusters such as hydrated electrons.

2.2.4 Reflectron Time-of-Flight Mass Spectrometer

As illustrated in Fig. 2.9, the reflectron TOF/MS, located between the laser interaction region and the detector of the primary TOF/MS, is used in the fragment studies in this work. Fragment studies are mainly used in studying the fragmentation that is induced by the pump laser and also in examining whether fragmentation takes place in the field-free region in the primary TOF/MS. The reflectron TOF/MS is composed of three major components: the decelerator, the reflector, and the detector assembly.

The mass gate, which is previously described in Section 2.2.3, is used to allow only a single anion species, the parent anions, to pass through the laser interaction region and then enter the reflectron TOF/MS. The anions, including the parent and fragment anions, pass through the center hole of the detector assembly and then drift into the deflector and reflector. The decelerator is composed of series of electrodes at increasing negative voltage gradients along the z axis. The reflector is made of two parallel plates that are floated at a negative high voltage. The parent and fragment anions experience the

field and are decelerated and reflected along the z axis and finally arrive at the detector and are collected.

The detector assembly of the reflectron TOF/MS is illustrated as a section view in the bottom panel of Fig. 2.9. A grounded stainless steel tube is coaxially placed with two specially made MCPs with center holes to allow the anions to drift through this detector region at a field-free condition. Those MCPs are also stacked in the chevron configuration and operated at ~2 KV. The signal is amplified and recorded by a digital oscilloscope (Lecroy 9361).

Simulated anion trajectories of anions with three different *m/e* settings and a uniform initial velocity are illustrated in the bottom right panel in Fig. 2.9. As shown in the trajectories, anions travel with different path lengths at different *m/e* settings. The flight time in the reflecton TOF/MS is also proportional to the square root of *m/e*.

The whole assembly of the reflectron TOF/MS is grounded when operating the primary TOF/MS and photoelectron spectrometer.

2.2.5. Magnetic-Bottle Photoelectron Spectrometer

PES is the major technique involved in this thesis. A magnetic-bottle photoelectron spectrometer, illustrated in Fig. 2.10, is located at the laser interaction region and is normal to the primary TOF/MS axis (z axis). It includes three major components: a strong permanent magnet, solenoid assembly, and detector.

A permanent strong magnet is placed under the laser interaction region while the solenoid assembly is on the opposite side. The highly non-uniform magnetic field, created by the strong permanent magnet and the magnetic field of the solenoid,

parallelizes the emitted photoelectrons from different solid angles and directs them through the solenoid assembly to the detector. [5-10]

The solenoid assembly is in a six-layer structure, as illustrated in the onset of Fig. 2.10, including graphite coating, Teflon tubing, solenoid, Teflon sheet, and μ-metal sheet, in order of inner layer through outside. The solenoid was made by wrapping the non-magnetic copper wire (JCH wire, 14 AWG) around the OFH copper tube (Thyssen-TMX Division, 2.5" O.D. and 26" long). The thick 14 AWG wire is used in the solenoid to keep the resistance low and to prevent the assembly from overheating. The solenoid is supplied with a ~3.8V and 1.0A DC voltage to generate the desired magnetic field.

Teflon tubing and sheets are placed immediately inside and outside the solenoid to provide electric insulation and also work as heat sinks. The high magnetically permeable μ-metal sheet (Mm-Metal, 0.015" thickness) wraps from the outside to reduce the influence of Earth's magnetic field.

The detector is located on the very top of the PES tube. The two-plate stack is also in the Chervon configuration and operated at ~2 KV. The signal is amplified and recorded by a digital oscilloscope (Lecroy, 9361).

The electron kinetic energy (*eKE*) of the photoelectron is determined by the flight time in this spectrometer. The *eKE* can be obtained by the following equation:

$$\frac{1}{\sqrt{eKE}} = \frac{1}{\sqrt{m_e}}\frac{1}{D}t - \sqrt{\frac{2}{m_e}}\frac{t_0}{D} \qquad \textbf{2.1}$$

The slope and the intercept of the above equation can be obtained by calibration to known PES. In this thesis, the PES is usually calibrated by the vibration progressions of the oxygen anion before experiments.[11]

2.3. Femtosecond Laser System

A high-power femtosecond laser system is used in these experiments to ensure the maximum overlap of the laser beam with sufficient peak power and the molecular beam. The laser system includes the femtosecond laser oscillator, the regenerative amplifier, and optics for manipulating the pulses, as shown in Fig. 2.11.

The femtosecond oscillator and amplifier used in this work is a commercial Ti:Sapphire based system manufactured by Spectra Physics. The self-mode-locked Ti:Sapphire oscillator, Tsunami, is pumped by a diode-pumped solid-state Nd:YLF laser Millennia Vs at 5 W and generates a 82-MHz 80-fs pulse train at 800 nm with a total power of 0.6–0.8 W. The output femtosecond is then directed into the TSA amplifier for amplification.

The TSA amplifier has three major components: stretcher, amplifiers, and compressor. The 80-fs pulses from the Tsunami are stretched by a grating-mirror setup to ~200 ps. The stretched pulse is then directed onto the Ti:Sapphire crystal in the amplifier compartment.

The amplification of TSA is done by a three-stage amplifier, one regenerative and two linear amplifiers. Each amplifier uses one Ti:Sapphire crystal. The regenerative and first linear amplifier is pumped by a Nd:YAG laser (Spectra Physics, Quanta Ray Lab-130) and the second linear amplifier is pumped by another Nd:YAG laser (Spectra Physics, Quanta Ray Lab-150). The amplified beam is then collimated to ~1-cm diameter and directed to the compressor. A grating-mirror setup then compresses the pulse to a width of ~110 fs. The output energy of the TSA at 800 nm is ~25 mJ/pulse.

The output beam from the TSA is characterized and monitored in real time by a

single-pulse autocorrelator (Positive Light SSA). The 800-nm output pulse is then frequency doubled by a type-I BBO second harmonic crystal. The second harmonic output (400 nm) pulse and the residual fundamental (800 nm) pulse are then separated by a dichroic mirror (harmonic separator). The 400-nm pulses then pass through a hollow-prism retroreflector mounted on a computer controlled linear motion stage (Aerotech, ATS-150-250-0-20P-NC-NM with controller Unidex 100) to control the time delay between the pump and probe pulses. The fundamental pulse passes through a fixed delay line to provide a comparable delay of the 400-nm pulse to ensure the temporal overlap of two pulses is achievable. Polarization of each beam is changed by a half wave plate and verified by a polarizer. Both beams are then directed onto the optical breadboard attached to the molecular beam machine.

On the breadboard, two beams are collimated to a beam size of ~3 mm (diameter). Two beams are then combined by another dichroic mirror and then directed into the molecular beam machine through the entrance window. A fast photodiode (Thorlabs DET-220) is placed at the exit window of the chamber to measure the arriving time of the laser pulse, which is used as a time-zero reference for the time-of-flight photoelectron spectrometer.

2.4. Synchronization and Data Acquisition System

The synchronization system in this work triggers the laser pulse, the ion source, and the detecting systems. It is especially important, since measurements are done by timing the arrival of particles (anions and electrons in mass and photoelectron spectrometer, respectively) at the detectors.

The diagram of the synchronization system is illustrated in Fig. 2.12 and the time table is shown in Fig. 2.13. The key issue of this setup is to synchronize the femtosecond laser pulse and the TOF/MS (high-voltage pulser for the repeller and accelerator) with no significant jitter, since the femtosecond laser output from TSA is not exactly at 20 Hz. It has up to a ±12-ns jitter because pulses are amplified from selected seeding pulses from the Tsunami oscillator, whose repetition rate is ~82 MHz. The following scheme is used in order to solve the jitter problem. A TTL master clock at 20 Hz synthesized by a pulse generator (Wavetek 182A) and the photodiode signal of Tsunami are sent to the synchronization module (Spectra Physics, SM-1) and a pulse that is synchronized to the Tsunami output pulse is synthesized at ~20 Hz (±12 ns). This pulse is then sent to the delay generator, #1(Stanford Research System, DG-535) and a delayed pulse (~350 μs delay) is sent to the controller unit of the TSA (Spectra-Physics SDG II) to control the TSA output timing. Another TTL pulse with no delay is then sent to another delay generator, #2 (Stanford Research System, DG-535). The output channels from delay generator, #2 are sent to the high-voltage pulser to control the timing of the high-voltage pulses for the repeller and accelerator of the primary TOF/MS and also other electronics. With this setup, all the electronics other than the nozzle controller are synchronized to the laser pulses. The nozzle controller does not need to be synchronized to this clock because the gas pulse duration is many orders greater than 12 ns and the jitter would not be an issue here.

Data acquisition is done automatically using a home-built computer program written in Microsoft Visual Basic 6.0 (See Appendix). The program controlled the instruments and retrieved data from the instruments through a General Purpose Interface

Bus (GPIB) interface by a National Instrument PCI-GPIB interface card. The flow chart of this computer program is shown in Fig. 2.14. Briefly, the program commands the motion stage to the desired position and then sends a request to the oscillator to start average data. Once the average on the digital oscilloscope is finished, the program is held until it receives the SRQ signal of the GPIB interface, which indicates the acquisition is done and then dumps the data to the memory and the hard drive in the computer. The program then moves the stage to the next position to perform the next acquisition. The program will repeatedly run loops until the signal-to-noise ratio is satisfactory.

In the hydrated electron cluster experiment (Chapter 3), Boxcar gated integrators (Stanford Research System, SR250) and an analog-to-digital converter (Stanford Research System, SR245) were used to obtain the time-resolved transient. However, this data acquisition system was upgraded to the current setup, which has the capability of three-dimensional time-resolved PES recording. More importantly, post-processing of the data can be done on the raw data obtained through this program. Careful slicing of the photoelectron in different energy windows can be used to getting the time-resolved transients for different species.

References

(1) Paik, D. H., Ph.D. Thesis, California Institute of Technology, Pasadena, CA 2004.

(2) Even, U.; Jortner, J.; Noy, D.; Lavie, N.; Cossart-Magos, C. *J. Chem. Phys.* **2000**, *112*, 8068.

(3) Wiley, W. C.; McLaren, I. H. *Rev. Sci. Instrum.* **1955**, *26*, 1150.

(4) Cotterr, R. J. *Time-of-Flight Mass Spectrometry: Instrumentation ans Application in Biological Research*; American Chemical Society: Washington, DC, 1997.

(5) Kruit, P.; Read, F. H. *J. Phys. E Sci. Instrum.* **1983**, *16*, 313.

(6) Greenblatt, B. J.; Zanni, M. T.; Neumark, D. M. *Chem. Phys. Lett.* **1996**, *258*, 523.

(7) Handschuh, H.; Ganteför, G.; Eberhardt, W. *Rev. Sci. Instrum.* **1995**, *66*, 3838.

(8) Rademann, K.; Rech, T.; Kaiser, B.; Even, U.; Hensel, F. *Rev. Sci. Instrum.* **1991**, *62*, 1932.

(9) Markovich, G.; Pollack, S.; Giniger, R.; Cheshnovsky, O. *J. Chem. Phys.* **1994**, *101*, 9344.

(10) Wang, L. S.; Cheng, H. S.; Fan, J. W. *J. Chem. Phys.* **1995**, *102*, 9480.

(11) Travers, M. J.; Cowles, D. C.; Ellison, G. B. *Chem. Phys. Lett.* **1989**, *164*, 449.

Figure Captions

Figure 2.1: Molecular Beam Machine — Chambers

Figure 2.2: Vacuum System Block Diagram

Figure 2.3: Molecular Beam Machine — Section View

Figure 2.4: Nozzle Assembly

Figure 2.5: Thermal Electron Source

Figure 2.6: New Sample Delivery System

Figure 2.7: Pulsed Electron Gun

Figure 2.8: Primary Time-of-flight Mass Spectrometer

Figure 2.9: Reflectron Time-of-flight Mass Spectrometer

Figure 2.10: Magnetic-bottle Photoelectron Spectrometer

Figure 2.11: Femtosecond Laser System

Figure 2.12: Synchronization Setup Block Diagram

Figure 2.13: Synchronization Timing Table

Figure 2.14: Flow Chart of the Data Acquisition Program

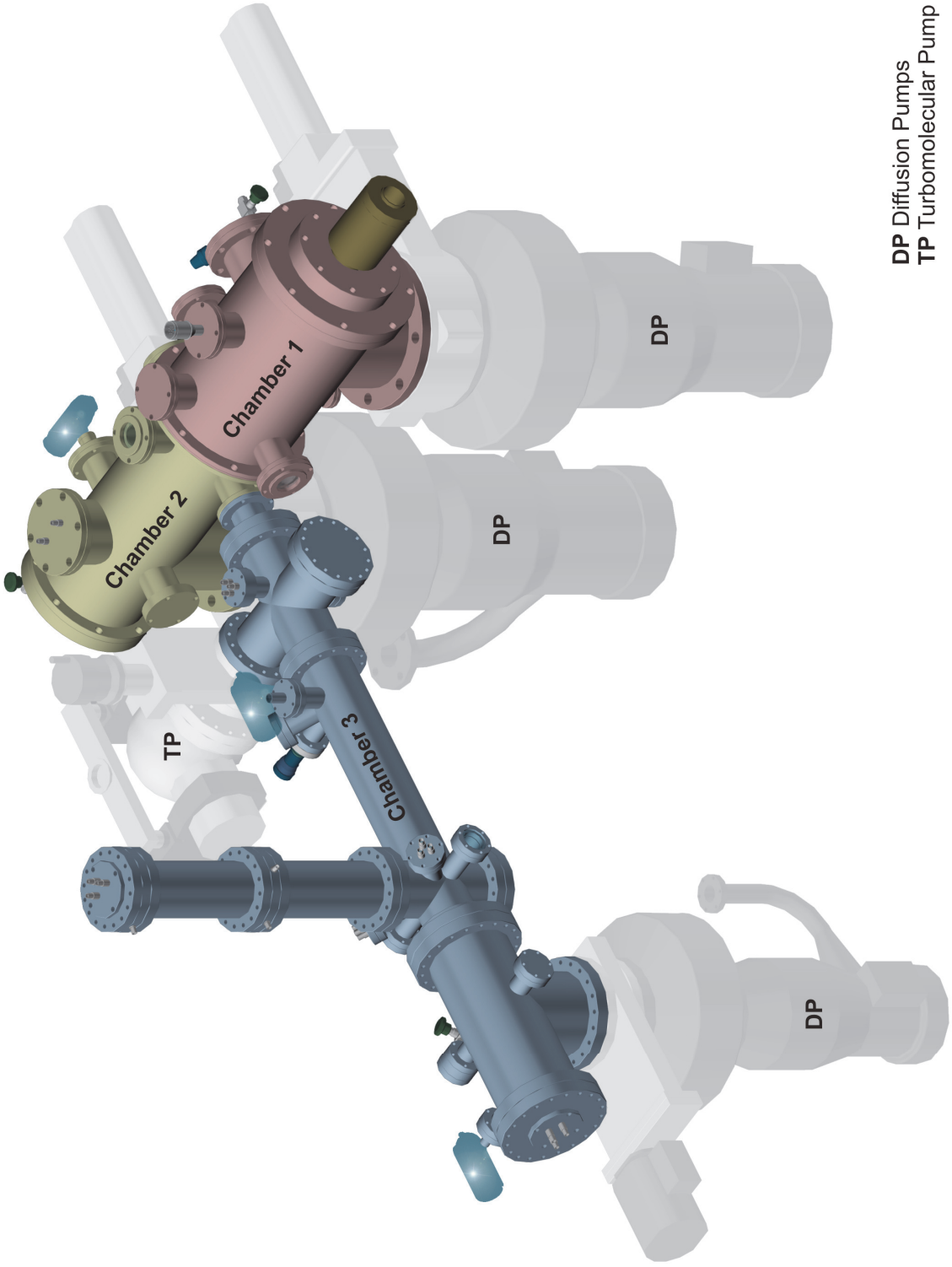
DP Diffusion Pumps
TP Turbomolecular Pump
Chamber 1
Chamber 2
Chamber 3
DP
DP
DP
TP

Figure 2.1

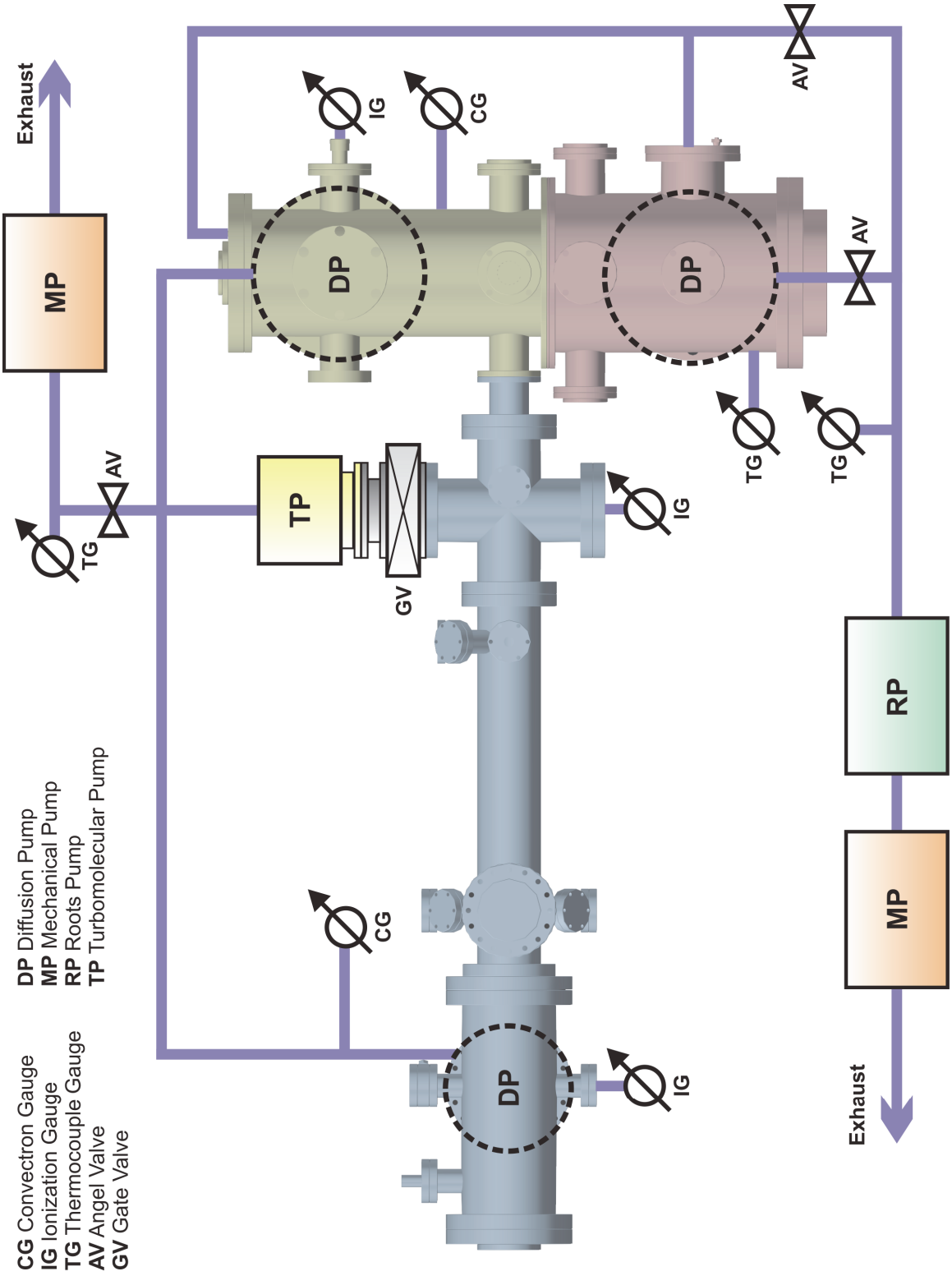
Exhaust
MP
AV
TG
TP
GV
IG
CG
DP
AV
TG
TG
RP
MP
Exhaust
DP Diffusion Pump
MP Mechanical Pump
RP Roots Pump
TP Turbomolecular Pump
CG Convectron Gauge
IG Ionization Gauge
TG Thermocouple Gauge
AV Angel Valve
GV Gate Valve

Figure 2.2

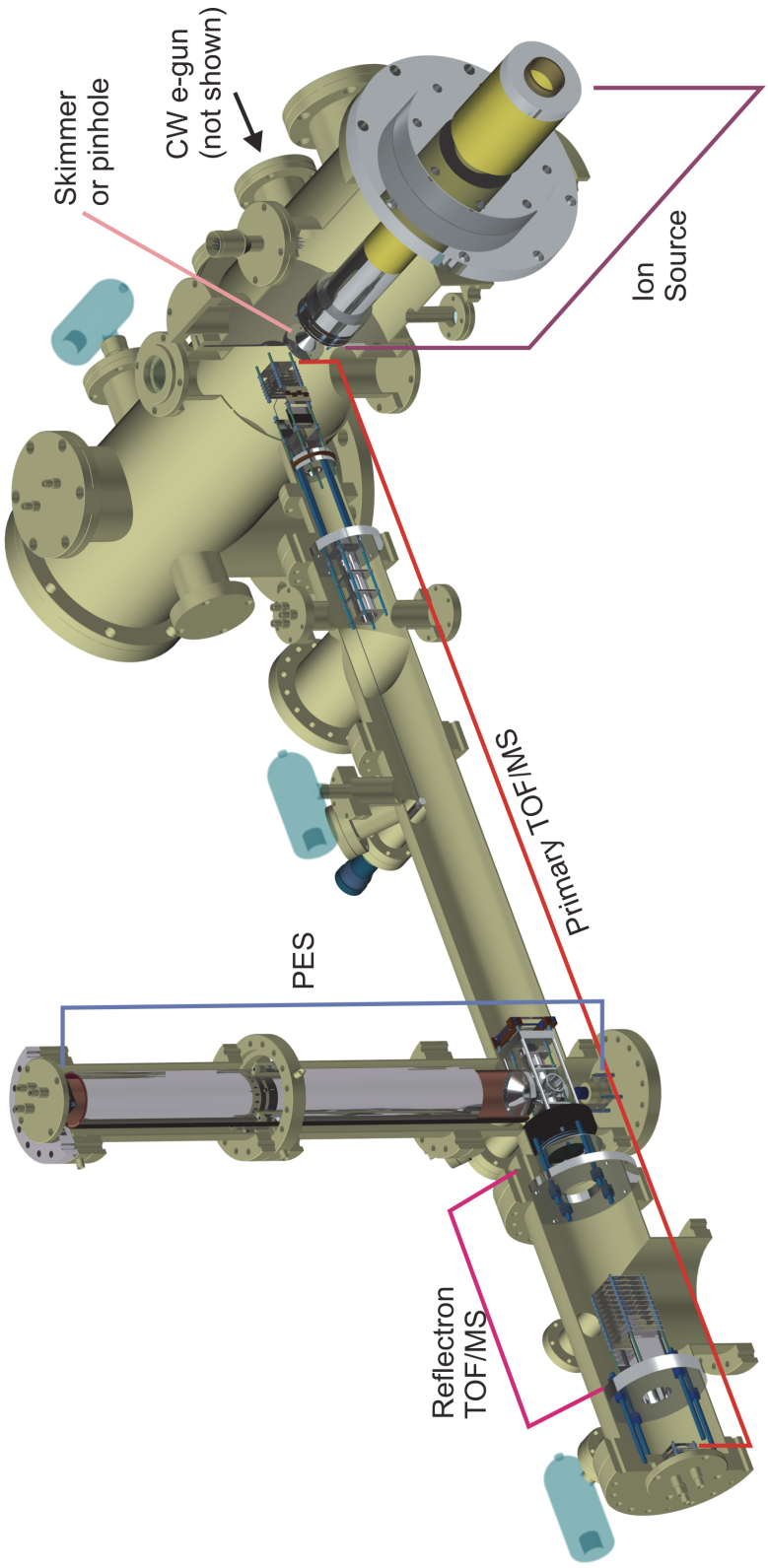
Skimmer
or pinhole
CW e-gun
(not shown)
Ion
Source
Primary TOF/MS
PES
Reflectron
TOF/MS

Figure 2.3

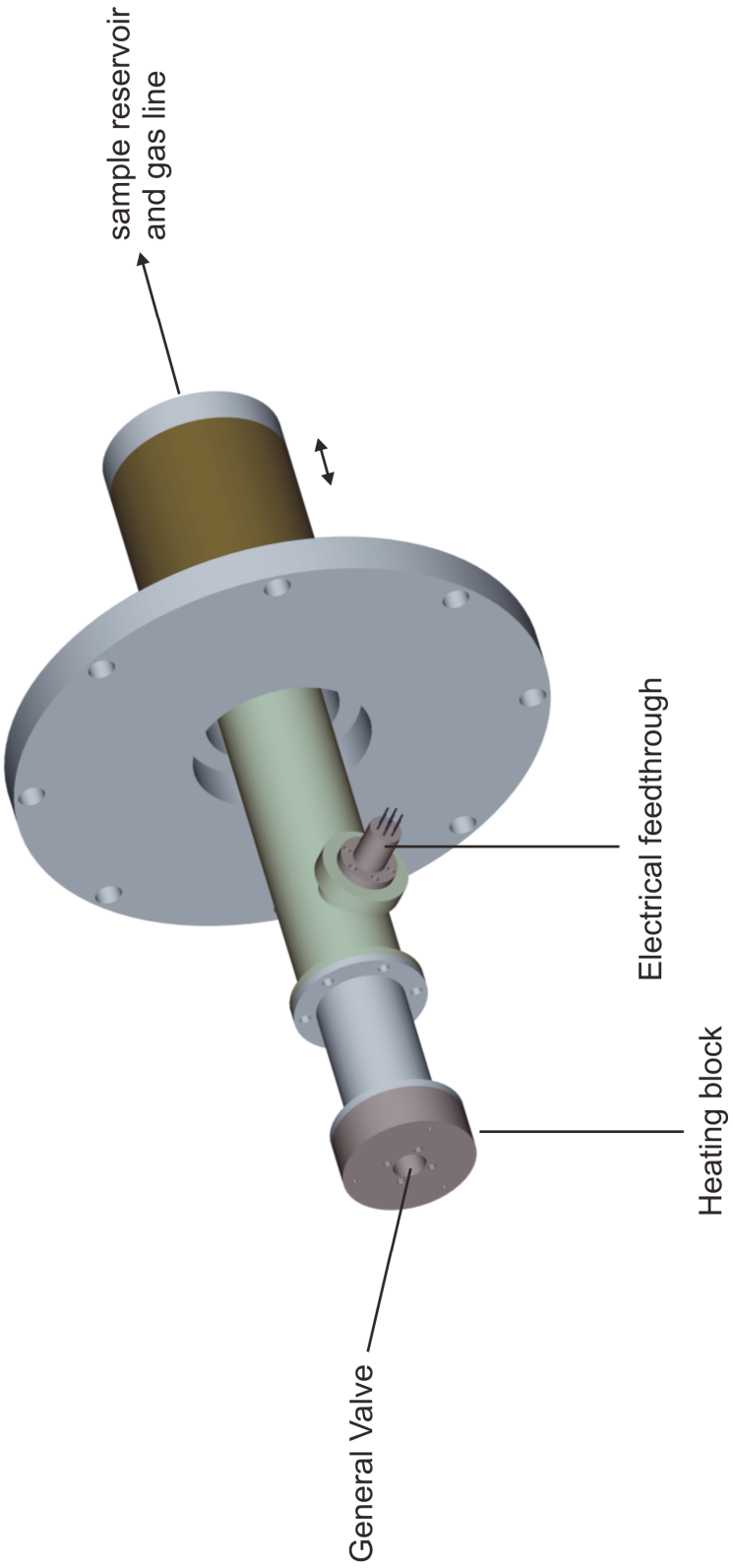
sample reservoir
and gas line
Electrical feedthrough
Heating block
General Valve

Figure 2.4

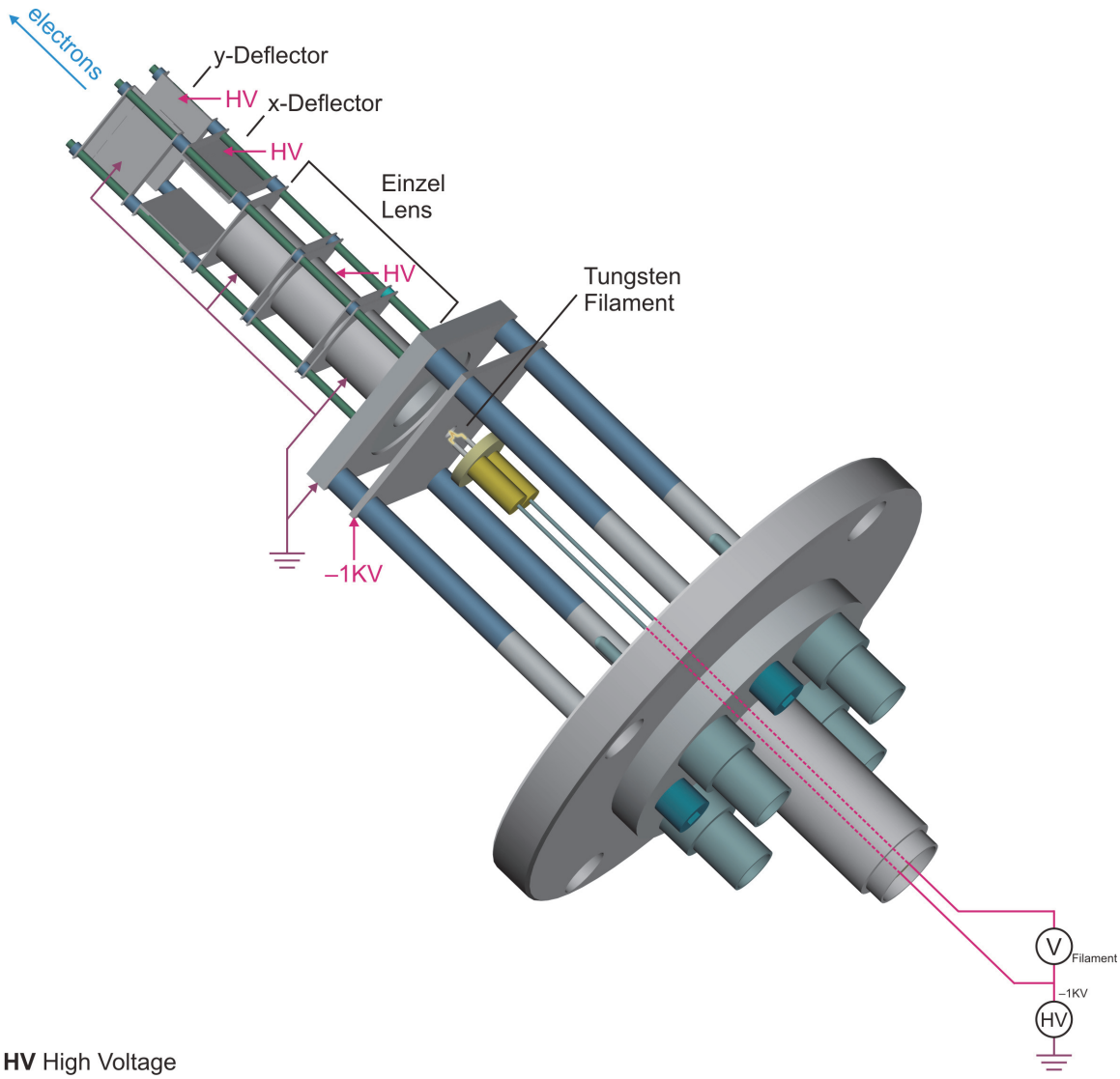

HV High Voltage

Figure 2.5

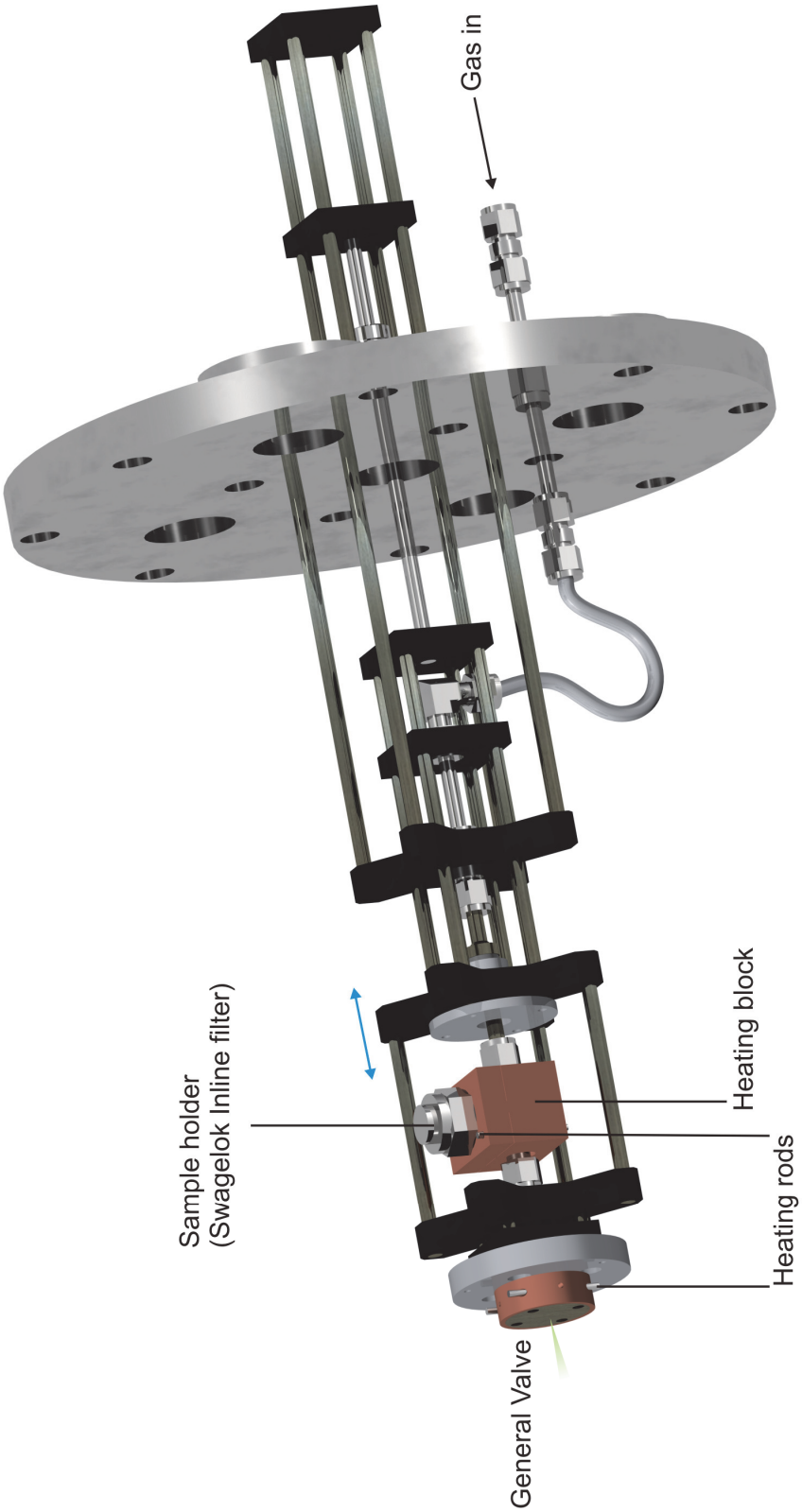
Gas in
Sample holder
(Swagelok Inline filter)
Heating block
Heating rods
General Valve

Figure 2.6

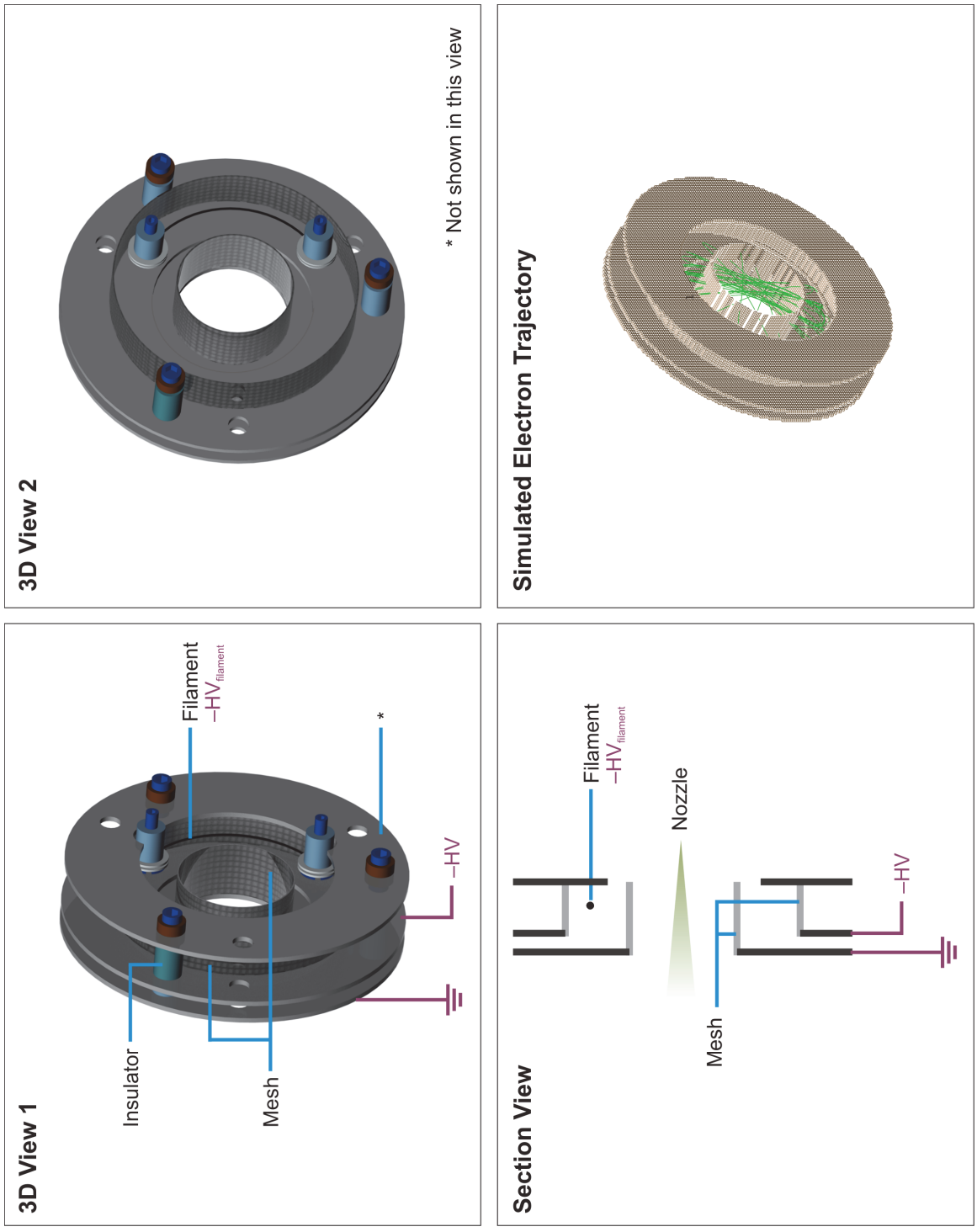
3D View 2
* Not shown in this view
Simulated Electron Trajectory
3D View 1
Filament
–HV filament
*
–HV
Insulator
Mesh
Section View
Filament
–HV filament
Nozzle
–HV
Mesh

Figure 2.7

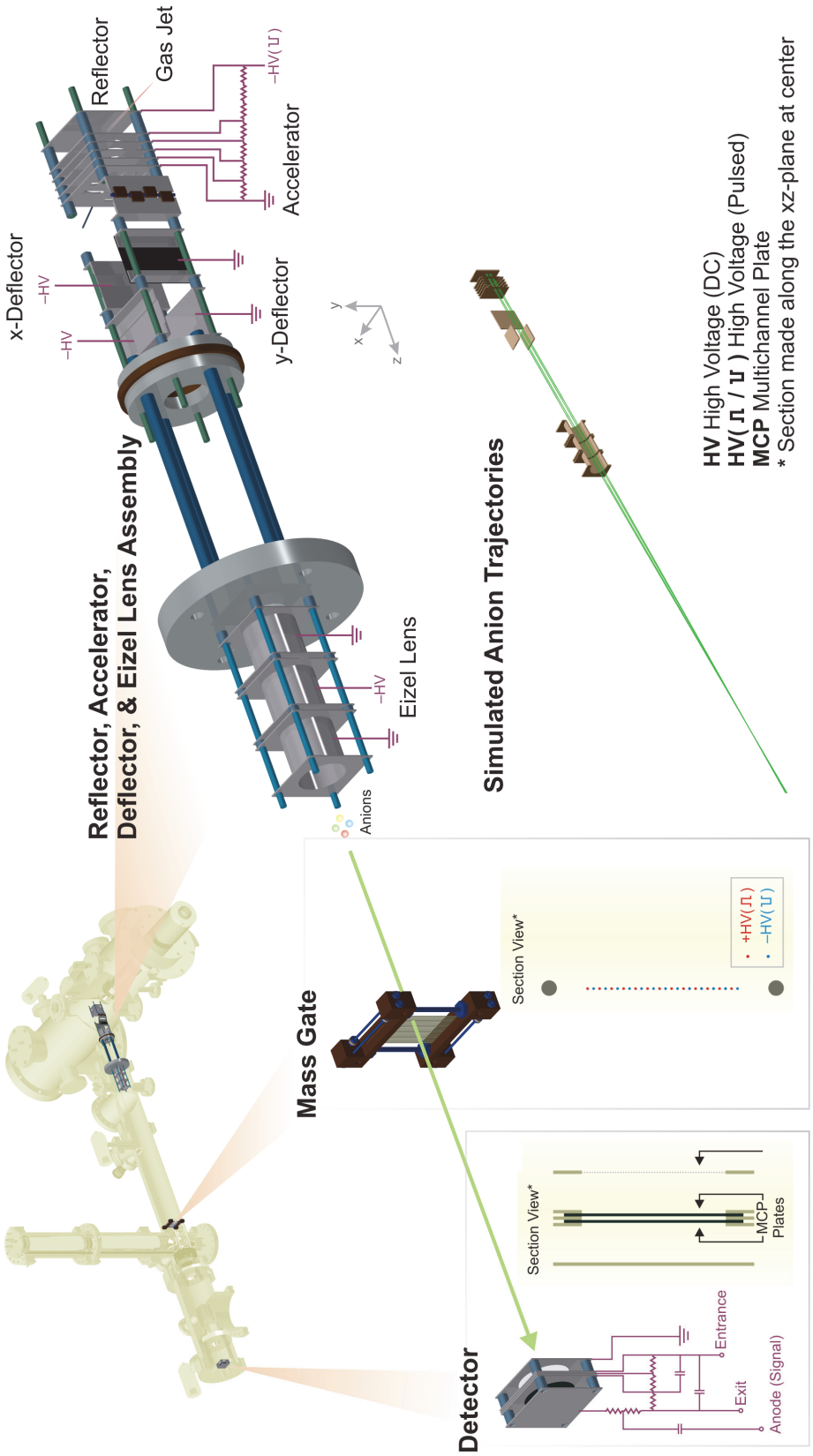
Reflector
Gas Jet
–HV(Д)
Accelerator
x-Deflector
–HV
–HV
y-Deflector
y
x
z
Reflector, Accelerator,
Deflector, & Eizel Lens Assembly
–HV
Eizel Lens
Anions
Simulated Anion Trajectories
HV High Voltage (DC)
HV(Д / Ц) High Voltage (Pulsed)
MCP Multichannel Plate
* Section made along the xz-plane at center
Mass Gate
Section View*
+HV(Д)
–HV(Ц)
Detector
Section View*
MCP
Plates
Entrance
Exit
Anode (Signal)

Figure 2.8

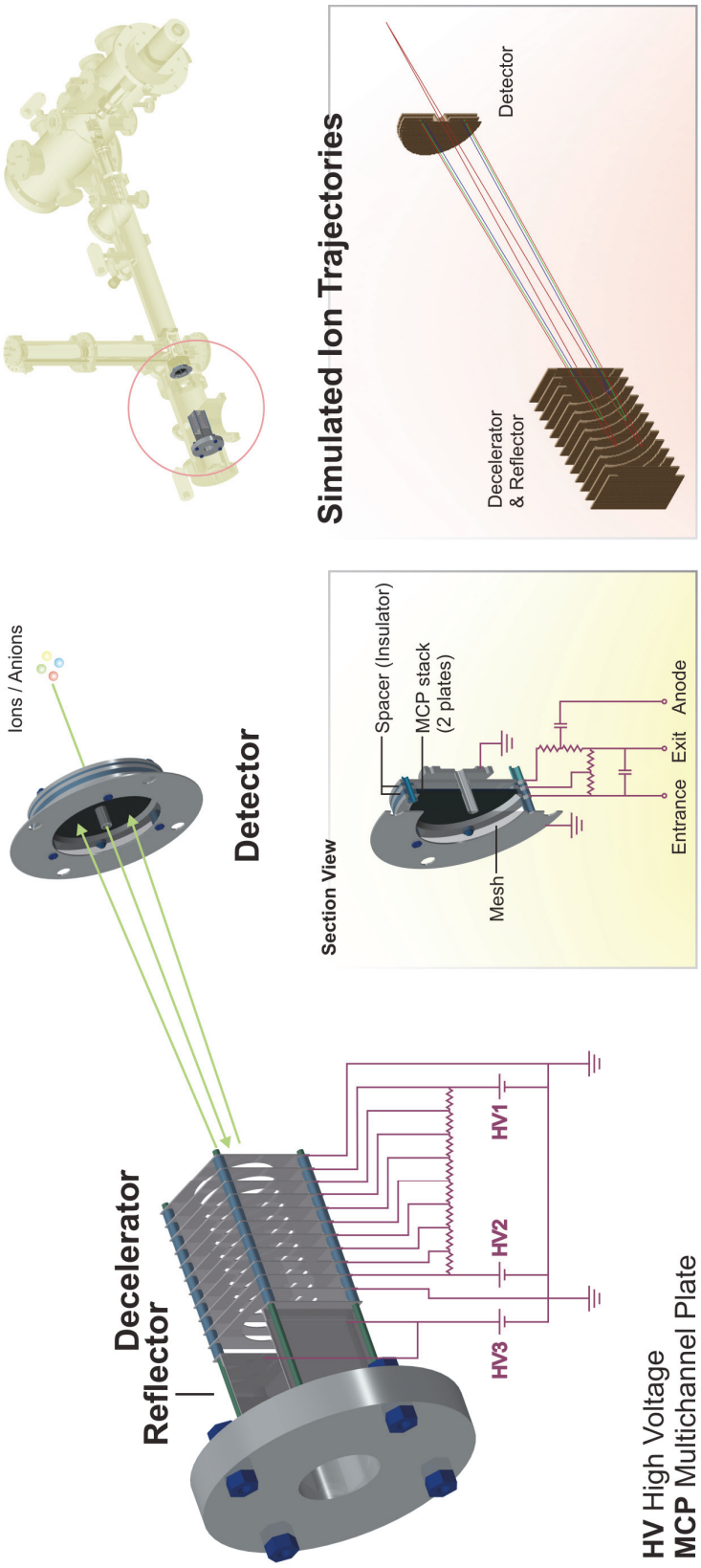
Simulated Ion Trajectories
Detector
Decelerator & Reflector
Section View
Spacer (Insulator)
MCP stack (2 plates)
Mesh
Entrance
Exit
Anode
Ions / Anions
Detector
Decelerator
Reflector
HV1
HV2
HV3
HV High Voltage
MCP Multichannel Plate

Figure 2.9

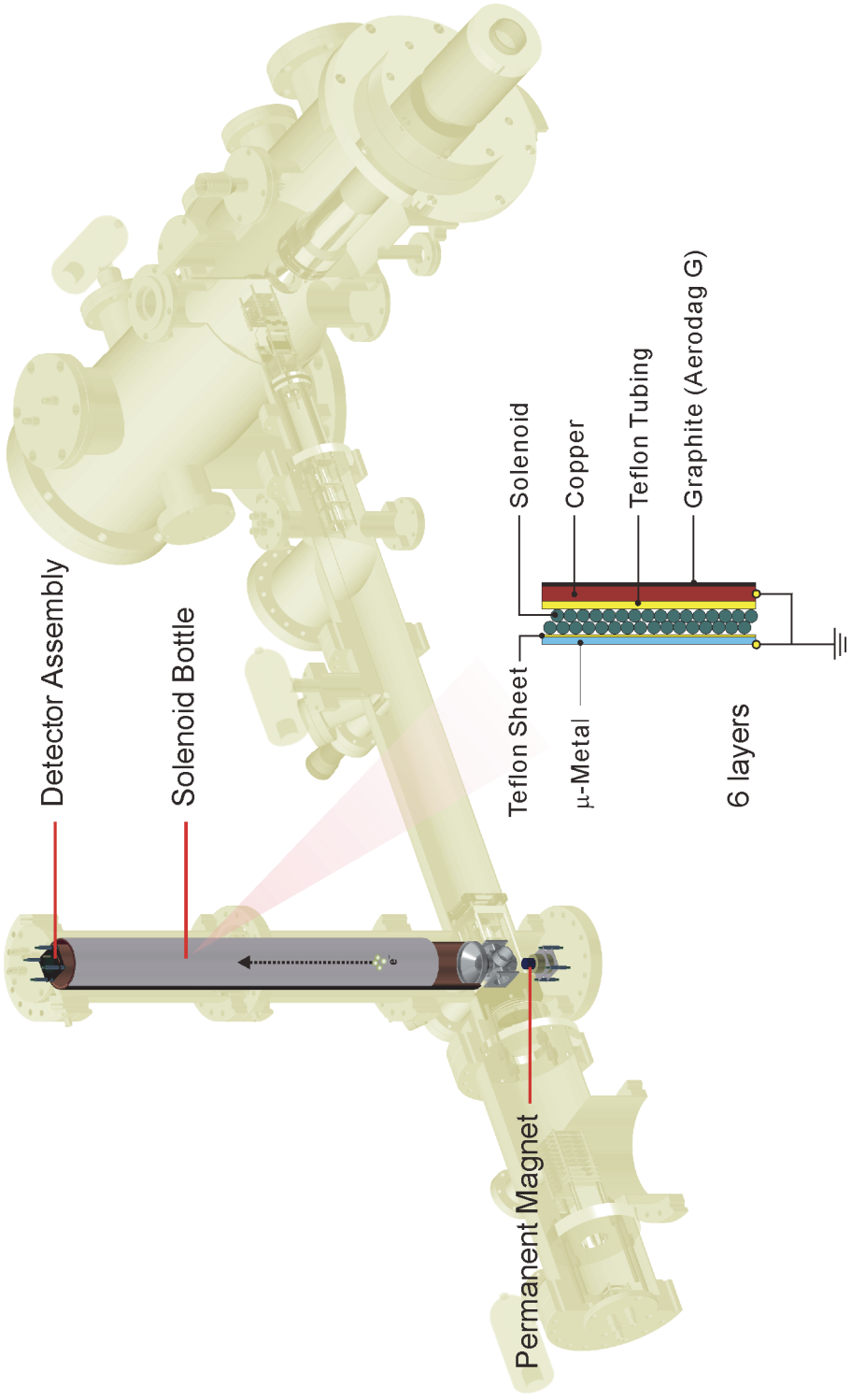
Detector Assembly
Solenoid Bottle
Permanent Magnet
Solenoid
Copper
Teflon Tubing
Graphite (Aerodag G)
Teflon Sheet
μ-Metal
6 layers

Figure 2.10

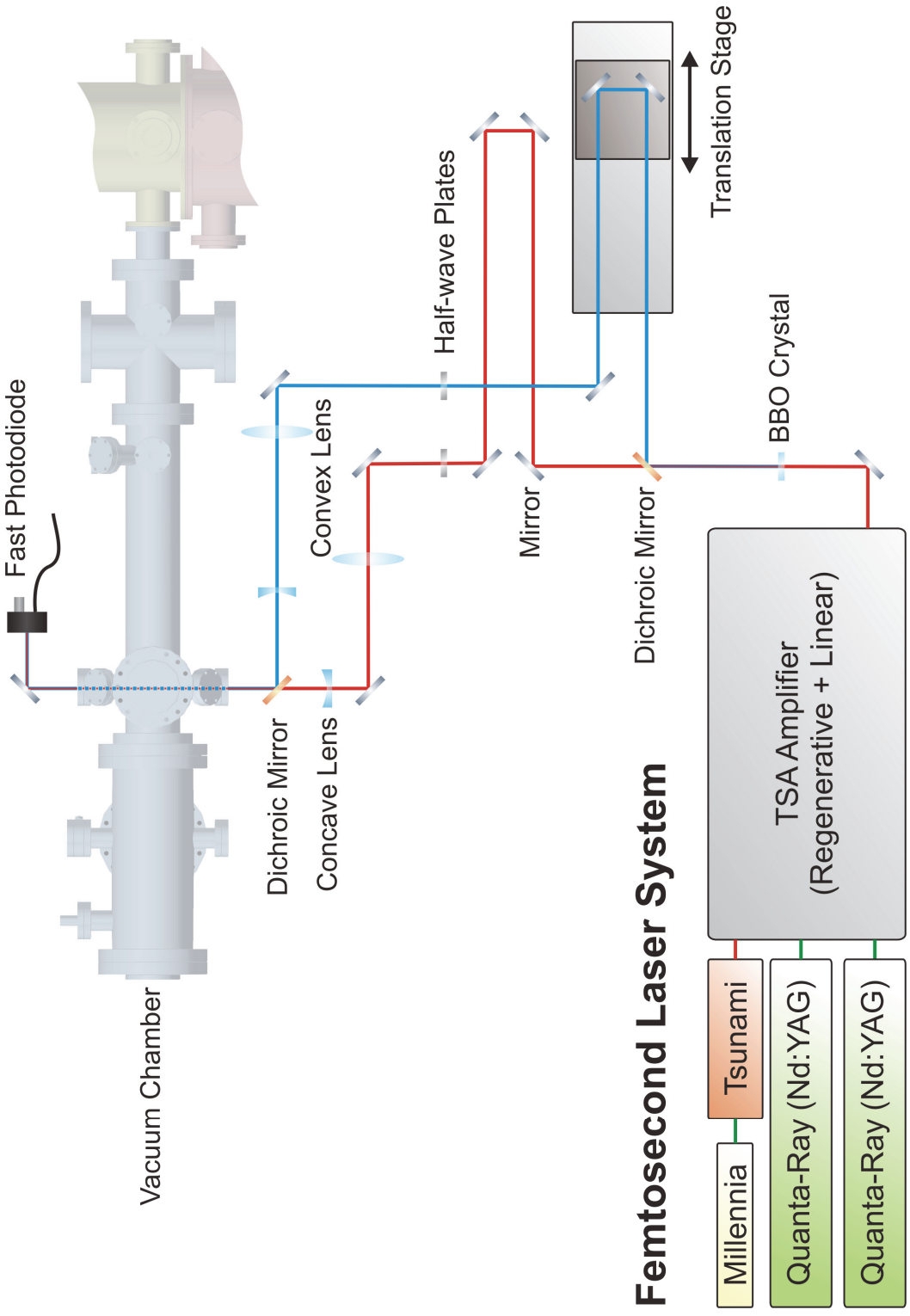
Fast Photodiode
Vacuum Chamber
Dichroic Mirror
Concave Lens
Convex Lens
Half-wave Plates
Mirror
Dichroic Mirror
Translation Stage
BBO Crystal
Femtosecond Laser System
TSA Amplifier
(Regenerative + Linear)
Millennia
Tsunami
Quanta-Ray (Nd:YAG)
Quanta-Ray (Nd:YAG)

Figure 2.11

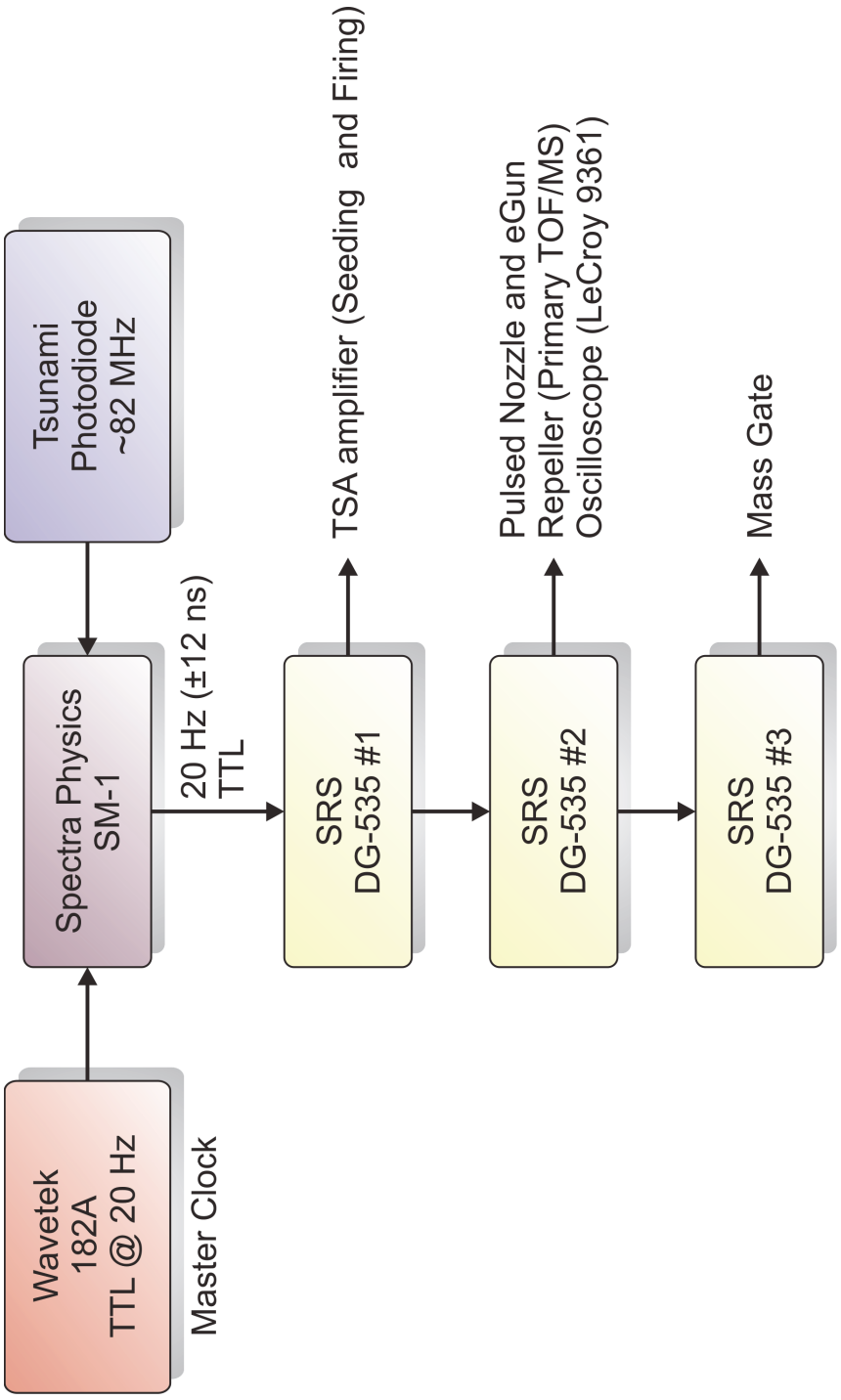
Tsunami
Photodiode
~82 MHz
Spectra Physics
SM-1
20 Hz (±12 ns)
TTL
SRS
DG-535 #1
TSA amplifier (Seeding and Firing)
SRS
DG-535 #2
Pulsed Nozzle and eGun
Repeller (Primary TOF/MS)
Oscilloscope (LeCroy 9361)
SRS
DG-535 #3
Mass Gate
Wavetek
182A
TTL @ 20 Hz
Master Clock

Figure 2.12

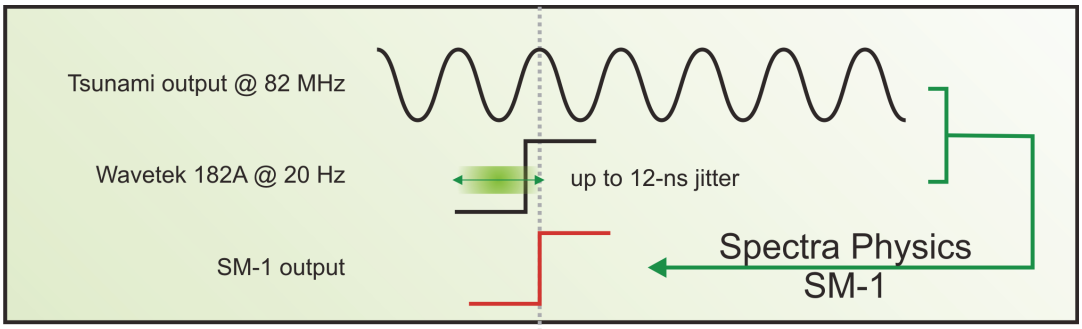

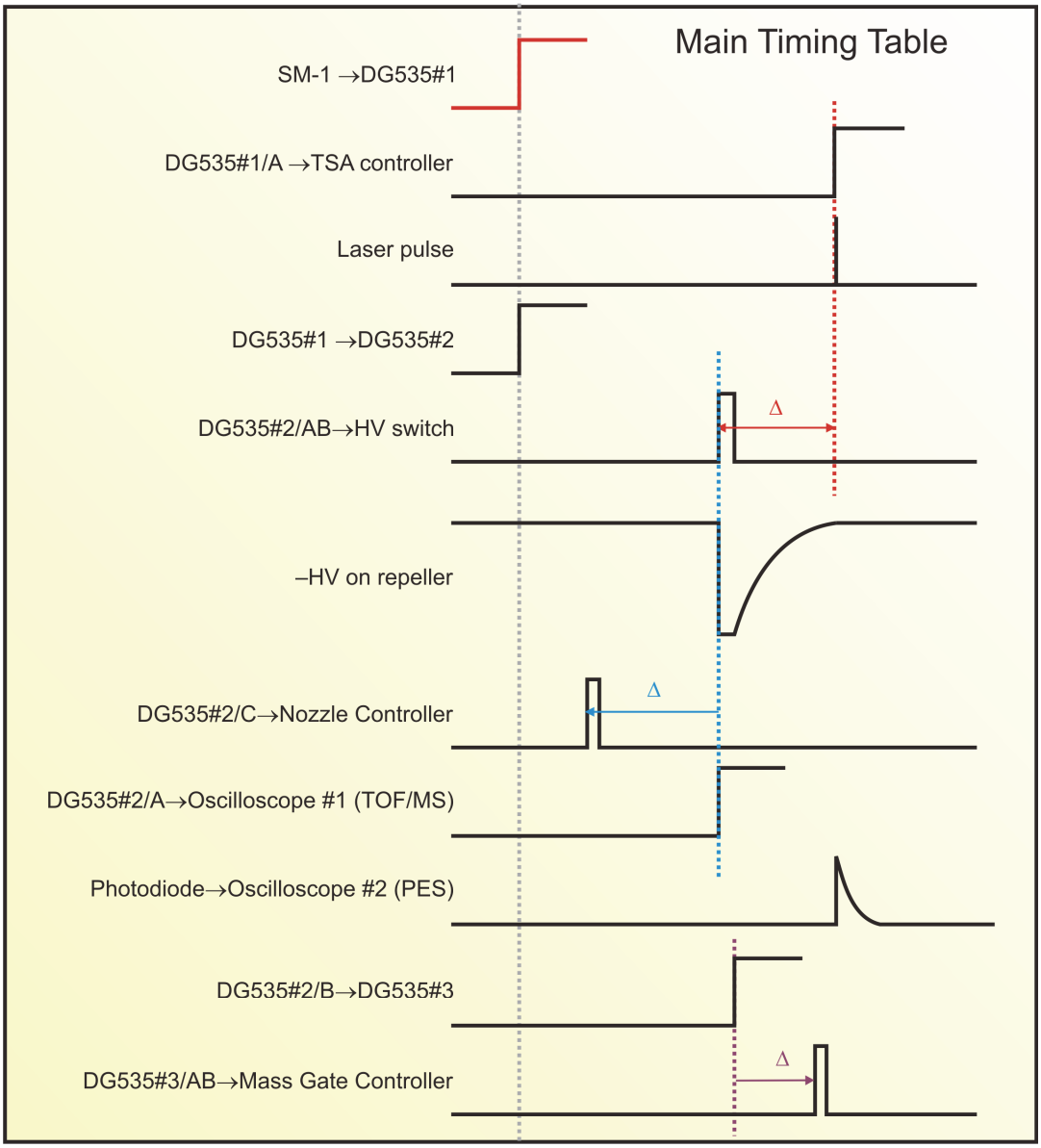

These two time tables are at different timescales.

Figure 2.13

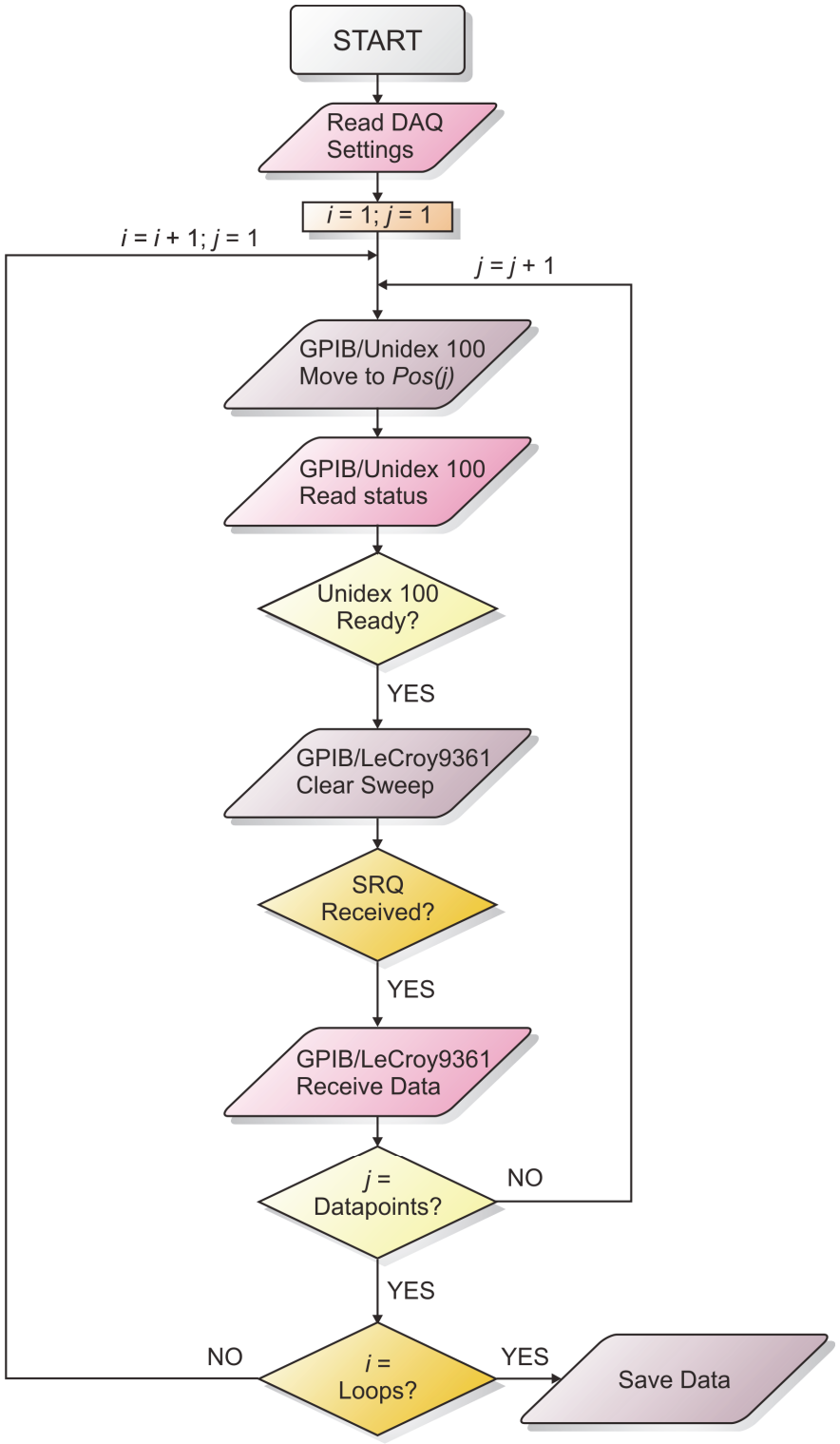
START
Read DAQ Settings
i = 1; j = 1
i = i + 1; j = 1
j = j + 1
GPIB/Unidex 100 Move to Pos(j)
GPIB/Unidex 100 Read status
Unidex 100 Ready?
YES
GPIB/LeCroy9361 Clear Sweep
SRQ Received?
YES
GPIB/LeCroy9361 Receive Data
j = Datapoints?
NO
YES
NO
i = Loops?
YES
Save Data

Figure 2.14

CHAPTER 3.

Electrons in Finite-Sized Water Cavities:

Hydration Dynamics Observed in Real Time†

†adapted from Paik, D. H.; Lee, I. R.; Yang, D. S.; Baskin, J. S.; Zewail, A. H. *Science* **2004**, *306*, 672.

Abstract

We directly observed the hydration dynamics of an excess electron in the finite-sized water clusters of $(H_2O)_n^-$ with n = 15, 20, 25, 30, and 35. We initiated the solvent motion by exciting the hydrated electron in the cluster. By resolving the binding energy of the excess electron in real time with femtosecond resolution, we captured the ultrafast dynamics of the electron in the presolvated ("wet") and hydrated states and obtained, as a function of cluster size, the subsequent relaxation times. The solvation time (300 femtoseconds) after the internal conversion [140 femtoseconds for $(H_2O)_{35}^-$] was similar to that of bulk water, indicating the dominant role of the local water structure in the dynamics of hydration. In contrast, the relaxation in other nuclear coordinates was on a much longer time scale (2 to 10 picoseconds) and depended critically on cluster size.

3.1. Introduction

The nature of the solvated electron, which was first observed in liquid ammonia in 1864, continues to pose several fundamental problems. When the solvent medium is water, the hydrated electron becomes essential to a myriad of physical, chemical, and biological processes. In a simple picture of an electron in a cavity, the description of the hydrated electron state structure is analogous to that of a hydrogen atom, with a ground state of *s*-type and an excited state of *p*-type character. However, the hydrated electron is far more complex, because of the ultrafast dynamics of structural change, solvation, and recombination. After postulation of the existence of the hydrated electron and the discovery of its absorption, experimental and theoretical efforts have focused on studies in bulk water in which the "cavity" is surrounded by a continuum of other water molecules.

A key issue for understanding electron hydration is knowledge of the time-scales involved: the motion of water molecules toward the equilibrium structure and the lifetime of the electron in the different states it occupies. In bulk water, early femtosecond transient absorption studies [1,2] resolved electron hydration dynamics using excitation by two ultraviolet photons to eject bound electrons from water molecules or solute anions. During the succeeding decade, different research groups have provided a vast amount of experimental data on the time scales of relaxation and the theoretical underpinnings of the hydrated electron system.[3-12] Among these was the first three-pulse experiment,[3] in which a population of ground-state hydrated electrons created by an initial laser pulse was subsequently studied using two additional pulses, the first of which excited the electrons from the *s*- to the *p*-state and the second of which probed either state. More

recently, studies have been made with pulses as short as 5 fs in order to elucidate the different relaxation pathways.[5,9] In these bulk studies, there remain unanswered questions, especially regarding the microscopic molecular structure and dynamics of hydration.

Mesoscopic clusters [13,14] are ideal for forming finite-sized nanoscale water cavities for electron hydration, and because of the charge of the electron, it is in principle possible to select a particular size of cluster and study its isolated structure and dynamics. Results from such studies provide insight into the bulk behavior. For example, accurate spectra of neutral water dimers are predictive of the properties of larger clusters and bulk water.[15] For electrons in water clusters, Haberland and coworkers [16] first reported the experimental observation of $(H_2O)_n^-$ clusters, and, in a series of comprehensive studies, the Johnson [17-19] and Bowen [20,21] groups have elucidated the size dependence of spectroscopic properties, examining the role of the core motif in reaching bulk hydration.

The structure of these finite-sized clusters has been studied both experimentally and theoretically, addressing the issue of surface and interior electron binding.[18,20,22-24] Theoretical studies [23,24] of small $(H_2O)_n^-$ clusters, $n \leq 14$, predict that the electron lies at the surface. Earlier calculations by the groups of Landman and Jortner [22] indicated that for small clusters ($n \leq 32$), the electron tends to remain on the surface, whereas for the larger ones (n = 64 and 128), the electron is in the interior. Recent work for n = 24 indicates that although three isomers (with the electron inside or outside at the surface) are energetically similar, the vertical detachment energy closest to the experimental value is that of the isomer with the electron inside.[25] Despite these extensive studies, the only report of real-time dynamics of water cluster anions has been that of a preliminary *p*-state lifetime, limited by laser pulse duration, for a cluster of unspecified size.[19]

We present here direct observation of the femtosecond dynamics of electrons in water clusters varying in size up to n = 35. We focused our attention on the dynamics in systems with different solvation cavities (n = 15, 20, 25, 30, and 35). The finite-sized clusters were selectively intercepted by femtosecond pulses to promote the electron from the *s*- to the *p*-state (Fig. 3.1A).[26] We followed subsequent relaxation dynamics by monitoring the evolution of the photoelectron (PE) spectrum with kinetic energy resolution.[27] The latter proved critical, as did the resolution of kinetic energy of ions, [28] for deciphering different pathways of dynamics. This PE energy resolution allowed us to address whether hydration proceeds while the electron is in the ground (*s*-type) and/or excited (*p*-type) states. For the cavity sizes under study, the behavior observed can be correlated to that of bulk-type hydration.

3.2. Experimental

We generated the negatively charged water clusters by crossing a continuous electron beam (1 keV) with a jet of water vapor, using nitrogen as a carrier gas at 150 to 250 kPa. After 100 μs of drift time, application of a properly timed voltage pulse accelerated $(H_2O)_n^-$ clusters into the field-free time-of-flight region, where the desired size was intercepted with femtosecond laser pulses.[29] A typical cluster size distribution is shown in Fig. 3.1B. The laser pulses (110 fs) were generated from a Ti:sapphire oscillator and amplified by regenerative and multipass amplifiers. The 800-nm laser output was frequency doubled to generate a 400-nm pulse. The residual 800-nm light was used as the excitation pulse, and the 400-nm laser pulse, delayed in time, was used as the probe to photodetach electrons. Photoelectrons were collected by a magnetic-bottle PE

spectrometer, and the metastable anions and photofragments were detected by a linear reflectron mass spectrometer. We recorded transients by integrating the PE intensity in selected electron kinetic energy (eKE) windows as a function of the delay time.

3.3. Results and Discussion

A conceptual illustration of our experiments and methodology is shown in Fig. 3.2. When a particular size of $(H_2O)_n^-$ is selectively excited by the 800-nm femtosecond laser pulse, the excess electron is promoted to the *p*-state (Fig. 3.2A). The coordinate-labeled solvation represents all nuclear motions of the solvent that strongly affect the electrostatic environment and thus the energy of the electron. As a result of the electronic transition, the electron charge distribution is significantly changed, driving a rearrangement of water molecules around the electron that corresponds to displacement along the solvation coordinate with characteristic time τ_p. Similarly, when the excited state relaxes down to the ground state by internal conversion with characteristic time τ_{ic}, displacement along the solvation coordinate will reverse, and the solvent will move back toward its original configuration with characteristic time τ_s. Because the pump photon energy, which is several times greater than the binding energy of surface water molecules,[30] is retained in these isolated clusters, the flow of energy from the solvation coordinate into other nuclear coordinates will lead to the eventual evaporation of water molecules (Fig. 3.2A, left). The fact that 800-nm absorption ultimately leads to evaporation is confirmed by our mass spectra of anionic fragments and has been reported elsewhere.[31]

The PE spectra were used to follow these dynamics and disentangle the pathways.

The energy level diagram (Fig. 3.2B) shows qualitatively how the energy content in the solvation coordinate of the anion is expected to affect the eKE of the electron ejected upon absorption of the 400-nm probe pulse. Franck-Condon considerations indicate that the eKE distribution broadens asymmetrically as the amount of energy in the solvation coordinate increases in a given electronic state (yellow to red); a change in electronic state causes the spectrum to shift position (yellow to blue). The degree of broadening depends on the relative flatness and equilibrium position displacement of the neutral's and anion's solvation coordinate potentials. With this picture in mind, solvation dynamics in both the *p*- and *s*-states can be followed by monitoring the dependence on probe delay time of the production of detached electrons with various values of eKE (e.g., the energies labeled *a*, *b*, and *c* in Fig.3.2B).

The PE spectrum of $(H_2O)_{35}^-$ upon irradiation by the 400-nm femtosecond pulse confirmed ejection of the excess electron by vertical detachment, producing the characteristic eKE distribution (Fig. 3.3A, top). When the clusters were irradiated by both 800-nm and 400-nm pulses, the PE spectrum changed with delay time, as indicated in the difference spectra (Fig. 3.3A, bottom). The same spectra are also shown in a three-dimensional representation (Fig. 3.3B). It is apparent that different regions of the PE spectrum exhibit distinct temporal behaviors, and we focused only on the three particular regions labeled *a*, *b*, and *c*. As indicated by the ribbons in Fig. 3.3B, at high eKE above the onset of the PE spectrum (region *a*), a new peak appeared at time zero and disappeared by 0.7 ps. The PE intensity near the onset (region *b*) decayed with time, whereas the PE signal near the peak of the spectrum (region *c*) displayed an abrupt drop at time zero and a rise at positive time.

To quantify the trends shown by the ribbons in Fig. 3.3B, we obtained transients by integrating the PE intensity as a function of the delay time for each energy window. The same forms of apparent temporal behaviors were evident for both n = 30 and n = 35 clusters (Fig. 3.3C). The greater level of detail provided by the transients revealed that the fast decay for region *a* is not limited by laser pulse duration, as the asymmetry is evident, and there are two distinct time scales of decay for region *b*. We also compared with region *b* results obtained for $(D_2O)_{30}^-$ and $(D_2O)_{35}^-$. For $(H_2O)_n^-$, n = 15, 20, and 25, only transients for region *b* were measured (Fig. 3.4A).[32]

The temporal behavior observed in the time-dependent PE spectra of $(H_2O)_{30}^-$ and $(H_2O)_{35}^-$ elucidates the ultrafast dynamics. The instantaneous rise and the fast decay in region *a* (at high eKE) represent vertical excitation to the *p*-state followed by rapid relaxation to the *s*-state. As discussed earlier, an isolated peak of *a*-type character should rise within our pulse duration and decay with the *p*-state lifetime. Moreover, this peak temporally changes at an eKE shift of 1 eV, which corresponds to the *s*- to *p*-state energy gap,[19] as predicted conceptually (Fig. 3.2B). In bulk water,[4,5,33] the inertial solvent motions (libration) are expected to occur before the internal conversion. In the clusters, the decay of the *a*-peak gives the time scale for population transfer to the *s*-state, with an effective time constant, τ_{eff}, for inertial motion and internal conversion (τ_p and τ_{ic}). Single exponential fits to the region *a* data give corresponding τ_{eff} values of 170 fs (n = 30) and 140 fs (n = 35) (Fig. 3.3C). Given the short time scale of these motions, coherent effects may be present,[4,34] but a kinetic description suffices for the behavior observed here.

After the internal conversion, the electron becomes presolvated in the ground state, and solvation of the electron (τ_s) follows, as revealed by the short time behavior in

regions *b* and *c*. Relaxation (τ_r) after solvation can be most clearly seen in the long time behavior in region *b* (Fig. 3.4A, right). To account for the delayed return of population from the *p*- to the *s*-state, a proper kinetic analysis must also include the influence of τ_{eff} on the transients of regions *b* and *c*.[35] The results (Figs. 3C and 4A) give s values of 300 fs (the range for the clusters studied was ±150 fs with our current analysis) and τ_r values ranging from 2 to 10 ps, depending on cluster size (Fig. 3.4A). For the different clusters *n* = 15 to *n* = 35 (Fig. 3.4B), the time scale of solvation was within a factor of two and was similar to that of electrons in bulk water. It was also on the order of the time scale of the diffusive rotational and translational motions of bulk water around molecular probes [33]. The solvent rearrangement time we obtained here for the *s*-state of these large clusters is about the same as that found for electron hydration after excitation of a charge transfer band of $I^-(H_2O)_n$ for $n = 5$ and $n = 6$.[36] Such weak size dependence and the similarity between bulk and clusters indicate that the dynamics of hydration are in large part controlled by the local structure of water molecules in immediate contact with the electron.

The longer relaxation times are determined by the energy content in the *s*-state, the rate of intramolecular vibrational energy redistribution (IVR), and hydrogen-bond breakage (Fig. 3.4, B and C). Because these times increase with cluster size, we excluded both time-dependent solvation and IVR as rate-determining and considered evaporation. Manifestation of evaporation in the transients was expected because the process alters the PE spectra as a result of change in cluster size and internal energy. We calculated the statistical rate constants for clusters undergoing evaporation by one water molecule ($1/\tau_{evp}$). Using Rice-Ramsperger-Kassel-Marcus theory,[37] we obtained rate constants that

were slower or much slower than the experimental observation, depending on the particular values of frequencies and the reaction barrier; for example, for n = 35, τ_{evp} ranged from 1 ns to 15 μs versus the observed value of 10 ps. The discrepancy would indicate a nonstatistical behavior.[40] However, there have been reports that such clusters may live for much longer times,[31] and because the internal energy needs to be determined, the results for the $(H_2O)_n^-$ and $(D_2O)_n^-$ systems should be extended with variation of energy and cluster initial temperature. The experimental time scale for relaxation (2 to 10 ps) of the clusters at finite temperature is not that different from that of hydrogen-bond making/breaking dynamics in bulk at room temperature [33].

3.4. Conclusion

Our observations demonstrate that solvation dynamics in mesoscopic hydrated electron clusters can be probed directly in real time. From the energy- and time-resolved PE spectra, we were able to follow the ultrafast processes that occur in the presolvated and hydrated states of the electron. With size-selection capability, we also observed the behavior of the rates of solvation and relaxation as a function of cluster size. For the clusters studied, our time-resolved data display solvation dynamics similar to those of the hydrated electron in bulk water, suggesting a local-water-structure model for hydration, and the pathways of electronic relaxation, solvation, and hydrogen-bond breakage have distinctly resolvable time scales. Mesoscopic scale clusters can thus provide the elementary dynamics and, as such, represent simplified model systems to study the behavior of bulk systems.

References and Notes

(1) Migus, A.; Gauduel, Y.; Martin, J. L.; Antonetti, A. *Phys. Rev. Lett.* **1987**, *58*, 1559.

(2) Long, F. H.; Lu, H.; Eisenthal, K. B. *Phys. Rev. Lett.* **1990**, *64*, 1469.

(3) Alfano, J. C.; Walhout, P. K.; Kimura, Y.; Barbara, P. F. *J. Chem. Phys.* **1993**, *98*, 5996.

(4) Yokoyama, K.; Silva, C.; Son, D. H.; Walhout, P. K.; Barbara, P. F. *J. Phys. Chem. A* **1998**, *102*, 6957.

(5) Baltuška, A.; Emde, M. F.; Pshenichnikov, M. S.; Wiersma, D. A. *J. Phys. Chem. A* **1999**, *103*, 10065.

(6) Assel, M.; Laenen, R.; Laubereau, A. *Chem. Phys. Lett.* **2000**, *317*, 13.

(7) Anderson, N. A.; Hang, K.; Asbury, J. B.; Lian, T. Q. *Chem. Phys. Lett.* **2000**, *329*, 386.

(8) Hertwig, A.; Hippler, H.; Unterreiner, A. N. *Phys. Chem. Chem. Phys.* **2002**, *4*, 4412.

(9) Pshenichnikov, M. S.; Baltuška, A.; Wiersma, D. A. *Chem. Phys. Lett.* **2004**, *389*, 171.

(10) Neria, E.; Nitzan, A.; Barnett, R. N.; Landman, U. *Phys. Rev. Lett.* **1991**, *67*, 1011.

(11) Yang, C. Y.; Wong, K. F.; Skaf, M. S.; Rossky, P. J. *J. Chem. Phys.* **2001**, *114*, 3598.

(12) Nicolas, C.; Boutin, A.; Levy, B.; Borgis, D. *J. Chem. Phys.* **2003**, *118*, 9689.

(13) Castleman, A. W.; Bowen, K. H. *J. Phys. Chem.* **1996**, *100*, 12911.

(14) Johnson, M. A.; W.C., L.; Farrar, J. M., Saunders Jr., W. H., Eds.; Wiley-InterScience: New York, 1988; Vol. 20, p 591.

(15) Goldman, N.; Saykally, R. J. *J. Chem. Phys.* **2004**, *120*, 4777.

(16) Armbruster, M.; Haberland, H.; Schindler, H. G. *Phys. Rev. Lett.* **1981**, *47*, 323.

(17) Ayotte, P.; Johnson, M. A. *J. Chem. Phys.* **1997**, *106*, 811.

(18) Ayotte, P.; Weddle, G. H.; Bailey, C. G.; Johnson, M. A.; Vila, F.; Jordan, K. D. *J. Chem. Phys.* **1999**, *110*, 6268.

(19) Weber, J. M.; Kim, J.; Woronowicz, E. A.; Weddle, G. H.; Becker, I.; Cheshnovsky, O.; Johnson, M. A. *Chem. Phys. Lett.* **2001**, *339*, 337.

(20) Coe, J. V.; Lee, G. H.; Eaton, J. G.; Arnold, S. T.; Sarkas, H. W.; Bowen, K. H.; Ludewigt, C.; Haberland, H.; Worsnop, D. R. *J. Chem. Phys.* **1990**, *92*, 3980.

(21) Coe, J. V.; Earhart, A. D.; Cohen, M. H.; Hoffman, G. J.; Sarkas, H. W.; Bowen, K. H. *J. Chem. Phys.* **1997**, *107*, 6023.

(22) Barnett, R. N.; Landman, U.; Cleveland, C. L.; Jortner, J. *J. Chem. Phys.* **1988**, *88*, 4429.

(23) Sobolewski, A. L.; Domcke, W. *Phys. Chem. Chem. Phys.* **2003**, *5*, 1130.

(24) Kim, J.; Park, J. M.; Oh, K. S.; Lee, J. Y.; Lee, S.; Kim, K. S. *J. Chem. Phys.* **1997**, *106*, 10207.

(25) Khan, A. *J. Chem. Phys.* **2004**, *121*, 280.

(26) The Fig. 3.1A depictions and use of the standard *s* and *p* designations for the solvated electron states in bulk cavities are not meant to imply that, for all clusters, the excess electron must be bound in the interior of the clusters.

(27) Stolow, A.; Bragg, A. E.; Neumark, D. M. *Chem. Rev.* **2004**, *104*, 1719.

(28) Zhong, D. P.; Zewail, A. H. *J. Phys. Chem. A* **1998**, *102*, 4031.

(29) Paik, D. H.; Kim, N. J.; Zewail, A. H. *J. Chem. Phys.* **2003**, *118*, 6923.

(30) Arnold, S. T.; Morris, R. A.; Viggiano, A. A.; Johnson, M. A. *J. Phys. Chem.* **1996**, *100*, 2900.

(31) Campagnola, P. J.; Posey, L. A.; Johnson, M. A. *J. Chem. Phys.* **1991**, *95*, 7998.

(32) Each transient of regions *b* and *c* also includes a fast response-limited negative component due to the vertical detachment by the 800-nm pump pulse the photon energy of which exceeds that of the detachment to the neutral. For small clusters (n = 15, 20, and 25), the photodetachment process is increasingly favored over the transition to the bound *p*-state because of spectral shift,[19] and this accounts for the small amplitude of the decay component (region *b*) and the fact that neither the peak near time zero in region *a* nor the rise component in region *c* were detected.

(33) Pal, S. K.; Zewail, A. H. *Chem. Rev.* **2004**, *104*, 2099.

(34) Kummrow, A.; Emde, M. F.; Baltuška, A.; Pshenichnikov, M. S.; Wiersma, D. A. *J. Phys. Chem. A* **1998**, *102*, 4172.

(35) We employed the scheme of consecutive population flow and selective population window (PE probing) and performed least-squares fitting. With experimentally determined τ_{eff} values for the initial state decay and the rise of the first intermediate of n = 30 and n = 35, the separation in time scales of the femtosecond and picosecond decays allows values of τ_s and τ_r to be extracted by the global fits. The validity of the model was supported by the pronounced dip in the region b transients of $(D_2O)_{30}^-$ and $(D_2O)_{35}^-$ (Figure 3.3C).

(36) Lehr, L.; Zanni, M. T.; Frischkorn, C.; Weinkauf, R.; Neumark, D. M. *Science* **1999**, *284*, 635.

(37) Vibrational frequencies were estimated from those calculated for small clusters.[38,39] Calculation for different size clusters differed only in the number of modes used. Thus, it is assumed that significant structural changes, for instance transition from the surface to interior states,[20,22] do not occur as cluster size

increases. The reaction coordinate was taken to be 260 cm^{-1},[39] the dissociation energy to be 2700 cm^{-1},[15] and the vibrational frequencies to remain the same at the transition state. The initial internal energy of the cluster is assumed to be the highest thermal energy of stable clusters (dissociation energy); the drift time before excitation is 100 μs, but clusters with higher internal energy may persist during this time. For the degeneracy factor of the reaction coordinate, we take half of the water molecules to be surface-bound and thus subject to dissociation.

(38) Smith, D. M. A.; Smets, J.; Elkadi, Y.; Adamowicz, L. *J. Chem. Phys.* **1997**, *107*, 5788.

(39) Kim, J.; Suh, S. B.; Kim, K. S. *J. Chem. Phys.* **1999**, *111*, 10077.

(40) Diau, E. W. G.; Herek, J. L.; Kim, Z. H.; Zewail, A. H. *Science* **1998**, *279*, 847.

(41) We thank M. A. Johnson and K. H. Bowen for helpful communication. Supported by the National Science Foundation.

Figure Captions

Figure 1:

(A) Schematic representation of the *s*- and *p*-states of the hydrated electron, based on Fig. 14 of Ref. 5. **(B)** Experimental mass spectrum of $(H_2O)_n^-$ generated by the ion source in our apparatus. A series of $O_2^-(H_2O)_n$ peaks is seen at low mass; amu atomic mass units.

Figure 2:

(A) A schematic illustration of the solvation and evaporative dissociation exhibited in the hydrated electron clusters. The upward arrow represents the excitation to the *p*-state. The relaxation and dissociation pathways are depicted and labeled by their characteristic times as follows: τ_p; solvation in *p*-state; τ_{ic}, internal conversion; τ_s, solvation in *s*-state; τ_r, relaxation and evaporation; $h\nu$, photon energy. **(B)** Probing of different transient states of the solvated electron by energy and time resolution. Left: An energy-level diagram illustrating the changes in PE distribution originating from anion populations with different electronic and solvation energies. The upward arrows indicate the 400-nm probe pulse that detached the electron, and the downward arrows correspond to the kinetic energy of the detached electron (the eKE). Right: The resulting PE spectra are plotted together on a common energy axis, with *a*, *b*, and *c* indicating points with differing sensitivities to the location of the transient state. The distribution shown is for a moderate weakening of the force constant and displacement of minimum position between the anion and the neutral potentials, as confirmed by Franck-Condon calculation. Asterisk indicates an excited electronic state.

Figure 3:

(A) Top: PE spectrum of $(H_2O)_{35}^-$ obtained by irradiation with the 400-nm pulse only. Bottom: Time-dependent PE difference spectra at several time delays of the 400-nm probe pulse relative to the 800-nm excitation pulse. Each spectrum was constructed by subtracting the reference at 100 ps from the PE spectrum at the time specified. Regions *a*, *b*, and *c* indicate the energy windows of interest. **(B)** Three-dimensional representation of the time-dependent PE spectra. The intensity trends in regions *a*, *b*, and *c* are indicated by yellow, red, and blue ribbons. **(C)** Femtosecond transients of $(H_2O)_{30}^-$ and $(H_2O)_{35}^-$ obtained by integration of the three different gated regions (*a*, *b*, and *c*) as a function of delay time. The transients of region *b* for $(D_2O)_{30}^-$ and $(D_2O)_{35}^-$ are also shown.

Figure 4:

(A) Femtosecond transients of $(H_2O)_n^-$ (where n = 15, 20, 25, 30, or 35) obtained by integration of the PE signals in region *b*. The short- and long-range scans are shown in the left and right columns, respectively. **(B)** Time constants τ_s (squares) and τ_r (circles) versus cluster size n. The solid curves indicate the observed trends. **(C)** Observed relaxation rate $1/\tau_r$ (circles) and the scaled RRKM rates for the hydrogen-bond breakage $1/\tau_{evp}$ (triangles). The RRKM rate is scaled by 11,000 to match the observed rate for n = 35. The solid curves indicate the observed trend, and the dashed curve indicates the theoretical trend.

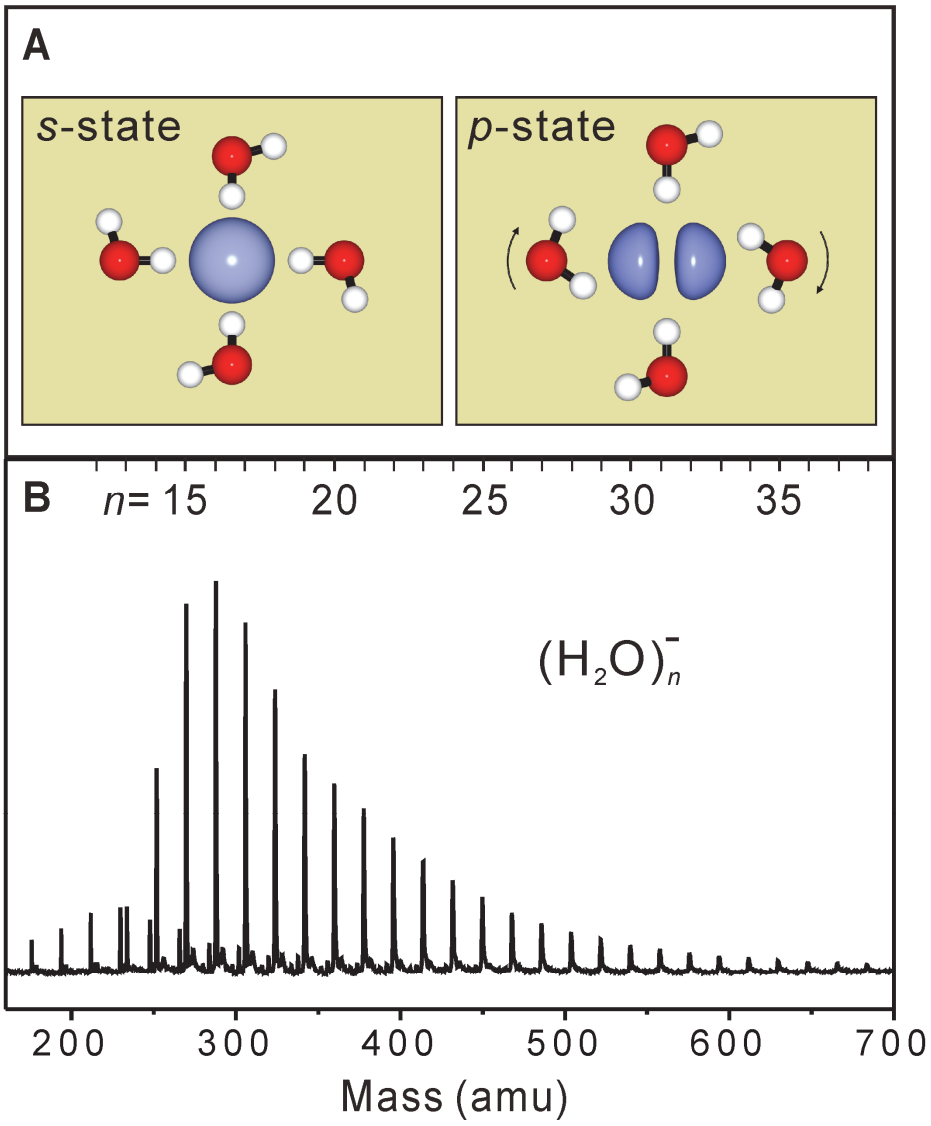
A
s-state
p-state
B
n= 15
20
25
30
35
(H2O)n-
200
300
400
500
600
700
Mass (amu)

\

Figure 3.1

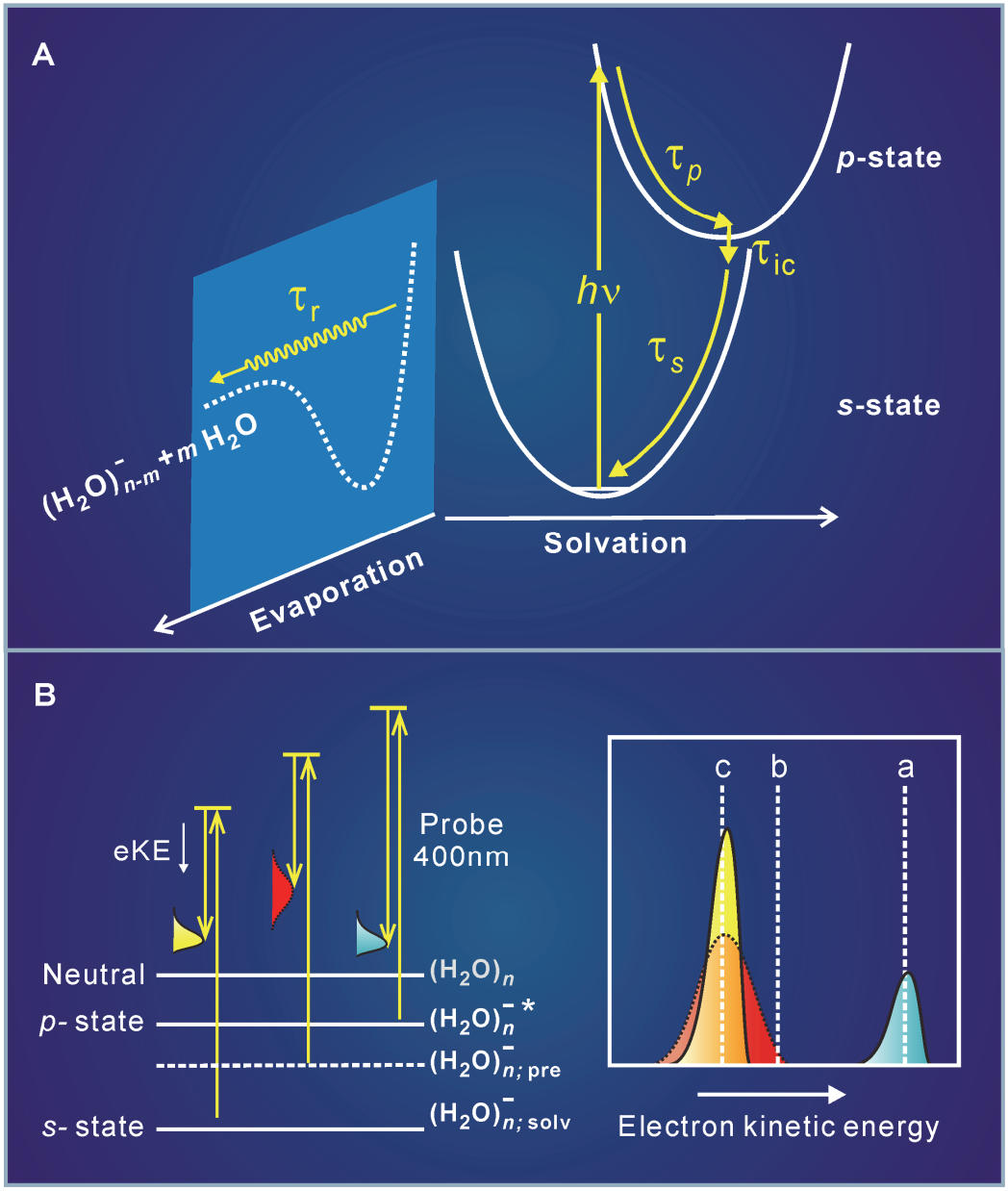
A
τ_p
p-state
τ_{ic}
$h\nu$
τ_s
s-state
τ_r
$(H_2O)^-_{n-m}+m\ H_2O$
Solvation
Evaporation
B
eKE
Probe
400nm
Neutral
$(H_2O)_n$
p- state
$(H_2O)^{-*}_n$
$(H_2O)^-_{n;\ pre}$
s- state
$(H_2O)^-_{n;\ solv}$
c
b
a
Electron kinetic energy

`Figure 3.2

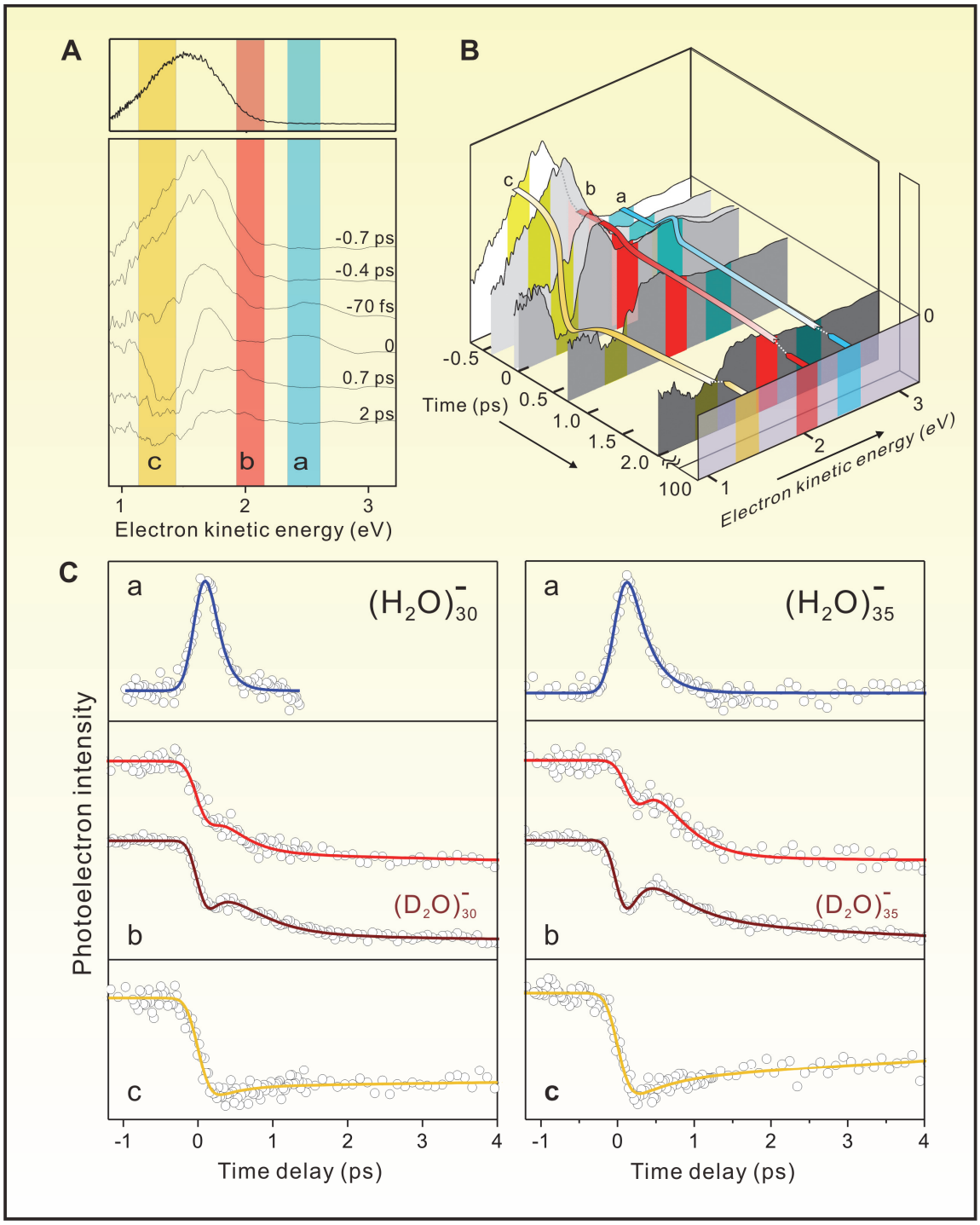
A
-0.7 ps
-0.4 ps
-70 fs
0
0.7 ps
2 ps
c
b
a
1
2
3
Electron kinetic energy (eV)
B
c
b
a
-0.5
0
0.5
1.0
1.5
2.0
100
Time (ps)
0
1
2
3
Electron kinetic energy (eV)
C
a
$(H_2O)^-_{30}$
$(H_2O)^-_{35}$
Photoelectron intensity
$(D_2O)^-_{30}$
$(D_2O)^-_{35}$
b
c
-1
0
1
2
3
4
Time delay (ps)

Figure 3.3

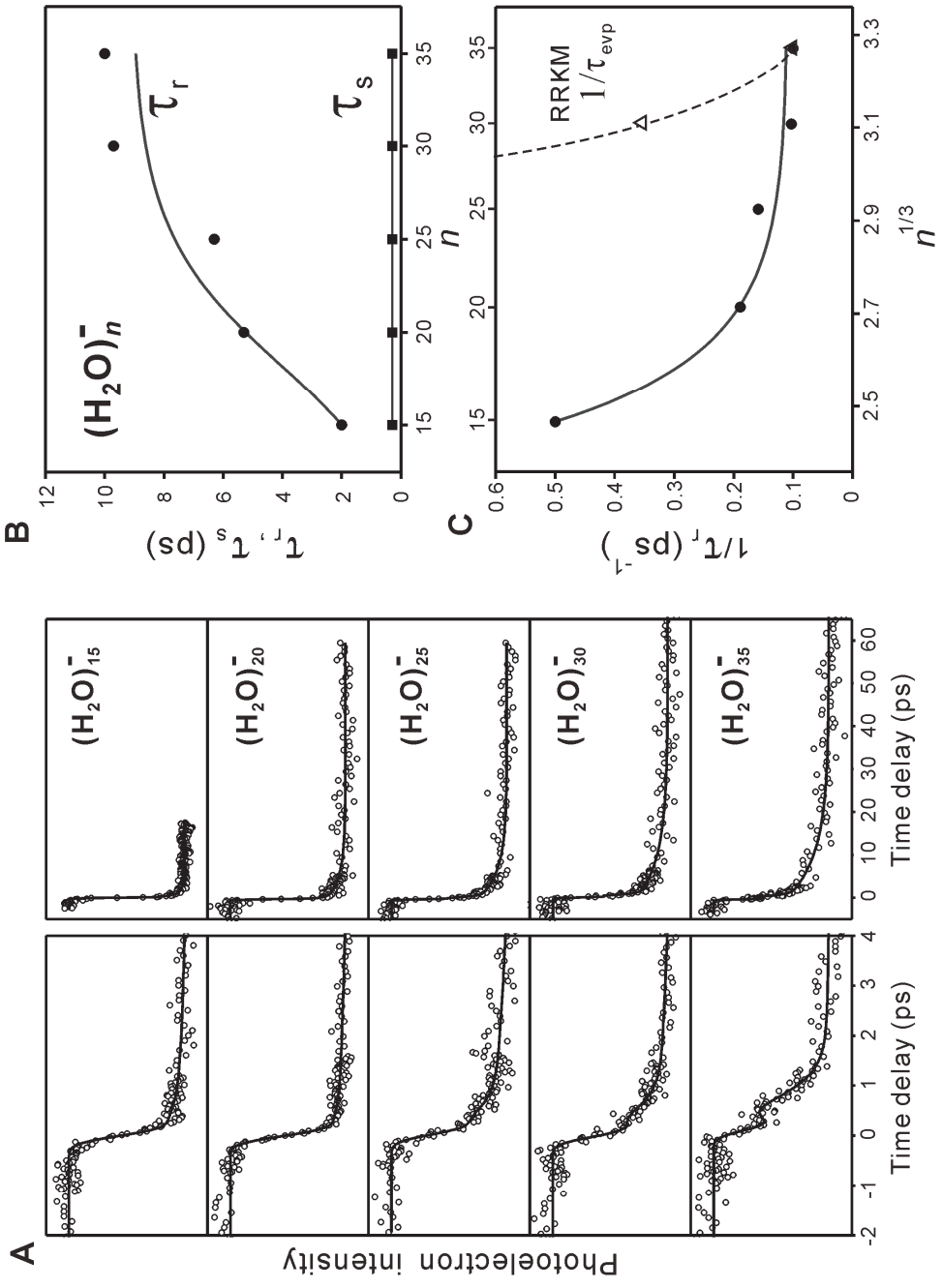
A
Photoelectron intensity
$(H_2O)^-_{15}$
$(H_2O)^-_{20}$
$(H_2O)^-_{25}$
$(H_2O)^-_{30}$
$(H_2O)^-_{35}$
Time delay (ps)
Time delay (ps)
B
$(H_2O)^-_n$
τ_r
τ_s
τ_r, τ_s (ps)
n
C
RRKM
$1/\tau_{evp}$
$1/\tau_r$ (ps^{-1})
$n^{1/3}$

Figure 3.4

CHAPTER 4.

Dynamics of Electron in Ammonia Cages:

The Discovery System of Solvation†

†adapted from Lee, I. R.; Lee, W.; Zewail, A. H. *ChemPhysChem* **2008**, *9*, 83.

Abstract

Two centuries ago solvated electrons were discovered in liquid ammonia and a century later the concept of the solvent cage was introduced. Here, we report real time study of the dynamics of size-selected clusters, n = 20 to 60, of electrons in ammonia, and, for comparison, that of electrons in water cages. Unlike the water case, the observed dynamics for ammonia indicates the formation, through a 100-femtosecond temperature jump, of a solvent collective motion in a 500-fs relaxation process. The agreement of the experimental results — obtained for a well-defined n, gated electron kinetic energy, and time delay — with MD theory suggests the critical and different role of the kinetic energy and the librational motions involved in solvation.

4.1. Introduction

The discovery in 1808 by Humphry Davy [1] that alkali metals dissolved in liquid ammonia give rise to a deep-blue colored solution has generated a wide range of research addressing the nature of solvated electrons, that are important in many research fields.[2,3] After the first publication by Weyl,[4] it was later hypothesized [5] that the color change is due to the absorption of electrons that are trapped in cavities created by solvent molecules. Theoretical considerations by Ogg [6] supported this hypothesis and suggested that the individual electrons are self-trapped, or caged, in the solvent cavity, hence the "solvated electron." He also pointed out that the ground state of a solvated electron is similar to the *s*-orbital of a hydrogen atom and the absorption of an infrared photon promotes the electron to the excited state, which is similar to a *p*-orbital.

Central to the solvation problem are questions that relate to the nature of the cavity structure and dynamics of electron-solvent interactions. Microscopic clusters are ideal structures for the investigation of solvation dynamics at the molecular scale.[7-10] They provide the capability of preparing finite-sized clusters for possibly emulating the core cavity and the possibility for following trends as the cluster size reaches the so-called bulk-type behavior. Clusters of solvated electrons in water are a prototype example of such studies using infrared [11] and photoelectron (PE) spectroscopy.[12-14] These studies are unique specially for comparison with the theoretical findings [15,16] and with studies made in bulk water; see reference [14] for discussion.

Negatively charged water and ammonia clusters were first observed by Haberland *et al*.[17,18] and studied using mass spectrometry.[17-20] Bowen and coworkers,[21] in their study using PE spectroscopy, showed a new range of cluster size, n = 41–1100, and,

as discussed below, indicated their embryonic relationship to solvated electrons, especially as n increases. Neumark and his coworkers,[22] for the $I^-(NH_3)_n$, with n = 4 - 15, system were able to monitor the dynamics following the charge transfer to the solvent. In liquids, the only study we are aware of is that reported recently by Vöhringer and co-workers.[23] On the theoretical side, the central issue of electron localization has been addressed by Barnett *et al.* [24-26], while MD simulations by Klein and coworkers [27-30] have elucidated the timescales of electron dynamics. Electron localization in an internal state occurs for $n \geq 32$, and in contrast to the water case this internal localization in ammonia is not preceded by a stable well-bound surface state for smaller cluster sizes, due to the nature of electron-molecule and intermolecular interactions.[24,25] The study of dynamics of such cluster cages is challenging due to the exceptional sensitivity required to carry out PE detection on the ultrashort timescale in this system.

Here, we report the study of solvation dynamics of electrons made in finite-sized clusters of ammonia with n = 20 to 60. Both the steady-state and time-resolved PE spectra are obtained, thus resolving the elementary dynamics involved in solvation. The excitation with femtosecond near-infrared pulses and the probing with UV femtosecond pulses, at fixed time delays and gated kinetic energies of the electron, provide the timescale of the conversion to the ground *s*-state and the subsequent ground-state dynamics evidenced in a highly damped oscillation. Significantly, the temporal behavior elucidates the predicted theoretical change of kinetic energy with time,[30] and is on a timescale significantly longer than that of the dissipative dynamics observed in the bulk liquid.[23] The results reported follow the linear dependence for electron binding energy with cavity radius ($n^{-1/3}$), with molecular size n = 20–60, giving the correct slope, in a

dielectric solvation model, and the binding energy for bulk media. For lower *n* clusters, the PE spectra have several peaks, but for larger *n* only one peak is observed, and we studied the temporal behavior for both ranges.

The concept of the experiment is illustrated schematically in Fig. 4.1. Briefly, the size-selected clusters were produced by attaching an electron to a beam of ammonia molecules and then selecting the desired cluster in a mass spectrometer. The electron was promoted from the *s*-state to the *p*-state by absorption of an 840-nm pulse. This absorption is followed by a delayed 420-nm probe pulse for photodetaching the electron. By gating the electron kinetic energy (eKE) at different time delays between the two pulses, we can follow the dynamics for a selected cluster size, in the range of *n* shown in Fig. 4.1. As discussed below and elsewhere,[14] because of Franck-Condon consideration, the use of kinetic energy gating is essential for the identification of dynamics on *s*- or *p*-state.

4.2. Results and Disscussion

The cluster distribution obtained here (Fig. 4.1) shows that the lowest *n* value is 13, compared to 30 [17,18] and 41,[21] and that the distribution is more shifted toward the smaller size clusters. This shifting originates from our utilization of a high-pressure nozzle, which is known to provide very efficient cooling. As mentioned above, theoretical studies predict that, unlike the water system, in ammonia clusters the electron is internally localized with no binding when $n < 32$;[24,25] at low temperatures (90K) smaller clusters may form.[31] The extent of localization in small water clusters has been the subject of recent experimental investigations.[11,32] Thus, it is important to investigate the

dynamics in clusters with at least 30 solvent molecules, and to compare with those at lower n, as discussed below.

The steady-state PE spectra are shown in Fig. 4.2A for different n. They were recorded using the 420-nm excitation and calibrated against the PE spectrum of O_2^-.[33] Using a dielectric continuum model,[21,25,34] where the molecular cluster is described by a dielectric cavity of radius $R = r_s\, n^{-1/3}$ (r_s is the mean radius of the molecular constituent), gives $\mathrm{VDE}(R) = \mathrm{VDE}(\infty) + B\, n^{-1/3}$, where in the plot of VDE against $n^{-1/3}$ the intercept represents the value of VDE in the bulk and the slope B is determined by the effective radius of a single solvent molecule and the optical and static dielectric constants. The peak positions marked in the PE spectra of Fig. 4.2A when plotted against $n^{-1/3}$ give the linear relationship shown in Fig. 4.2B. The slope and intercept of the linear plot agree well with those reported by the Bowen group.[21] The intercept is 1.5 eV consistent with the value of 1.27–1.45 eV obtained by photoelectric electron threshold measurement in bulk liquid.[35,36] A slope of 3.0 eV is also close to that of 3.08 eV obtained using the parameters of B for ammonia.[21]

For $(NH_3)_{50}^-$, the vertical detachment energy (VDE) measured in this work is 0.62 eV, which is consistent with Bowen's reported value of 0.59 ±0.1 eV [21]. A single peak was observed for the large size clusters, but for the smaller clusters some structure in the PE spectra is evident. This suggests that the peak for $n \geq 50$ follows the behavior of internally solvated electron.[21] The peaks at lower binding energy for $n \leq 30$ reflect similar behavior, and the others at higher binding energies may originate from different structural isomers.[32] Given these results we now examine the dynamics for different cluster sizes.

Time-resolved PE spectra were recorded, and for all clusters there is no

observable change beyond the time delay of 1.8 ps. We examined the difference spectra, obtained by subtracting the PE signal of 1.8 ps from that before time zero (–0.8 ps), and compared to the steady-state spectra, as shown in Fig. 4.2C. The nearly perfect overlap of these two spectra suggests that there is no significant "product" formation after the system reaches steady state at 1.8 ps; only depletion by the pump photon is evident. With these results, we conclude that isomerization and fragmentation of clusters on the ps timescale are insignificant.

The PE spectra collected at 400 fs and 800 fs are displayed in Fig. 4.3A and 4.3B, respectively. The spectra were calibrated, by subtraction, against the one obtained at 1.8 ps. As shown, the PE spectra display either an increase or a decrease but in different regions of the electron kinetic energy. Integrating the yellow-shaded area in Fig. 4.3A gives the transient presented in Fig. 4.4B and 4.4C for n = 20 and 50, respectively. A femtosecond depletion of PE signal at time zero is observed, but this depletion is followed by a transient response. The depletion (step function) is due to the depopulation by the fs pump pulse. Fig. 4.4A presents the residual signal, showing a highly damped oscillation with a half-period of 800 fs and damping time constant of 0.5 ps. We repeated the experiments for the other clusters studied and found, within our signal to noise, no significant change of the transient behavior.

Comparing the behavior of the PE spectra to that found in water, shown in Fig. 4.3C and 4.3D, indicates major differences. For water, the increase and decrease, with respect to the steady-state PE spectra (the zero line), change in concert with time. For ammonia, only the increase peak becomes smaller with time, while no significant change can be visualized for the small decrease peak within the signal level shown. In other words, the

difference spectra for ammonia behave in an opposite way from that of water and show no signature of recovery of the cold state, suggesting that the relaxation model of water is strictly inapplicable. However, for both, the *p*-state converts to the ground state in ~150 fs, consistent with the less than 100-fs value reported in liquid ammonia [23] and the ~150 fs in water clusters.[12-14] For ammonia, the lifetime was obtained from the transients at PE energy of ~3.4 eV (i.e., much higher energy) for all clusters; we observed only a peak located at $t = 0$. Following excitation, and at $t = 0$, the UV fs pulse probes the *p*-state population resulting in the PE energy being much higher than that of the *s*-state.

From the above results and with the help of Fig. 4.1(inset) we can describe the elementary processes involved. The absorption of a near IR photon promotes the electron from the *s*-state to the *p*-state. This is followed by an ultrafast internal conversion that results in the formation of a coherent wavepacket on the *s*-state. Because of Franck–Condon selectivity in probing to the state of the neutral species, coherent motions can be detected. The contrast with hydrated electron dynamics is evidenced in the following observations. As shown in Fig. 4.3, for the water system, at early time, we observed the depletion of population of the "cold" state and the rise of the "hot" state. With time, the cold state increases in population and the hot one decreases, entirely consistent with irreversible relaxation dynamics, and with consideration of Franck-Condon probing: the cold state probing is at lower PE energy than the hot state (see Fig. 4.3C). We note that for a given cluster, the total energy is conserved in a microcanonical system but energy relaxation occurs because the solvent defines the bath modes in the energy redistribution.

For the ammonia system, although the observed temporal response can be fit to the consecutive reaction model described above and in ref. 14 with rise/decay time

constants of 50/200 fs, the situation is different due to the following. As shown in Fig. 4.3A at t = 0.4 ps, the apparent high-energy peak corresponds to a decrease while the apparent lower energy one corresponds to an increase, which is inconsistent with the picture described above. Moreover, if there is significant cold-state population we should be able to detect it at our probe wavelength as evidenced in the steady-state PE spectrum shown. Accordingly, the major peak in Fig. 4.3A is due to the hot *s*-population being in a coherent state; with a motion away from the Franck–Condon region the signal decreases and complete relaxation to the cold state is not observed on the timescale studied. The relatively small peak at ~2.7 eV (and possibly ~2.35 eV) is consistent with a limited spreading of the wave packet following the initial preparation; spreading in configuration space corresponds to narrowing in energy space. Consistent with this picture is the relative decrease in the amplitude of the transient as the cluster increases in size (larger number of modes), even though the *p*-state population continues to increase for larger *n* clusters. This increase in the *p*-state population is based on the rise in intensity of the PE signal from the electronic excited *p*-state at ~3.4 eV (not shown).

Theoretical molecular dynamics (MD) calculations by Klein and coworkers [27-30] have addressed the problem of electron wave packets in pseudoparticles (to mimic liquid ammonia), and these studies are relevant to compare with our results. In their approach they separate the time scales of the solvent motion and certain classical degrees of freedom that describe the *s*-state of the electron. In this separation, the role of solvent libration motions and longer time phonon-like oscillations is highlighted. An important point was made in this study by Klein and co-workers: the quantum kinetic energy is only weakly coupled to the solvent librations, which occur on the time scale of tens of

femtoseconds. The kinetic energy is thus a better probe of the longer-time dynamics. In the study presented here the cavity is made of a rigid ("solid-like") cluster structure (temperature is below 200 K [21]) and its probing provides the longer-time dynamics with the high-frequency libration motion being suppressed.

In Fig. 4.4D and 4.4E, we compare the calculated MD for the quantum kinetic energy change with time (Fig. 4.4E). The reported damped oscillation with a period of τ_p^{KE} of ~0.8 ps is remarkably on a much longer time scale than that of the librational and inertial motions.[37,38] A period in the kinetic energy is half that of a harmonic wave packet motion, and for a harmonic potential the period is independent of the internal energy. The agreement with the damped profile observed experimentally in the PE probing is surprisingly good, given the above discussed considerations.

The observed behavior in the water cluster system and in liquid ammonia can now be rationalized. For water clusters, the internal temperature ("liquid-like") and the unique mobility of the hydrogen-bond network makes dominance solvation by the libration motions. Indeed, fast damped oscillatory motion was observed in liquid water (850 cm^{-1}) and assigned to solvent libration motion.[39,40] For electrons in liquid ammonia,[23] the relaxation is ultrafast and was found to occur in 150 fs, following the internal conversion to the *s*-state. Rossky and co-workers [16] have performed an instant normal mode analysis on solvated electrons and suggested two types of motion: a lower frequency motion (0-400 cm^{-1}), which is mainly due to diffusion (translational) motion, and another, the intermediate frequency (400–1200 cm^{-1}) range, which is dominated by the contribution of librational motion. On our time scale, if present, these will dominate in the range of 30 to 80 fs.

The similarity of the cluster work reported here to the study in the liquid state of ammonia [23] is in the *T*-jump achieved on the ground *s*-state. For both cases, because the $p \rightarrow s$ conversion takes place in less than 100 fs, the population prepared is in a nonequilibrium state, which can be ascribed to an instant rise in temperature. Based on the change in density, Lindner *et al.* [23] estimated a solvent shell increase of 1 Å at the excitation used (1.4 μm). It is interesting that in our case an average speed of 1 Å ps^{-1} implies an angstrom expansion during the period. The self-diffusion coefficient in liquid ammonia is 1 $Å^2$/ps,[41] implying a length scale of angstrom(s) during a picosecond dynamics. Finally, the electron diffusion of a Gaussian packet was calculated [30] to be 0.6 $Å^2$ ps^{-1} (in liquid it is 1.9 $Å^2$ ps^{-1} [42]). Thus, on the time scale of our experiments, the average length scale maintained is < 1 Å. Coherence in solvent cages is a reflection of the strength of solvent-solvent interactions, which control the degree of rigidity at finite temperatures.[43]

4.3. Conclusion

Much of the progress made in understanding solvated electrons in ammonia has come from studies of bulk properties, and more recently from studies of energetic with cluster size dependence for convergence to liquid state properties. The nature of the cage, since its proposal a century ago, was first elucidated theoretically by Jortner,[44] Mott,[45] and others, but the dynamics at the molecular level has not been directly observed. In this work, we report our first contribution to real time dynamics in solvent structures with up to 60 ammonia molecules, and similarly for water. These studies of dynamics, which turned out — because of the required high sensitivity — to be extremely challenging for

the ammonia system, elucidate the different time scales involved in the relaxation of the cage to the ground state and the wave packet motion of electron-solvent cages. The induced *s* to *p* polarization on the femtosecond time scale leads to expansion of the cage, which may be related to Bjerrum defects due to changes in ammonia bonding around the electron.[45] The different solvent motions for electron interaction with water (libration) and ammonia (phonon-like) and the extent of cage rigidity determine the observed difference in solvation dynamics.

4.4. Experimental

The experiments were carried out in our apparatus, which integrates a femtosecond laser system with a molecular beam machine equipped for electron attachment, mass selection, and laser pulse interrogation. Details are given in reference 47. Briefly, The laser pulses (110 fs) were generated from a Ti:sapphire oscillator and amplified by a regenerative multipass amplifier. The 840-nm laser output was split into two beams. One beam (~4 mJ per pulse) was used as the pump pulse for excitation. The other one was frequency doubled by a BBO crystal to generate the 420-nm laser pulses (~0.6 mJ per pulse). The 420-nm laser pulses, delayed in time, were used as a probe to photodetach the electron. The polarization of the pump pulse was set at the magic angle (54.7°) with respect to the probe pulse in order to suppress the influence of anisotropy in the rotational motion. The electrons were collected by a magnetic-bottle PE spectrometer and the PE spectra were recorded with an oscilloscope and transferred to a computer for analysis.

The ammoniated electron clusters were made using an Even-Lavie high pressure

pulsed nozzle.[48] Diluted ammonia anhydrous (~0.5% in helium) at the total pressure of ~50 kPa was expanded into the vacuum chamber through the pulsed nozzle at 20 Hz repetition rate, and then intercepted immediately with a continuous electron impact source (~150 eV). The gas mixture was then passed through a skimmer with a 6-mm diameter orifice and was directed into the time-of-flight mass spectrometer. The application of properly timed high-voltage pulse accelerated the clusters into the field-free time-of-flight region where the desired size was intercepted with the femtosecond laser pulses.

References

(1) Edwards, P. P. *Adv. Inorg. Chem.* **1982**, *25*, 135.

(2) Edwards, P. P. *Nature* **1988**, *331*, 564.

(3) Edwards, P. P.; Rao, C. N. R.; Kumar, N.; Alexandrov, A. S. *ChemPhysChem* **2006**, *7*, 2015.

(4) Weyl, W. *Ann. Phys.* **1863**, *197*, 601.

(5) Kraus, C. A. *J. Am. Chem. Soc.* **1908**, *30*, 1323.

(6) Ogg, R. A. *Phys. Rev.* **1946**, *69*, 668.

(7) Johnson, M. A.; Lineberger, W. C. In *Technique for the Study of Ion-Molecule Reactions*; Farrar, J. M., Saunders Jr., W. H., Eds.; Wiley-interscience: New York, 1988; Vol. 20, p 591.

(8) Castleman, A. W.; Bowen, K. H. *J. Phys. Chem.* **1996**, *100*, 12911.

(9) Neumark, D. M. *J. Chem. Phys.* **2006**, *125*.

(10) Cheng, P. Y.; Baskin, J. S.; Zewail, A. H. *Proc. Natl. Acad. Sci. USA.* **2006**, *103*, 10570; see also commantary Castleman Jr., A. W.; Jena, P.. *Natl. Acad. Sci. USA.* **2006**, *103*, 10552.

(11) Hammer, N. I.; Shin, J. W.; Headrick, J. M.; Diken, E. G.; Roscioli, J. R.; Weddle, G. H.; Johnson, M. A. *Science* **2004**, *306*, 675.

(12) Bragg, A. E.; Verlet, J. R. R.; Kammrath, A.; Cheshnovsky, O.; Neumark, D. M. *Science* **2004**, *306*, 669.

(13) Bragg, A. E.; Verlet, J. R. R.; Kammrath, A.; Cheshnovsky, O.; Neumark, D. M. *J. Am. Chem. Soc.* **2005**, *127*, 15283.

(14) Paik, D. H.; Lee, I. R.; Yang, D. S.; Baskin, J. S.; Zewail, A. H. *Science* **2004**, *306*, 672.

(15) Jordan, K. D. *Science* **2004**, *306*, 618.

(16) Yang, C. Y.; Wong, K. F.; Skaf, M. S.; Rossky, P. J. *J. Chem. Phys.* **2001**, *114*, 3598.

(17) Haberland, H.; Schindler, H. G.; Worsnop, D. R. *Ber. Bunsen. Phys. Chem.* **1984**, *88*, 270.

(18) Haberland, H.; Ludewigt, C.; Schindler, H. G.; Worsnop, D. R. *Surf. Sci.* **1985**, *156*, 157.

(19) Kondow, T. *Buturi* **1989**, *44*, 486.

(20) Kondow, T.; Nagata, T.; Kuchitsu, K. *Z. Phys. D: At., Mol. Clusters* **1989**, *12*, 291.

(21) Sarkas, H. W.; Arnold, S. T.; Eaton, J. G.; Lee, G. H.; Bowen, K. H. *J. Chem. Phys.* **2002**, *116*, 5731.

(22) Frischkorn, C.; Zanni, M. T.; Davis, A. V.; Neumark, D. M. *Faraday Discuss.* **2000**, 49.

(23) Lindner, J.; Unterreiner, A. N.; Vöhringer, P. *ChemPhysChem* **2006**, *7*, 363.

(24) Barnett, R. N.; Landman, U.; Cleveland, C. L.; Kestner, N. R.; Jortner, J. *Chem. Phys. Lett.* **1988**, *148*, 249.

(25) Barnett, R. N.; Landman, U.; Cleveland, C. L.; Kestner, N. R.; Jortner, J. *J. Chem. Phys.* **1988**, *88*, 6670.

(26) Barnett, R. N.; Landman, U.; Nitzan, A. *Phys. Rev. Lett.* **1989**, *62*, 106.

(27) Sprik, M.; Impey, R. W.; Klein, M. L. *J. Chem. Phys.* **1985**, *83*, 5802.

(28) Marchi, M.; Sprik, M.; Klein, M. L. *Faraday Discuss. Chem. Soc.* **1988**, 373.

(29) Sprik, M.; Klein, M. L. *J. Chem. Phys.* **1988**, *89*, 1592.; see also erratum, Sprik, M.; Klein, M. L. *J. Chem. Phys.* **1989**, *91*, 7614.

(30) Sprik, M.; Klein, M. L. *J. Chem. Phys.* **1989**, *91*, 5665.

(31) Marchi, M.; Sprik, M.; Klein, M. L. *J. Chem. Phys.* **1988**, *89*, 4918.

(32) Verlet, J. R. R.; Bragg, A. E.; Kammrath, A.; Cheshnovsky, O.; Neumark, D. M. *Science* **2005**, *307*, 93.

(33) Travers, M. J.; Cowles, D. C.; Ellison, G. B. *Chem. Phys. Lett.* **1989**, *164*, 449.

(34) Barnett, R. N.; Landman, U.; Cleveland, C. L.; Jortner, J. *Chem. Phys. Lett.* **1988**, *145*, 382.

(35) Häsing, J. *Ann. Phys.(Leipzig)* **1940**, *37*, 509.

(36) Aulich, H.; Baron, B.; Delahay, P.; Lugo, R. *J. Chem. Phys.* **1973**, *58*, 4439.

(37) Stratt, R. M.; Maroncelli, M. *J. Chem. Phys.* **1996**, *100*, 12981.

(38) Pal, S. K.; Zewail, A. H. *Chem. Rev.* **2004**, *104*, 2099 and reference therein.

(39) Emde, M. F.; Baltuŝka, A.; Kummrow, A.; Pshenichnikov, M. S.; Wiersma, D. A. *Phys. Rev. Lett.* **1998**, *80*, 4645.

(40) Kummrow, A.; Emde, M. F.; Baltuska, A.; Pshenichnikov, M. S.; Wiersma, D. A. *J. Phys. Chem. A* **1998**, *102*, 4172.

(41) O'reilly, D. E.; Peterson, E. M.; Scheie, C. E. *J. Chem. Phys.* **1973**, *58*, 4072.

(42) *Kinetics of Nonhomogeneous Processes*; Freeman, G. R., Ed.; Wiley: New York, 1987.

(43) Liu, Q. L.; Wang, J. K.; Zewail, A. H. *Nature* **1993**, *364*, 427.

(44) Jortner, J. *J. Chem. Phys.* **1959**, *30*, 839.

(45) Catterall, R.; Mott, N. F. *Adv. Phys.* **1969**, *18*, 665; see also ref. 46.

(46) Cohen, M. H.; Thompson, J. C. *Adv. Phys.* **1968**, *17*, 857.

(47) Paik, D. H.; Kim, N. J.; Zewail, A. H. *J. Chem. Phys.* **2003**, *118*, 6923.

(48) Even, U.; Jortner, J.; Noy, D.; Lavie, N.; Cossart-Magos, C. *J. Chem. Phys.* **2000**, *112*, 8068.

(49) This work was financially supported by the National Science Foundation and the Air Force Office of Scientific Research.

Figure Captions

Figure 4.1:

Experimental mass spectrum of electrons in ammonia cages (clusters) generated in our apparatus. The mass axis gives the indicated solvent cluster size with number n. In the inset, the conceptual scheme of the experimental methodology is presented.

Figure 4.2:

Photoelectron (PE) spectra, detachment energies, and temporal changes for size-selected clusters. **(A)** Steady-state PE spectra for n = 20, 30, 40, 50, or 60, obtained by femtosecond-pulse irradiation at 420 nm. The electron kinetic energy (eKE) and electron binding energy (eBE) are given in electron volts (eV). **(B)** The plot of the vertical detachment energy (VDE), obtained from the marked positions in Figure 4.2A against $n^{-1/3}$ gives a linear relationship. Least-squares fitting (red line) of the data provides the slope and intercept values indicated. **(C)** Comparison of the PE difference signal [S(−0.8 ps)−S(1.8 ps); red] and the signal obtained at steady-state (black). The PE spectra are for n = 20 and 50. Spectra are scaled for careful comparison.

Figure 4.3:

Femtosecond-resolved transient photoelectron spectra of ammonia (n = 20) and water (n = 35) clusters. For ammonia, the yellow-shaded area indicates the energy window of interest; for steady-state PE spetra, see Figure 4.2A. For (**A**) and (**B**), the spectra were integrated over ±100 fs to enhance the signal-to-noise ratio. Note the change of the spectra with time. For water, the arrows represent the concerted time evolution of the population of hot and cold states, respectively. These spectra were taken in order to compare with the ammonia case for clusters of similar size.[14]

Figure 4:

Experimental femtosecond transients and theoretical molecular dynamics (MD) simulations. (**A**) Residual signal of the depletion obtained from the PE transient. (**B**) and (**C**) are transients obtained for n = 20 and 50, respectively, from the integration of the yellow-shaded area in Figure 4.3A; the red curves are the best fits. (**D**) and (**E**) are the experimental (**A**) and theoretical MD calculations. The temporal behavior is fitted (green curve) and gives $\tau_{\mathbf{p}}^{\mathbf{PE}}$ and a damping constant, $\tau_{\mathbf{d}}$. (**E**) Autocorrelation function of quantum kinetic energy, adapted from ref. 30; the oscillation period, $\tau_{\mathbf{p}}^{\mathbf{KE}}$ is taken from ref. 30, while the decay time constant, $\tau_{\mathbf{d}}$, is obtained from our fitting of their MD data

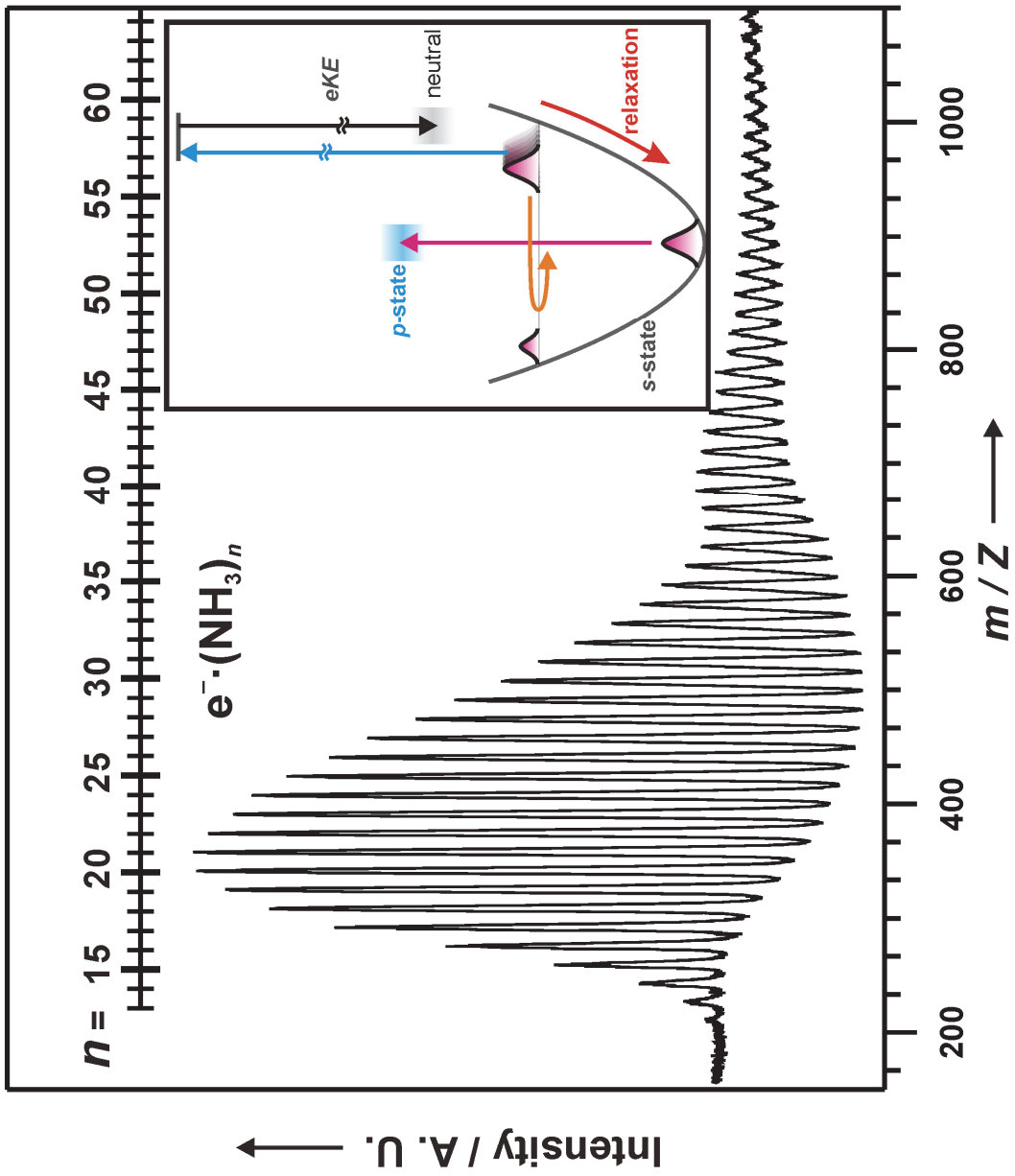
Intensity / A. U.
m / Z
200
400
600
800
1000
n = 15 20 25 30 35 40 45 50 55 60
e⁻·(NH3)n
eKE
neutral
relaxation
p-state
s-state

Figure 4.1

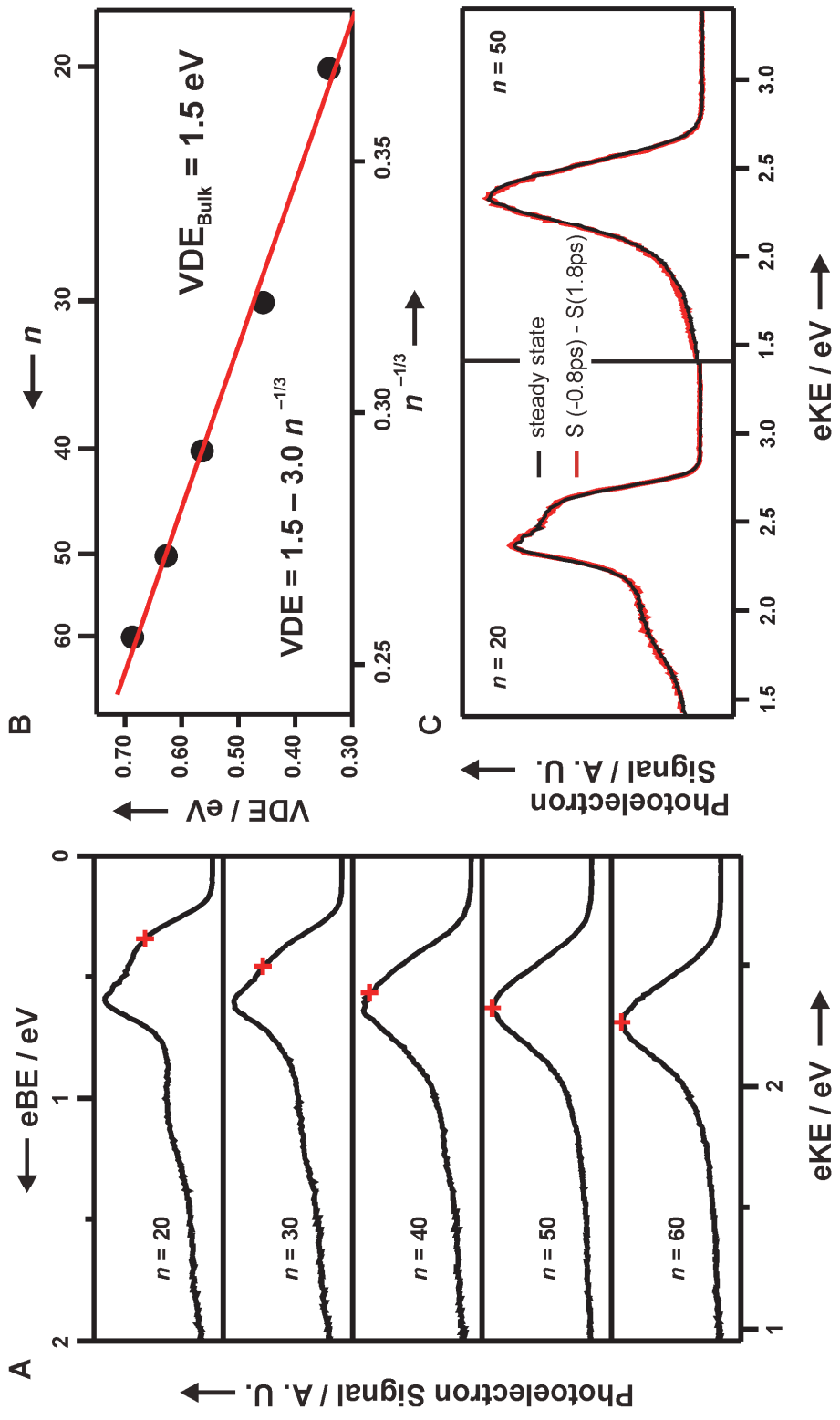
A
Photoelectron Signal / A. U.
eBE / eV
eKE / eV
n = 20
n = 30
n = 40
n = 50
n = 60
B
VDE / eV
n
VDE_Bulk = 1.5 eV
VDE = 1.5 – 3.0 n^-1/3
n^-1/3
C
Photoelectron Signal / A. U.
steady state
S (-0.8ps) - S(1.8ps)
n = 20
n = 50
eKE / eV

Figure 4.2

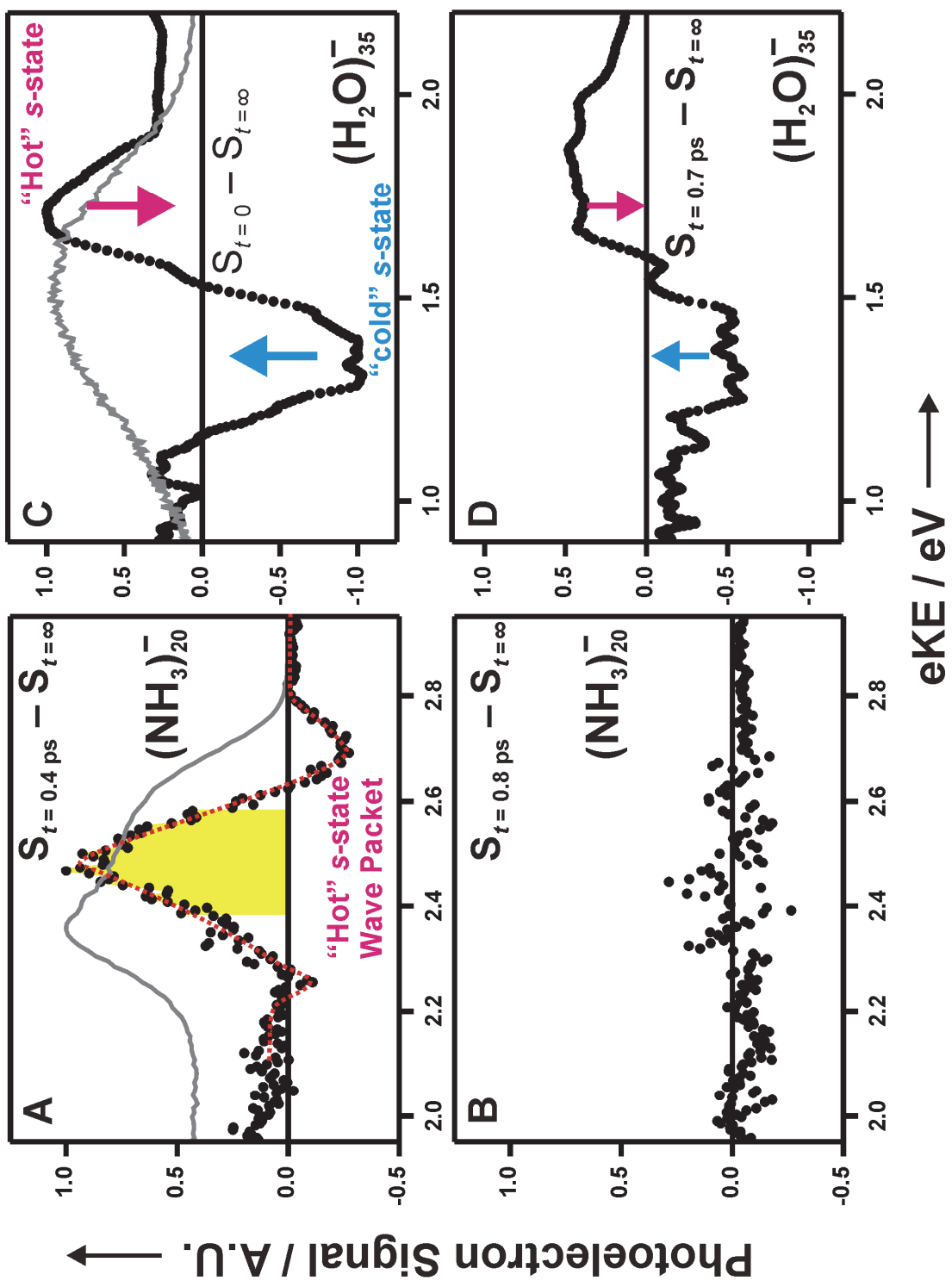
A
B
C
D
$S_{t=0.4\ ps} - S_{t=\infty}$
$(NH_3)_{20}^-$
"Hot" s-state
Wave Packet
$S_{t=0.8\ ps} - S_{t=\infty}$
$S_{t=0} - S_{t=\infty}$
"cold" s-state
$S_{t=0.7\ ps} - S_{t=\infty}$
$(H_2O)_{35}^-$
Photoelectron Signal / A.U.
eKE / eV

Figure 4.3

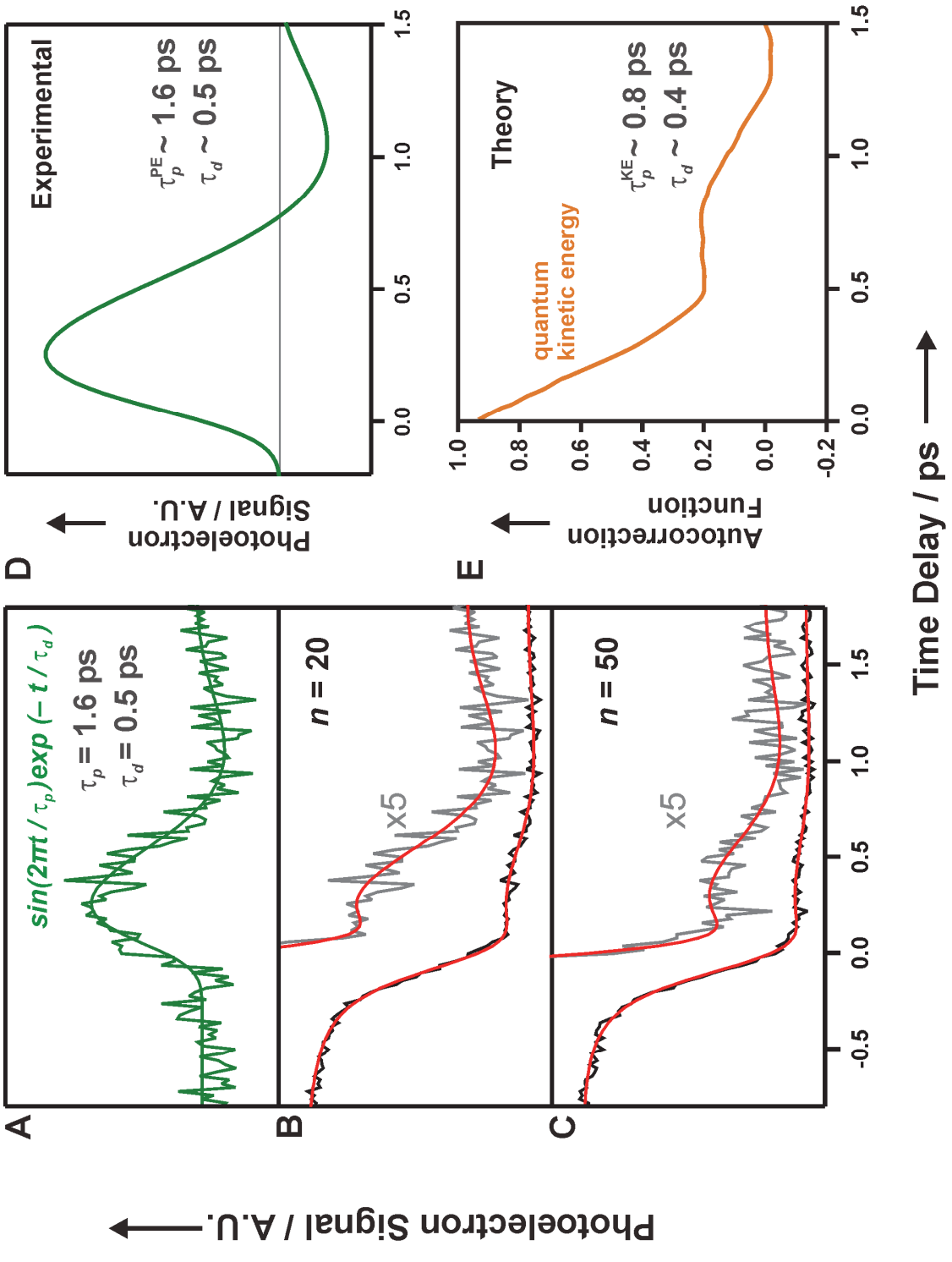
A
B
C
D
E
sin(2πt / τp)exp (– t / τd)
τp = 1.6 ps
τd = 0.5 ps
n = 20
n = 50
x5
x5
Photoelectron Signal / A.U.
Experimental
τpPE ~ 1.6 ps
τd ~ 0.5 ps
Photoelectron Signal / A.U.
Theory
quantum
kinetic energy
τpKE ~ 0.8 ps
τd ~ 0.4 ps
Autocorrection Function
Time Delay / ps

Figure 4.4

CHAPTER 5.

Primary Steps of the Photoactive Yellow Protein

Isolated Chromophore Dynamics and Protein Directed Function†

† adapted from Lee, I. R.; Lee, W.; Zewail, A. H. *Proc. Natl. Acad. Sci. U.S.A.* **2006**, *103*, 258.

Abstract

The cycle of the photoactive yellow protein (PYP) has been extensively studied, but the dynamics of the isolated chromophore responsible for transduction is unknown. Here, we present realtime observation of the dynamics of the negatively charged chromophore and detection of intermediates along the path of *trans*-to-*cis* isomerization using femtosecond mass selection/electron detachment techniques. The results show that the role of the protein environment is not in the first step of double-bond twisting (barrier crossing) but in directing efficient conversion to the *cis*-structure and in impeding radical formation within the protein.

5.1. Introduction

Photoactive yellow protein (PYP) is a water-soluble photoreceptor found in *Halorhodospira halophila* and related halophilic bacterial species.[1] The chromophore responsible for perception of light and phototactic response is a deprotonated *trans*-4-hydroxycinnamic acid (also known as *p*-coumaric acid) covalently linked to a cysteine residue of the protein via a thioester bond (Fig. 5.1). Light absorption of the PYP chromophore leads to the initiation of a complex photocycle involving several intermediates. With a variety of biophysical techniques,[2-5] it is concluded that the first intermediate (I_0) in the photocycle is formed within a few picoseconds, with the chromophore changing to the *cis* configuration, in a *trans*-to-*cis* isomerization process.[6-10] The intermediates at longer times have been trapped and identified by x-ray crystallography.[11,12]

The critical change of the chromophore in the primary process of isomerization is accompanied or followed by several other processes: proton transfer, protein conformational change, solvation, and disruption of hydrogen bonding. This complexity can be reduced if the chromophore in its true anionic, not neutral, structure can be studied free of perturbations. With model compounds, the solvent effect can be assessed by studying them in the solution phase.[13-17] However, the nature of intramolecular change and the timescales involved are still unknown. It is, therefore, desirable to study the primary isomerization dynamics of the PYP chromophore in isolation, especially in view of the fact that the mechanism for forming the first intermediate (I_0) is debatable.[2] A gas-phase spectroscopic study has already been reported,[18] but it was for the neutral molecule, not the anion structure in the protein.

In this work, we report direct observation of the dynamics of the isolated PYP anionic chromophore. To disentangle the role of protein binding and distant torsions, we preserved the central structure involved in the isomerization about the double bond but use the CH3 group for termination (see Fig. 5.1). The chromophore, hereafter called **P**, is excited with a femtosecond pulse from its ground state, the dark state in the protein, to the *trans* configuration using the mass-selected ions. For probing we use another femtosecond pulse to photodetach and resolve the photoelectrons at different kinetic energies. This resolution in time and energy provides the transient behavior of the intermediates involved. Remarkably, the **P**-chromophore shows primary step dynamics of twisting in 1 ps, which is essentially the same as that in the protein, indicating that the efficient, almost frictionless, transduction process by isomerization is central to the double bond. The meaning of pure double- vs. single-bond twisting is convoluted because of nuclear couplings and electronic/resonance delocalization (see conclusion). The role of the protein environment is primarily in directing the crossing to the ground-state *cis* structure and suppressing radical formation.

5.2. Results and Discussion

Fig. 5.2 shows the photoelectron spectra of the **P**-chromophore with and without the probe pulse. With the pump pulse alone (blue trace), a major peak was observed at ~0.2 eV (1 eV = 1.602×10^{-19} J) together with a broad and much less intense peak at ~2 eV; no signal was observed with the probe pulse alone. The sharp major peak at ~0.2 eV is identified as the photoelectron signal from single-photon excitation; its energy matches well with the difference between the photon energy of the pump pulse (3.1 eV) and the

vertical detachment energy of the anion to the radical ground state (~2.9 eV).[19] With both the probe and pump pulses overlapping at 200 fs, a new peak appears at ~0.9 eV in the electron kinetic energy, whereas the peak at ~0.2 eV is depleted (the red trace in Fig. 5.2). As shown below, these temporal changes are present because of the evolution from the *trans* to *cis* configuration with the formation of intermediates. Because of the clear separation in energy, low and high kinetic energy, it is possible to map out the dynamics of different species.

The temporal behavior at three windows of kinetic energies (**I–III** in Fig. 5.3) provides a stringent test of the nature of intermediates involved and the consistency of the rates. In Fig. 5.3, we display 15 such transients over different, short, and long timescales. Transients in the same row show temporal behaviors of a specific energy window, on different timescales, whereas those in the same column show the temporal behavior of different energy windows for a specific timescale. The clear trends in Fig. 5.3, depletion of the population in region **I**, decays (and coherence) in region **II**, and buildup and decay in region **III**, indicate that the dynamics involve three states of the chromophore: the initially launched population, the twisted intermediate, and the hot ground-state population of the *cis* form. To obtain the timescales involved and quantify the fraction of population for each structure, we invoked the following elementary steps:

$$\mathbf{P}_{\text{dark}} \xrightarrow{h\nu} \mathbf{P}^{*}_{t,e} \longrightarrow \mathbf{P}^{*}_{\theta} \longrightarrow \mathbf{P}_{c}$$

where $\mathbf{P}_{\text{dark}}$ is the structure in the ground state, $\mathbf{P}^{*}_{t,e}$ is the initially excited state, $\mathbf{P}^{*}_{\theta}$ is the twisted state, and $\mathbf{P}_{c}$ is the hot-ground state of the *cis* form. All of the transients were fit with the same parameter set in a global search. The results of the global fit are

shown as solid lines overlaid on the experimental transients in Fig. 5.3.

The agreement between the theoretical analysis and experimental results at different energies and the self-consistency among all transients are impressive and reflect the validity of the above picture with well-defined rates for the elementary steps involved. In detail, the population of the initially excited state, $\mathbf{P}^*$, bifurcates on the femtosecond timescale to produce the *trans* population (80%); the remaining fraction (20%, $\mathbf{P}_e^*$) autodetaches to form the corresponding radicals. This finding is evidenced in the decay of the population in region **II** (1 ps; 4 ps) and the recovery of population in region **I** (4 ps; 52 ps). Monitoring population in region **III**, we observed a clear buildup (1 ps) and a decay (52 ps). Accordingly, the high-energy region (**II**) results from the initial population (prompt response), and the low-energy region (**III**) results from the trapped, in a well, twisted intermediate. The isomerization by twisting occurs in 1 ps, whereas the twisted state ($\mathbf{P}_\theta^*$) decays in 52 ps. A damped coherent oscillation was observed in the decay of the population of region **II** (see Fig. 5.3), and it has a period of ~800 fs, corresponding to a vibrational frequency of ~40 cm^{-1}.

The above results are surprising for several reasons. First, isomerization time for the isolated chromophore is similar to that observed for the same chromophore in the solution phase (1.3 ps).[20,21] Second, unlike the protein case, the chromophore is free from backbone bonding and can undergo other torsions and rotations, and yet the isomerization time is similar to that of the protein (within a few picoseconds).[6-10] Third, the coherence, which reflects the involvement of low-frequency motion(s) in isomerization,[22] is preserved ongoing from the isolated molecule to the protein. For the chromophore in PYP,

these oscillations were reported to be ~50 and ~135 cm^{-1}.[23] One then must ask the following. Why is this nearly a frictionless dynamics? What is its significance to the function?

The structural change of the chromophore is a precursor to other dynamical events in the PYP function. After isomerization, protonation in the protein environment occurs, and the protein itself changes on a longer timescale. From theoretical calculations,[24,25] it was proposed that the *trans*-to-*cis* isomerization proceeds by, first, the passage through a small barrier for twisting around the double bond (coordinate θ) and then a search for a conical intersection (CI), which facilitates the internal conversion to the ground state. The same calculations [24] suggested that the protein promotes the isomerization of the chromophore by restricting the rotation of its *p*-hydroxyphenyl moiety.

Our experimental results given above indicate that the primary role of the chromophore is determined by the twisting around the central double bond (C2=C3) and that other motions involving the hydroxyphenyl or the sulfur linkage are relatively unimportant. In fact, careful examination of the trajectories in the molecular dynamics simulations [24] indicate that the C2=C3 motion occurs on the timescale of ~1 ps, significantly faster (factor of two) than the other bonds involved in the linkage to the protein. Thus, the chromophore twisting is nearly insensitive to the protein environment in that it does not occur by a typical barrier-crossing process with multiple "collisions" to cross over to the *cis* configuration. The ultrafast nature of the reaction ensures the high efficiency of the initial "molecular impulse," which then triggers subsequent changes in the protein.

This initial step is facilitated by the electronic excitation, which weakens the double bond (more antibonding character) and by (coherent) low-frequency motion(s) that brings the atoms into the needed configuration for efficient twisting.

The barrier height estimates range from 5 to 20 kcal/mol, and the effect of the environment on the height is debatable.[24,25] It is clear that at our wavelength the system is above the barrier energy. The degree of frictionless crossing is also clear from comparison with results for the same chromophore in solution. Upon varying the viscosity from 1 to 60 centipoise,[20,21] the fluorescence decay changes from 1.3 to 16 ps, indicating the effect of friction. The quantum yield of fluorescence in solution [26] and in the protein [27] is ~10^{-3} and increases by two orders of magnitude when the chromophore is locked around the double bond.[28] Again, this behavior suggests an ultrafast nonradiative crossing, but we now know that it is an intrinsic property of the isolated chromophore around its central double bond. The analogy with *trans*-stilbene, diphenyl ethylene, is relevant because the barrier is similarly low (~3 kcal/mol).[29]

In Fig. 5.4, we depict the potential energy along the twisting coordinate θ and the effect of a second coordinate(s) describing the coherent motion, for example, that of skeletal deformation(s). After barrier crossing, the population of the twisted state in the isolated chromophore can decay only by searching for the CI and/or by redistributing the energy by intramolecular vibrational-energy redistribution. The twisted configuration is in a well with a depth of ~1 eV.[30] For this intermediate, we measured 52 ps for its decay, but in the protein the formation of the ground-state *cis* isomer (I_0, the first intermediate of the PYP photocycle) is within a few picoseconds.[7-10] This large discrepancy suggests that the position of CI on the potential energy surface is dependent on the environment.

Groenhof *et al*. [24] proposed that the CI of the PYP chromophore *in vacuo* is located far from the reaction coordinate plane on the skeletal deformation coordinate(s), whereas it is near the reaction coordinate in the protein (see Fig. 5.4 Inset).

Nuclear motions, particularly those of low frequency, can promote intramolecular vibrational-energy redistribution to coordinates other than θ, and hence internal conversion at the CI would be delayed, explaining the slow decay of $\mathbf{P}_{\theta}^{*}$ population in the isolated chromophore; once the CI is reached, the crossing occurs in <1 ps. In the protein the twisted state can easily reach the CI near the reaction coordinate plane without the assistance of intramolecular vibrational-energy redistribution. We show this difference in Fig. 5.4 (perpendicular plane). The momentum carried by the twisted state along the reaction coordinate is conserved better in the protein than in the isolated system because of the ultrashort interaction time in the CI region, and therefore more *cis* isomers can be formed with high reaction quantum yield (0.24–0.64).[7,10,31,32] That is a critical design by the protein environment to enhance *trans*-to-*cis* isomerization in the PYP photocycle.

There is another influence for the protein. In the isolated chromophore, the internal conversion of the twisted state near the CI creates vibrationally hot ground-state *cis* molecules. The excess energy is released by ejecting an electron (autodetachment), and some of the anions convert to radicals, because of the lack of competing relaxation processes. In the protein, however, the energy can be released efficiently because of the presence of many degrees of freedom, and creating a radical by autodetachment is not a dominant process; the radical state, from our autodetachment experiments, lies near 2.9 eV above the ground state. Vibrational relaxation in the protein is highly efficient, as

indeed measured in the protein; the absorption of the formed *cis* molecules is that of an equilibrated species within a few picoseconds.[6-10] Consistent with our findings is the fact that the radical state was not observed in the PYP photocycle with single-photon absorption; only with multiphoton excitation of high-energy photons were radicals detected.[6]

5.2. Conclusion

The studies reported here on the anionic, isolated chromophore of PYP provide direct evidence of the ultrafast, nearly frictionless dynamics of the first step of isomerization. The key primary step involves structural change including the central double bond. As pointed out earlier, double-bond twisting must include the effect of nuclear couplings to other bonds and electronic/resonance effects. In a very recent report,[33] the gas-phase absorption spectrum of the PYP chromophore indicates that the excitation energy is lower than calculated value,[24] indicating that an excess vibrational energy is sufficient for double-bond twisting. Moreover, recent molecular dynamics calculations for the protein and *in vacuo* support the involvement of the double-bond twisting.[34] The protein environment is not significant in changing the low-energy barrier for twisting, but it is critical for the subsequent conversion to the *cis* form and for the impedance of radical formation during the cycle. The design by the protein is for an efficient ultrafast phototransduction and for directing the dynamics by reducing the phase space of many nuclear motions into that of the reaction coordinate, as observed here in the direct comparison of the behavior of isolated-chromophore and protein dynamics.

5.3. Materials and Mathods

The **P**-chromophore, 4-(3-oxobut-1-enyl)-phenolate anion, was prepared from 4-hydroxybenzylideneacetone (HBA; Alfa Aesar, Ward Hill, MA; 97%) by using pulsed electron impact (1 keV, 1.0 ms) and expansion with oxygen at ~200 kPa in a molecular beam. The temperature was ~80°C, and under these conditions we obtained the **P**-chromophore mass, which confirms the deprotonation of HBA. The anions were directed into a field-free time-of-flight region by applying a –2.0-kV electric pulse in a two-stage accelerator. The beam of the **P**-chromophore, which was separated from other ions by its mass, was interrogated by the two beams of femtosecond laser pulses. The laser pulse (110 fs) at 800 nm was generated from a Ti:sapphire oscillator and amplified by a regenerative and multipass amplifier. The amplified laser pulse was split into two parts. The first was frequency doubled by a type-I beta barium borate crystal, generating a 400-nm pulse, and was used as the pump pulse to excite the **P**-chromophore. The second part was used as the probe pulse. The polarization was set at the magic angle (54.7°), and the power of the pulse was 0.35 mJ for the pump and 3.6 mJ for the probe, collimated to ~3-mm diameter. The resulting photoelectrons were analyzed in our apparatus [35] by using a magnetic bottle photoelectron spectrometer. The powerful methodology of mass selection/electron detachment provided the needed resolution of species and state,[36-39] whereas the pump-probe femtosecond chemistry configuration allowed for the temporal resolution.

Ab initio calculations for geometry optimization and energy minimization of the **P**-chromophore and single-point energy calculation of its radical form were performed by using the GAUSSIAN 98 program [40] at the B3LYP/cc-pVTZ level of theory.

References and Notes

(1) Sprenger, W. W.; Hoff, W. D.; Armitage, J. P.; Hellingwerf, K. J. *J. Bacteriol.* **1993**, *175*, 3096.

(2) Larsen, D. S.; van Grondelle, R. *ChemPhysChem* **2005**, *6*, 828.

(3) Hellingwerf, K. J.; Hendriks, J.; Gensch, T. *J. Phys. Chem. A* **2003**, *107*, 1082.

(4) Cusanovich, M. A.; Meyer, T. E. *Biochemistry* **2003**, *42*, 4759.

(5) Borgstahl, G. E. O.; Williams, D. R.; Getzoff, E. D. *Biochemistry* **1995**, *34*, 6278.

(6) Larsen, D. S.; van Stokkum, I. H. M.; Vengris, M.; van der Horst, M. A.; de Weerd, F. L.; Hellingwerf, K. J.; van Grondelle, R. *Biophys. J.* **2004**, *87*, 1858.

(7) Groot, M. L.; van Wilderen, L.; Larsen, D. S.; van der Horst, M. A.; van Stokkum, I. H. M.; Hellingwerf, K. J.; van Grondelle, R. *Biochemistry* **2003**, *42*, 10054.

(8) Gensch, T.; Gradinaru, C. C.; van Stokkum, I. H. M.; Hendriks, J.; Hellingwerf, K. J.; van Grondelle, R. *Chem. Phys. Lett.* **2002**, *356*, 347.

(9) Imamoto, Y.; Kataoka, M.; Tokunaga, F.; Asahi, T.; Masuhara, H. *Biochemistry* **2001**, *40*, 6047.

(10) Devanathan, S.; Pacheco, A.; Ujj, L.; Cusanovich, M.; Tollin, G.; Lin, S.; Woodbury, N. *Biophys. J.* **1999**, *77*, 1017.

(11) Genick, U. K.; Soltis, S. M.; Kuhn, P.; Canestrelli, I. L.; Getzoff, E. D. *Nature* **1998**, *392*, 206.

(12) Genick, U. K.; Borgstahl, G. E. O.; Ng, K.; Ren, Z.; Pradervand, C.; Burke, P. M.; Šrajer, V.; Teng, T. Y.; Schildkamp, W.; McRee, D. E.; Moffat, K.; Getzoff, E. D. *Science* **1997**, *275*, 1471.

(13) Usman, A.; Mohammed, O. F.; Heyne, K.; Dreyer, J.; Nibbering, E. T. J. *Chem. Phys. Lett.* **2005**, *401*, 157.

(14) Changenet-Barret, P.; Espagne, A.; Plaza, P.; Hellingwerf, K. J.; Martin, M. M. *New J. Chem.* **2005**, *29*, 527.

(15) Changenet-Barret, P.; Espagne, A.; Charier, S.; Baudin, J. B.; Jullien, L.; Plaza, P.; Hellingwerf, K. J.; Martin, M. M. *Photochem. Photobiol. Sci.* **2004**, *3*, 823.

(16) Vengris, M.; van der Horst, M. A.; Zgrablic, G.; van Stokkum, I. H. M.; Haacke, S.; Chergui, M.; Hellingwerf, K. J.; van Grondelle, R.; Larsen, D. S. *Biophys. J.* **2004**, *87*, 1848.

(17) Larsen, D. S.; Vengris, M.; van Stokkum, I. H. M.; van der Horst, M. A.; Cordfunke, R. A.; Hellingwerf, K. J.; van Grondelle, R. *Chem. Phys. Lett.* **2003**, *369*, 563.

(18) Ryan, W. L.; Gordon, D. J.; Levy, D. H. *J. Am. Chem. Soc.* **2002**, *124*, 6194.

(19) Based on energetics obtained by *ab initio* calculation (see Materials and Methods), the peak at ~0.9 eV (pump-plus-probe) corresponds to probe detachment with the formed radical having 0.8 eV of excitation. The broad peak at ~2 eV (pump only), similarly, is a two-photon excitation.

(20) Espagne, A.; Paik, D. H.; Changenet-Barret, P.; Plaza, P.; Martin, M. M.; Zewail, A. H. *Photochem. Photobiol. Sci.* **2007**, *6*, 780.

(21) Espagne, A.; Paik, D. H.; Changenet-Barret, P.; Martin, M. M.; Zewail, A. H. *ChemPhysChem* **2006**, *7*, 1717.

(22) Pedersen, S.; Bañares, L.; Zewail, A. H. *J. Chem. Phys.* **1992**, *97*, 8801.

(23) Mataga, N.; Chosrowjan, H.; Taniguchi, S. *J. Photochem. Photobiol. C-Photochem. Rev.* **2004**, *5*, 155.

(24) Groenhof, G.; Bouxin-Cademartory, M.; Hess, B.; De Visser, S. P.; Berendsen, H. J. C.; Olivucci, M.; Mark, A. E.; Robb, M. A. *J. Am. Chem. Soc.* **2004**, *126*, 4228.

(25) Thompson, M. J.; Bashford, D.; Noodleman, L.; Getzoff, E. D. *J. Am. Chem. Soc.* **2003**, *125*, 8186.

(26) Changenet-Barret, P.; Plaza, P.; Martin, M. M. *Chem. Phys. Lett.* **2001**, *336*, 439.

(27) Meyer, T. E.; Tollin, G.; Causgrove, T. P.; Cheng, P.; Blankenship, R. E. *Biophys. J.* **1991**, *59*, 988.

(28) Chosrowjan, H.; Taniguchi, S.; Mataga, N.; Unno, M.; Yamauchi, S.; Hamada, N.; Kumauchi, M.; Tokunago, F. *J. Phys. Chem. B* **2004**, *108*, 2686.

(29) Baskin, J. S.; Bañares, L.; Pedersen, S.; Zewail, A. H. *J. Phys. Chem.* **1996**, *100*, 11920.

(30) When the population of $\mathbf{P}^*_{\theta}$ is promoted by the probe to form the corresponding radical, the radical would carry similar amount of vibrational energy (E_{vib}) as , because of Franck–Condon consideration. This energy is the sum of δ, the energy difference between the *trans* and twisted form of the radical, and Δ, the difference in their electron-kinetic-energy observed here to be ~0.5 eV. Small δ values are improbable, and if δ is ~0.5 eV, E vib would be ~1 eV, which matches well with the theoretical calculation (Ref. 25).

(31) van Brederode, M. E.; Gensch, T.; Hoff, W. D.; Hellingwerf, K. J.; Braslavsky, S. E. *Biophys. J.* **1995**, *68*, 1101.

(32) Meyer, T. E.; Tollin, G.; Hazzard, J. H.; Cusanovich, M. A. *Biophys. J.* **1989**, *56*, 559.

(33) Nielsen, I. B.; Boye-Peronne, S.; El Ghazaly, M. O. A.; Kristensen, M. B.; Nielsen, S. B.; Andersen, L. H. *Biophys. J.* **2005**, *89*, 2597.

(34) Yamada, A.; Ishikura, T.; Yamato, T. *Proteins* **2004**, *55*, 1063.

(35) Paik, D. H.; Kim, N. J.; Zewail, A. H. *J. Chem. Phys.* **2003**, *118*, 6923.

(36) Leopold, D. G.; Murray, K. K.; Miller, A. E. S.; Lineberger, W. C. *J. Chem. Phys.*

1985, *83*, 4849.

(37) Posey, L. A.; Deluca, M. J.; Johnson, M. A. *Chem. Phys. Lett.* **1986**, *131*, 170.

(38) Metz, R. B.; Weaver, A.; Bradforth, S. E.; Kitsopoulos, T. N.; Neumark, D. M. *J. Phys. Chem.* **1990**, *94*, 1377.

(39) Castleman, A. W.; Bowen, K. H. *J. Phys. Chem.* **1996**, *100*, 12911.

(40) Frisch, M. J.; Trucks, G. W.; Schlegel, H. B.; Scuseria, G. E.; Robb, M. A.; Cheeseman, J. R.; Zakrzewski, V. G.; Montgomery, J. A.; Stratmann, R. E.; Burant, J. C.; Dapprich, S.; Millam, J. M.; Daniels, A. D.; Kudin, K. N.; Strain, M. C.; Farkas, O.; Tomasi, J.; Barone, V.; Cossi, M.; Cammi, R.; Mennucci, B.; Pomelli, C.; Adamo, C.; Clifford, S.; Ochterski, J.; Petersson, G. A.; Ayala, P. Y.; Cui, Q.; Morokuma, K.; Malick, D. K.; Rabuck, A. D.; Raghavachari, K.; Foresman, J. B.; Cioslowski, J.; Ortiz, J. V.; Stefanov, B. B.; Liu, G.; Liashenko, A.; Piskorz, P.; Komaromi, I.; Gomperts, R.; Martin, R. L.; Fox, D. J.; Keith, T.; Al-Laham, M. A.; Peng, C. Y.; Nanayakkara, A.; Gonzalez, C.; Challacombe, M.; Gill, P. M. W.; Johnson, B. G.; Chen, W.; Wong, M. W.; Andres, J. L.; Head-Gordon, M.; Replogle, E. S.; Pople, J. A.; Gaussian 98, revision A.9; Gaussian, Inc.: Pittsburgh PA, 1998.

(41) We thank Prof. Monique M. Martin and Drs. Agathe Espagne and D. Hern Paik for stimulating discussion; the collaborative work on solution-phase studies are published elsewhere (Ref. 20 and 21). This work was supported by the National Science Foundation.

Figure Captions

Figure 5.1:

Structure of the PYP and its chromophore. **(A)** Structure of the PYP, from refs. 5 and 6. The chromophore structure is indicated. **(B)** Chemical structure of the PYP chromophore and **P**-chromophore used in this study.

Figure 5.2:

Photoelectron spectra of the **P**-chromophore obtained with pump femtosecond pulse (blue trace) and pump-plus-probe femtosecond pluses (red trace) at 200-fs delay. (Inset) Blowup of the energy region of 0–1.5 eV, in which energy windows for time-dependent transients are marked as **I**, **II**, and **III**. The windows allow for probing of $\mathbf{P}_e^*$, $\mathbf{P}_t^*$, and $\mathbf{P}_\theta^*$ (see text).

Figure 5.3:

Time-resolved dynamics of the **P**-chromophore. Shown are the photoelectron spectra at three different kinetic energies and different timescales. Transients in each row are from the same energy window, and those in the same column have the same timescale. The theoretical fits are the solid lines superimposed on the experimental transients. The damped coherent oscillations are shown in region II on the short timescale. Note the clear depletion and recovery in window **I** and prompt response and decay in window **II**. In window **III**, the buildup and decay is evident; some contribution (prompt response) for the overlap of windows also is observed.

Figure 5.4:

Conceptual potential energy surface for the primary dynamics of the **P**-chromophore. The rotation angle around the double bond is indicated by θ and the other coordinate(s) are denoted by a perpendicular plane (γ coordinate) with the CI. The initial excitation prepares a wave packet localized at the *trans* configuration, after bifurcation (see text). The 3D potential in Inset shows the energy surface of the chromophore in the protein environment (adapted from ref. 24). A cut in this surface displays a similar θ-dependence but with a much closer, to the reaction coordinate, CI.

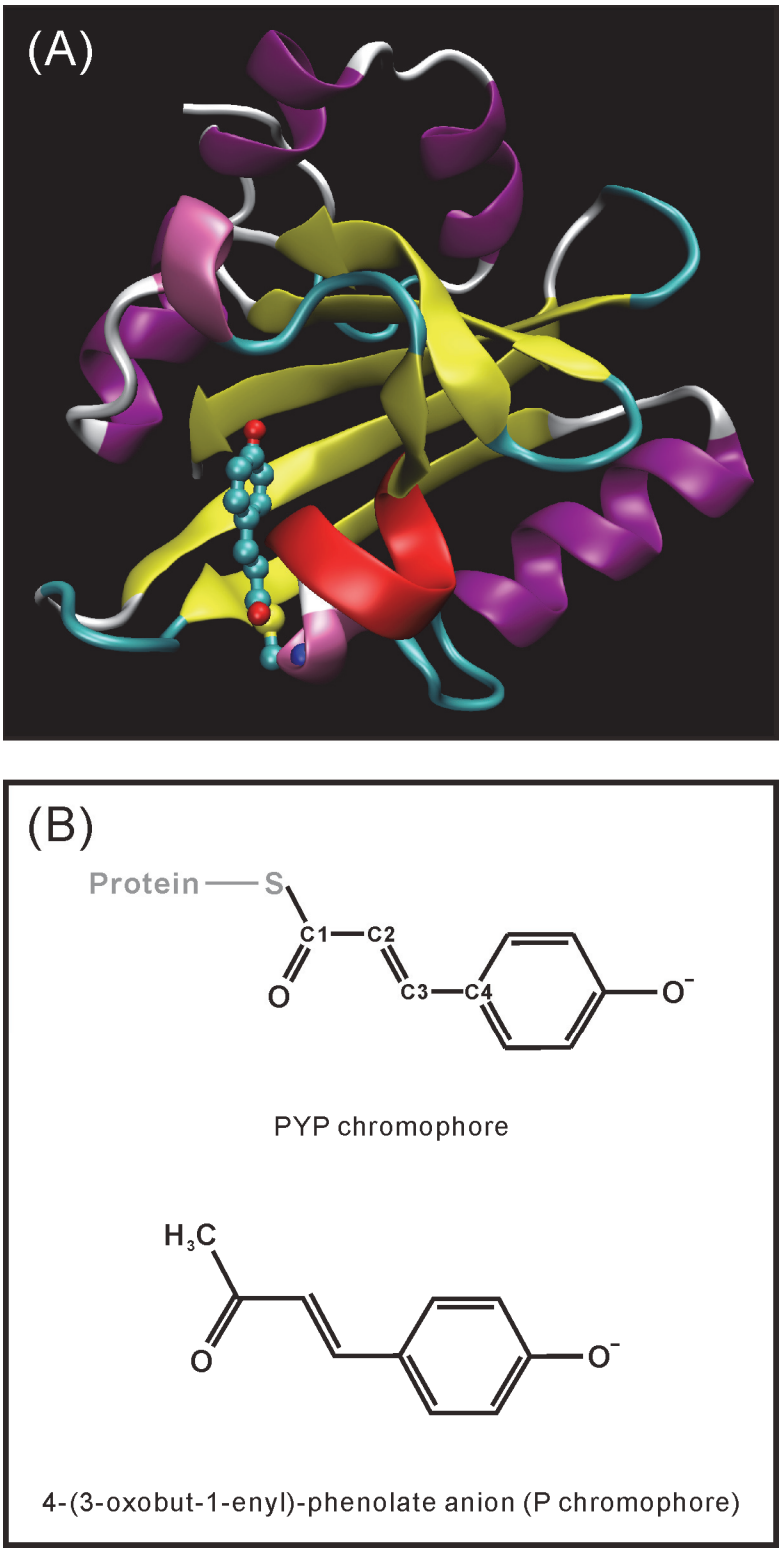
(A)
(B)
Protein — S
C1
C2
C3
C4
O
O⁻
PYP chromophore
H3C
O
O⁻
4-(3-oxobut-1-enyl)-phenolate anion (P chromophore)

Figure 5.1

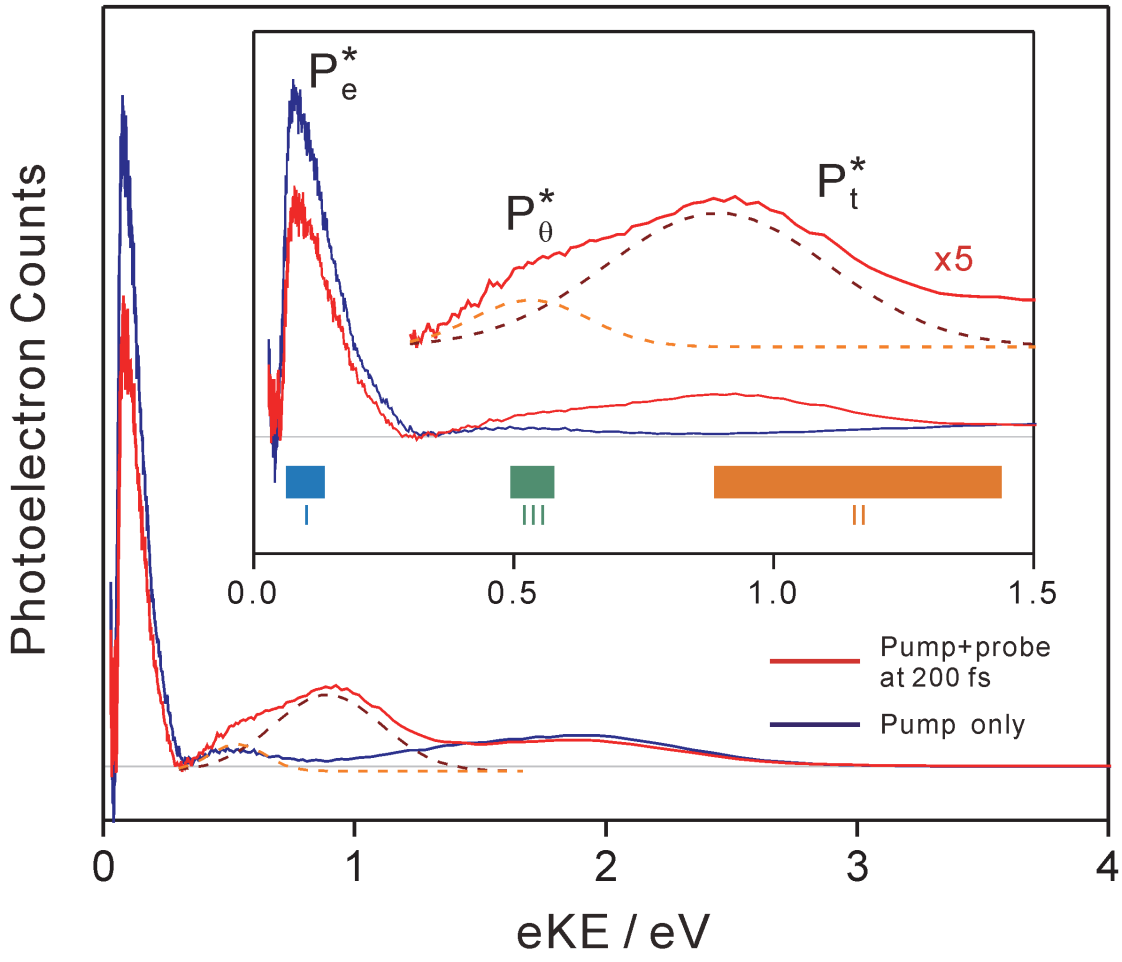
Photoelectron Counts
eKE / eV
0
1
2
3
4
P^*_e
P^*_θ
P^*_t
x5
I
III
II
0.0
0.5
1.0
1.5
Pump+probe at 200 fs
Pump only

Figure 5.2

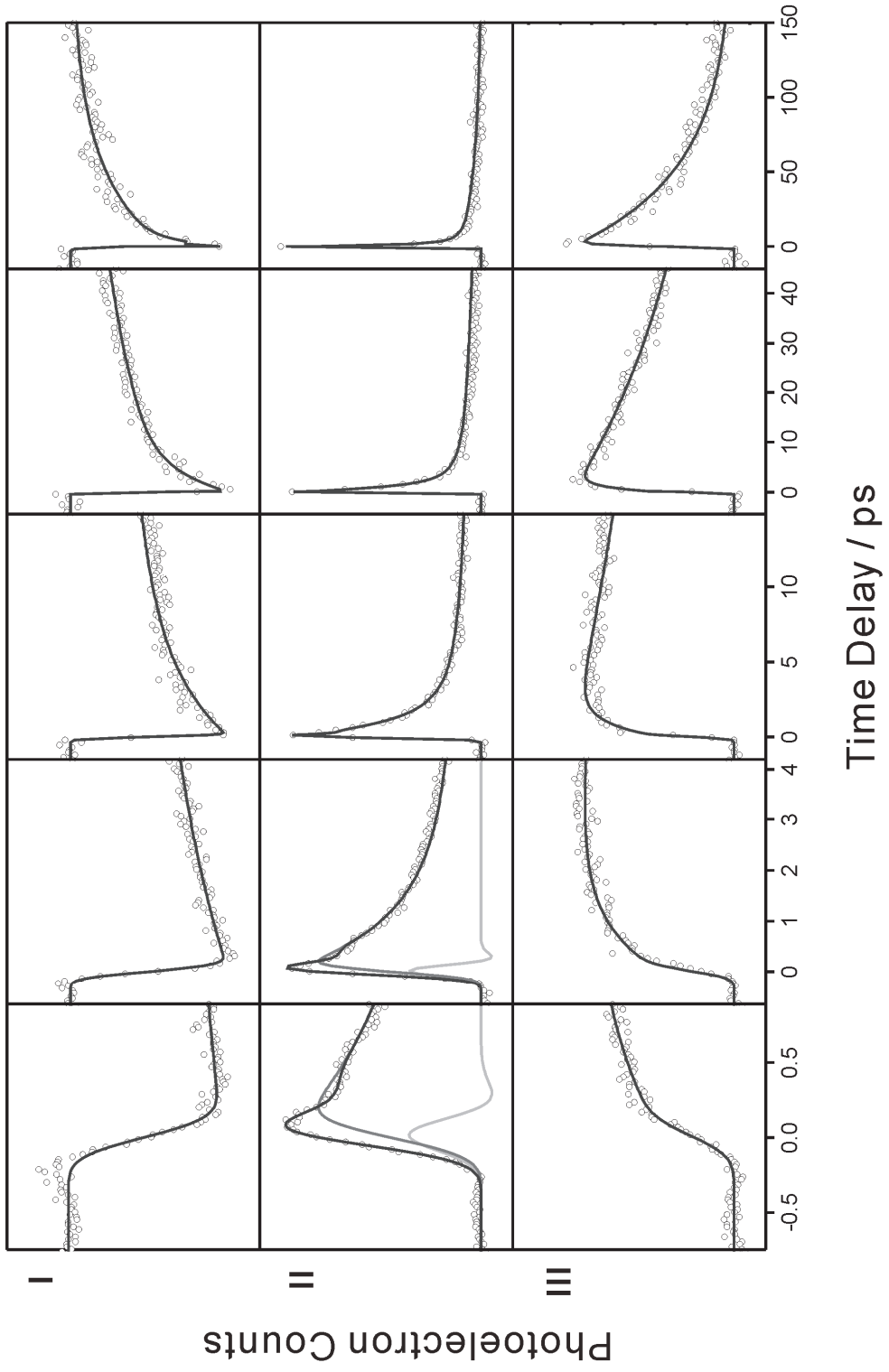
Photoelectron Counts
Time Delay / ps
-0.5
0.0
0.5
0
1
2
3
4
0
5
10
0
10
20
30
40
0
50
100
150

Figure 5.3

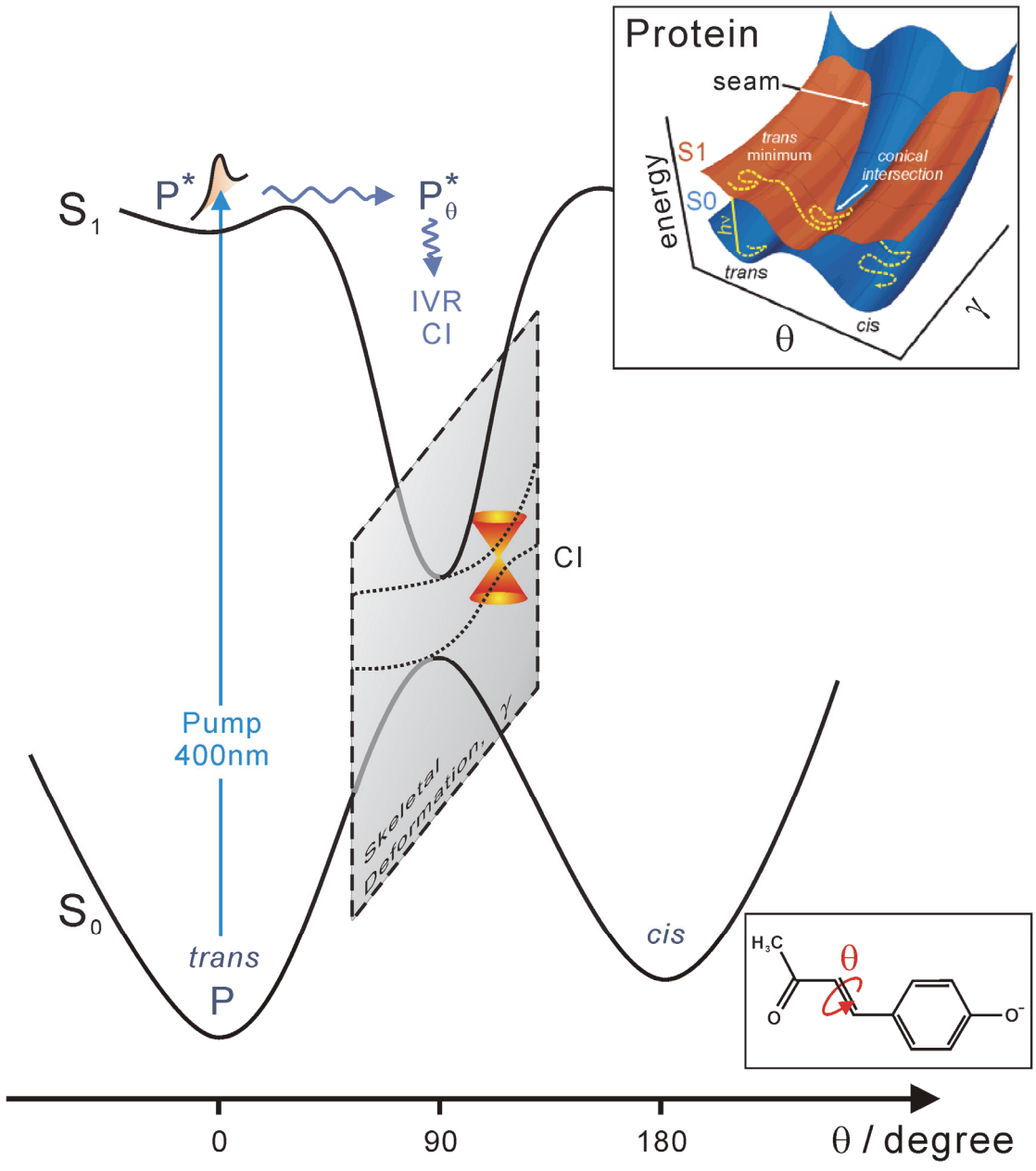
Protein
seam
trans
minimum
conical
intersection
S1
S0
energy
trans
cis
θ
γ
S1
P*
P*θ
IVR
CI
CI
Pump
400nm
S0
trans
P
cis
Skeletal
Deformation
γ
H3C
O
θ
O-
0
90
180
θ / degree

Figure 5.4

CHAPTER 6.

Direct Observation of the Primary Bond-Twisting Dynamics of Stilbene Anion Radical

† adapted from Lee, I. R.; Bañares, L.; Zewail, A. H. *J. Am. Chem. Soc.* **2008**, *130*, 6708.

Abstract

The anion radicals of stilbenes in the collisionless isolated phase were synthesized by electron attachment and their dynamics were observed in real time on the femtosecond time scale. The observed coherent vibrational motion (~42 cm^{-1}) and the primary dynamics (~650 fs) for the D_2 state are on a vastly different time scale (~10 ns) from that reported in solution.

6.1. Introduction

The isomerization of neutral stilbene, a model system for conformational twisting in chemical and biological chromophores, has been studied extensively in the past, both experimentally [1,2] and theoretically.[3] The central bond (vibrational) twisting and barrier crossing occur on the femtosecond to picosecond time scale in the isolated molecule [4-6] and in the condensed phase.[7] In contrast, for the anions (and cations) of stilbene, the results are very scarce and only available from studies in solid matrices,[8,9] and in solution using pulsed radiolysis methods.[10-12] This is because the ions are more difficult to study in the gas phase and, because of the very low density, the dynamics of twisting becomes even more challenging.

In this communication, we report real-time femtosecond (fs) observation of the primary bond-twisting on dynamics of *trans*- and *cis*-stilbene anion radicals made by electron attachment in a molecular beam and selected using mass spectrometry. Following the selection, a pulse of 110 fs intersected the anion beam to excite (400 nm) it into the D_2 state and a second pulse was delayed to photodetach an electron whose kinetic energy was resolved and monitored as a function of time.[13] Besides being the first study of the anion in the isolated collisionless phase, the results reported here provide the dynamics of the *cis*- (and *trans*-) configuration giving the time constant of ~650 fs for the primary step, with a coherent vibrational motion (~42 cm^{-1}) during the twisting along the multidimensional reaction coordinate. This is vastly different from the time constant of 10 ns reported in the solution-phase study.[12]

6.2. Results and Discussion

Fig. 6.1 depicts the energetics and the relevant experimental scheme. The steady-state and transient photoelectron spectra (PES) of both *trans*- and *cis*-stilbene anion radicals taken at 400 and 800 nm are shown in Fig. 6.2. The vertical detachment energy (VDE) obtained from both these spectra is ~0.6 eV. Using density functional theory (DFT) we calculated[15] energies of 0.61 (*trans*) and 0.59 eV (*cis*), which are in good agreement with the experimental value. The most noticeable difference in the PES of the isomers is the structure observed for 400-nm and 800-nm excitation of the *trans*-isomer, and the peak at ~1.5 eV.[16] The importance of these differences is in ruling out the possibility of a major contamination caused by the thermal isomerization channel during the sample delivery and ionization processes.

Transient difference PES at –0.9 ps and zero time delay, relative to that at 8 ps, are shown in the bottom panels of Fig. 6.2. Three energy windows centered at 1.2, 2.3, and 3.6 eV (3.9 eV for *cis*-isomer) have been investigated, and the corresponding transients are shown in Fig. 6.3 for both *trans*- and *cis*-stilbene anions. For the *trans*-isomer, the peak at ~1.5 eV eKE changes in concert with the major peak at ~2.5 eV eKE, again consistent of being for the same anion species. Despite the difference in steady-state PES, the measured transients in all three windows are similar in shape for both isomers.

The enhancement of PES in window **I** only appears at a time delay close to zero and, thus, the transients obtained in this window (left panel of Fig. 6.3) represent the initially excited state (D_s) dynamics, as evidenced from the energetic and the temporal behavior. The energies in windows **II** and **III** overlap in energy with those of the pump

and probe PES at steady state (see Fig. 6.2). In these two regions, the signal arises from the depopulation of the ground state by the pump or probe photons, which arrive prior to the detaching pulse (probe or pump, respectively). The fitted rise (decay) is on the time scale of the transient observed in window **I**, which is consistent with the dynamics of the initially excited D_2 state,[17] as described below. The behavior in window **III** is similar.

The transients in window **I** clearly show an ultrafast decay and a coherent oscillatory behavior. The fs initial decay component reflects the initial wavepacket motion away from the Franck–Condon(FC) region of D_2, which leads at longer time to the actual twisting along the reaction coordinate. Given this initial decay, the damped oscillation was described by a molecular response function, $M(t)$, which takes into account the buildup/decay of the population, together with the oscillatory behavior:

$$M(t) = \frac{k_1}{k_1 - k_2}(e^{-k_2 t} - e^{-k_1 t})\cos(\omega t + \varphi) \qquad (1)$$

where ω and φ are the frequency and phase of the oscillation, respectively. From the analysis, we obtained an initial wave packet motion on the time sale of k_1^{-1}~100 fs, but with the oscillatory behavior being on a much longer time scale (see Fig. 6.3): $T = 2\pi\omega^{-1}$ ~ 800 fs (42 cm^{-1}) and k_2^{-1} ~ 650 fs.

Several points can now be made regarding the dynamics. First, both the *cis*- and *trans*-isomers of the anion exhibit similar behavior, and this is very different situation from that of neutral *cis*/*trans* isomerization. For the neutral (S_1) *trans*, there exists a barrier of 3.4 kcal/mol while for this *cis* the potential is barrierless.[4,5] For the anion (D_2), the twisting process originates on a potential surface of similar forces for both isomers, perhaps because of the antibonding character acquired with the additional electron.

Second, the difference in time scales reported here with that of neutral *cis*-stilbene (k_2^{-1} = 307 fs, T = 360 fs)[4] is also consistent with the force field being weaker. The 42 cm^{-1} could be the reaction coordinate but we must consider other motions involving the phenyl rings.[4] Third, and finally, these results are at variance with previous experimental data from pulse radiolysis–flash photolysis experiments in the condensed phase.[12] The study in the solution phase suggests that only *cis* is capable of twisting, and with a time constant of ~10 ns (5 ns for lifetime) for the same D_2 state. This would indicate four orders of magnitude change in rate due to solvent interactions, a situation that was not found for neutral stilbenes. This disparity suggests a major solvent (friction and polarity) retardation, either in the barrier[18,19] or conical intersection[3] region.

6.3. Conclusion

In conclusion, the contribution made here indicates the significance of studying these anion dynamics in the isolated molecule, revealing the actual time scales in primary dynamics involved and the coherent vibration motion involved. The observed behavior for twisting is vastly different from that reported in the solution phase.

References and Notes

(1) Saltiel, J.; Sun, Y.-P. In Photochroism-Molecules and Systems; Dürr, H.; Bouas-Laurent, H. Eds.; Elsevier: Amsterdam, 1990; p 64-164 and references therein.

(2) Waldeck, D. H. Chem. Rev. 1991, 91, 415-436 and references therein.

(3) Levine, B. G.; Martínez, T. J. *Ann. Rev. Phys. Chem.* **2007**, *58*, 613 and references therein.

(4) Pedersen, S.; Bañares, L.; Zewail, A. H. *J. Chem. Phys.* **1992**, *97*, 8801.

(5) Baskin , J. S.; Bañares, L.; Zewail, A. H. *J. Phys. Chem.* **1996**, *100*, 11920 and references therein.

(6) Lee, I.-R.; Lee, W.; Zewail, A. H. *Proc. Nat. Acad. Sci. USA* **2006**, *103*, 258.

(7) Sension, R. J.; Repinec, S. T.; Szarka A. Z.; Hochstrasser R. M., *J. Chem. Phys.* **1993**, *98*, 6291.

(8) Shida, T.; Hamill, W. H. *J. Chem. Phys.* **1966**, *44*, 2375.

(9) Sazhnikov, V. A.; Rakhmatov, M.; Alfimov, M. V. *Chem. Phys. Lett.* **1980**, *71*, 33.

(10) Ebbesen, T. W. *J. Phys. Chem.* **1988**, *92*, 4581.

(11) Ishida, A.; Fukui, M.; Ogawa, H.; Tojo, S.; Majima, T.; Takamuku, S. *J. Phys. Chem.* **1995**, *99*, 10808.

(12) Majima, T.; Fukui, M.; Ishida, A.; Takamuku, S. *J. Phys. Chem.* **1996**, *100*, 8913.

(13) Stilbene radical anions were prepared using electron impact (200V) in our pulsed molecular apparatus (see ref. 14). The *trans*- or *cis*-compound was heated (120°C or 90°C) under 300 psi helium gas, and the gas mixture was then introduced into vacuum through an Even-Lavie pulsed nozzle at 20 Hz. For selection, the anions were directed to the time-of-flight mass spectrometer through a skimmer, and interrogated by the two fs laser pulses (pump: 400 nm, ~1.5 mJ; probe: 800 nm, ~1.5 mJ). Photoelectrons were analyzed using a magnetic-bottle spectrometer.

(14) Paik, D. H.; Kim, N. J.; Zewail, A. H. *J. Chem. Phys*. **2003**, *118*, 6923.

(15) DFT calculations with geometry optimization of *trans*- and *cis*-stilbene radical anions, and single-point energy of the neutral form, were performed using GAUSSIAN98 at the B3LYP/6-31G+(d,p) level of theory. (Frisch, M. J.; Trucks, G. W.; Schlegel, H. B.; Scuseria, G. E.; Robb, M. A.; Cheeseman, J. R.; Zakrzewski, V. G.; Montgomery, J. A.; Stratmann, R. E.; Burant, J. C.; Dapprich, S.; Millam, J. M.; Daniels, A. D.; Kudin, K. N.; Strain, M. C.; Farkas, O.; Tomasi, J.; Barone, V.; Cossi, M.; Cammi, R.; Mennucci, B.; Pomelli, C.; Adamo, C.; Clifford, S.; Ochterski, J.; Petersson, G. A.; Ayala, P. Y.; Cui, Q.; Morokuma, K.; Malick, D. K.; Rabuck, A. D.; Raghavachari, K.; Foresman, J. B.; Cioslowski, J.; Ortiz, J. V.; Stefanov, B. B.; Liu, G.; Liashenko, A.; Piskorz, P.; Komaromi, I.; Gomperts, R.; Martin, R. L.; Fox, D. J.; Keith, T.; Al-Laham, M. A.; Peng, C. Y.; Nanayakkara, A.; Gonzalez, C.; Challacombe, M.; Gill, P. M. W.; Johnson, B. G.;

Chen, W.; Wong, M. W.; Andres, J. L.; Head-Gordon, M.; Replogle, E. S.; Pople, J. A.; Gaussian 98, revision A.9; Gaussian, Inc.: Pittsburgh PA, 1998.)

(16) The peak of the *trans*-isomer at ~1.5-eV eKE is 0.9 eV higher in electron binding energy (eBE) when compared to the major peak at 0.6-eV eKE. However, the energy gap of S_1–S_0 or T_1–S_0 is higher than 0.9 eV. Thus, it is not due to the photodetachment of the electronically excited neutral states (S_1 or T_1). However, it is possible that autodetachment through the hot D_1 or D_0 state will produce this peak whose position and intensity are determined by the Franck–Condon overlap between the hot anion (D_1 or D_0) and neutral (S_0) state.

(17) The observed transient behavior in windows **II** and **III** represent both the fs depopulation of D_2 state, which should match the decay in window **I** (see text), and the prompt photodetachment (for window **II**), as expected.[6] For the window **III**, since it is at the probe region, the transient should be dominated by the photodetachment. However, the additional decay can be understood given the fact that the energy difference between window **I** and **III** (~ 2.4 eV) is consistent with the energy separation between T_1 and S_0 state (2.2 and 2.4 eV for *trans*- and *cis*-stilbene, respectively) of the neutral molecules. Thus, the decay should be that of the D_2 population, but with different probing (probe photon detaches the anion to the neutral T_1, instead of S_0, and result in electron of lower eKE), as observed here.

(18) Kim, H. J.; Staib, A.; Hynes, J. T. In *Femtochemistry and Femtobiology: Ultrafast Reaction Dynamics at Atomic-Scale Resolution*; Sundström, V. Eds.; Imperial College Press: Bjorkbörn, Sweden, 1996; pp 510-527 and references therein.

(19) Eisenthal, K, B, In *Femtochemistry and Femtobiology: Ultrafast Reaction Dynamics at Atomic-Scale Resolution*; Sundström, V., Ed.; Imperial College Press: Bjorkbörn, Sweden, pp 560-596 and references therein.

(20) LB gratefully acknowledges Del Amo Foundation and Research Vice-rectorate (acción especial no. AE10/07-15604) of Universidad Complutense de Madrid for financial support of travel for a two-month stay at Caltech and AZ for his hospitality. This work is supported by the National Science Foundation and the Air Force Office of Scientific Research.

Figure Captions

Figure 6.1:

The energetics and probing scheme are illustrated. The pump pulse (blue arrow) at 400 nm promotes the population from D_0 to D_2 of the anion. The delayed probe pulse (red arrow) at 800 nm then photodetaches the electron and yields the electron with kinetic energy shown as black arrow. The neutral S_0 is displayed and located at 0.6 eV above D_0 as obtained here from both the experiments and DFT calculations.

Figure 6.2

Transient and steady-state and photoelectron spectra (PES) of the *trans*- (**A**) and *cis*- (**B**) stilbene radical anions. Top panels: steady-state PES taken at 400 nm (blue) and 800 nm (red). Bottom panels: transient PES shown at two time delays. The difference was referenced to the spectra taken at 8 ps, where no further changes were observed (steady state). The brackets at the bottom indicate the energy windows of interest labeled as **I**, **II**, and **III** and centered at 3.6 (3.9 for *cis*), 2.3, and 1.2 eV, respectively.

Figure 6.3

Transient PES for *trans*- and *cis*- (insets) stilbene radical anions. Panels show the transients obtained by integrating the PES at the energy windows **I**, **II**, and **III** indicated (see Fig. 6.2), respectively. The red solid lines are the best fit to the experimental transients (black). In the top panel, the dashed lines give the different components contributing to the transients. The oscillatory behavior is shown in the residual signals (gray and green). Note that the plateau remains constant up to 80 ps; for window **I**, it is of the same origin as window **II** but for two-photon (400 nm) probing.

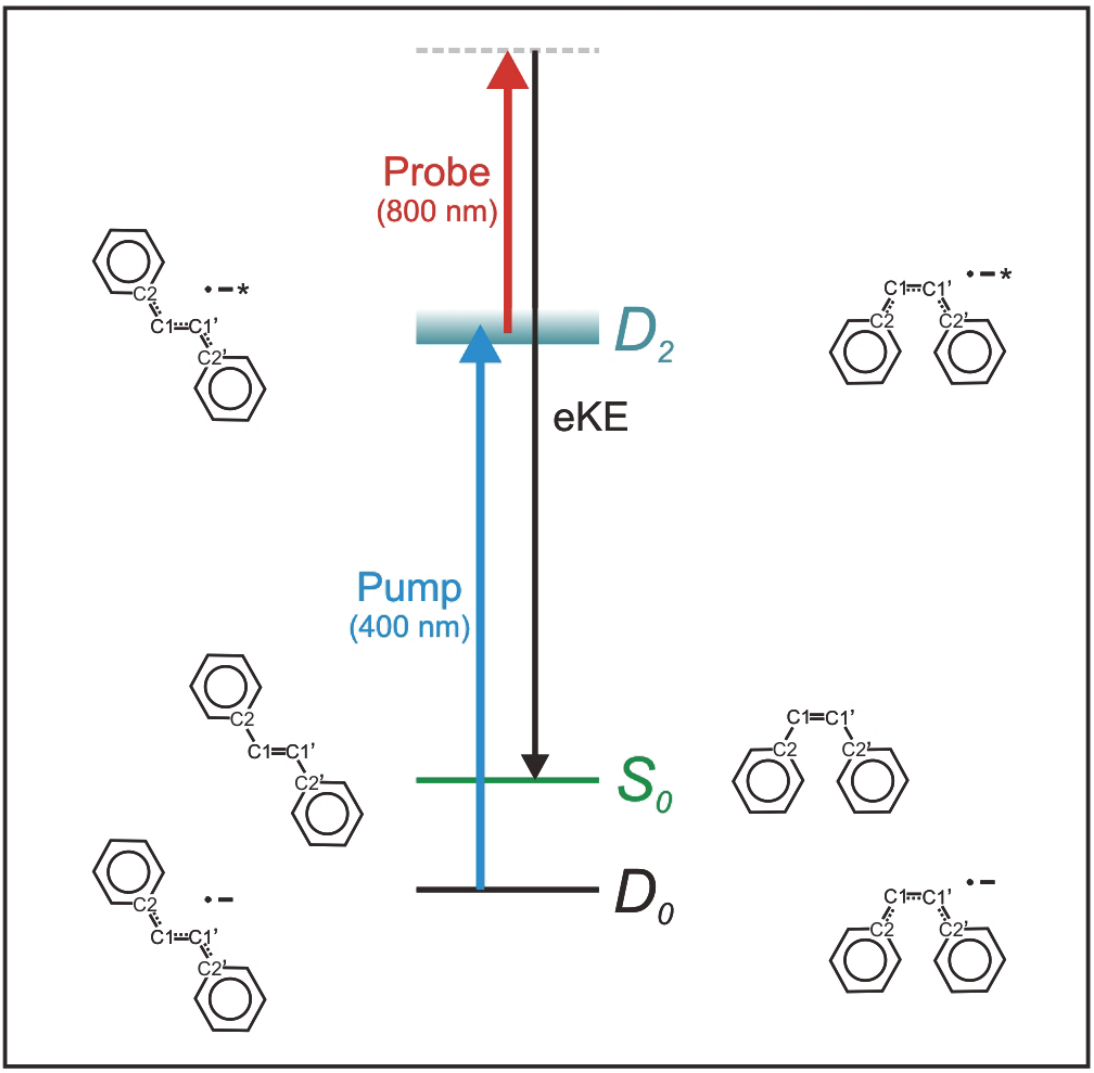

Figure 6.1

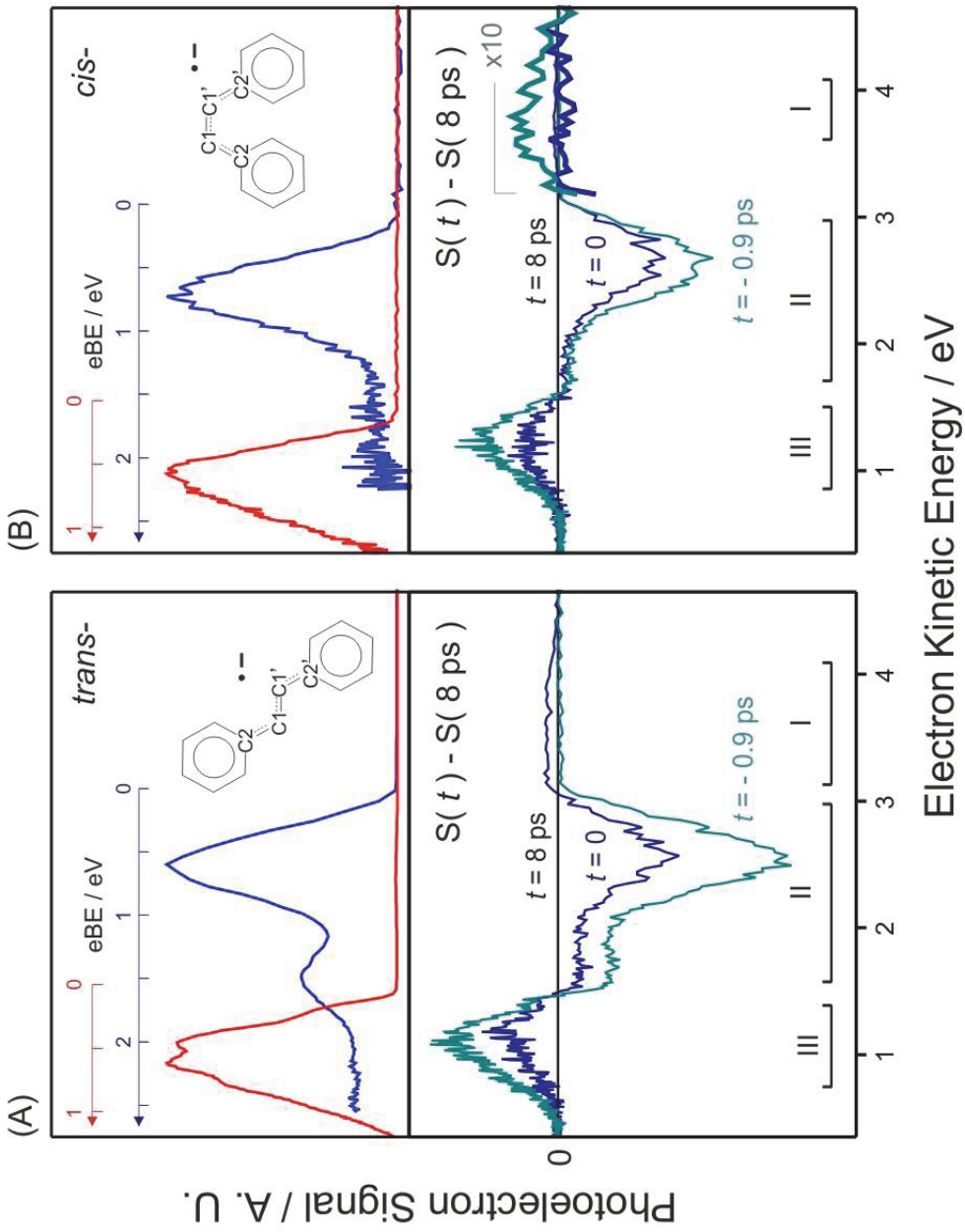
(A)
(B)
trans-
cis-
eBE / eV
S(t) - S(8 ps)
t = 8 ps
t = 0
t = - 0.9 ps
x10
I
II
III
Photoelectron Signal / A. U.
Electron Kinetic Energy / eV

Figure 6.2

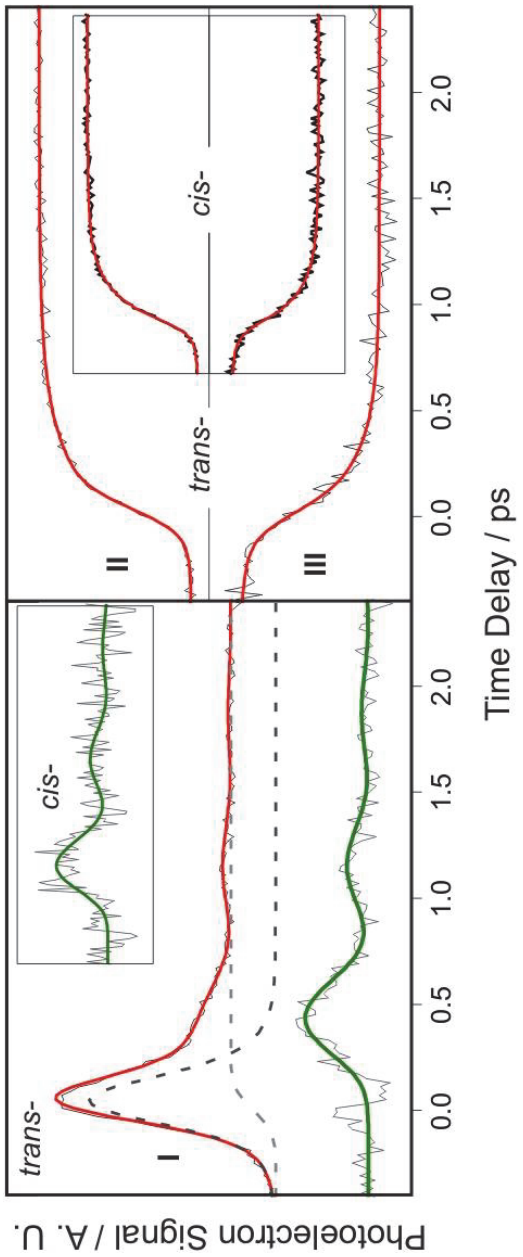
Photoelectron Signal / A. U.
Time Delay / ps
trans-
cis-
I
II
III
0.0
0.5
1.0
1.5
2.0

Figure 6.3

Appendix.

This section includes the home-built data acquisition program that is used in this thesis. The program is written in Microsoft Visual Basic 6. The screen shot is shown in page 122 and the program codes are given in page 124-144.

Requirement:

1. Hardware:

   Personal computer with a National Instrument PCI-GPIB interface card installed.

2. Software:

   National Instrument PCI-GPIB device driver.
   National Instrument Measurement Studio
   Microsoft Visual Basic 6.0

3. Include the following modules in the program:

   GlobalDec.bas
   GraphScope.bas
   GraphTransient.bas
   LeCroy9361.bas
   Niglobal.bas (from PCI-GPIB driver)
   Unidex100.bas
   Vbib-32.bas(from PCI-GPIB driver)

* Microsoft and Visual Basic are trademarks of Microsoft Coorperation.
* National Instrument and Measurement Studio are the trademakes of National Instrument Coorperation.

Main

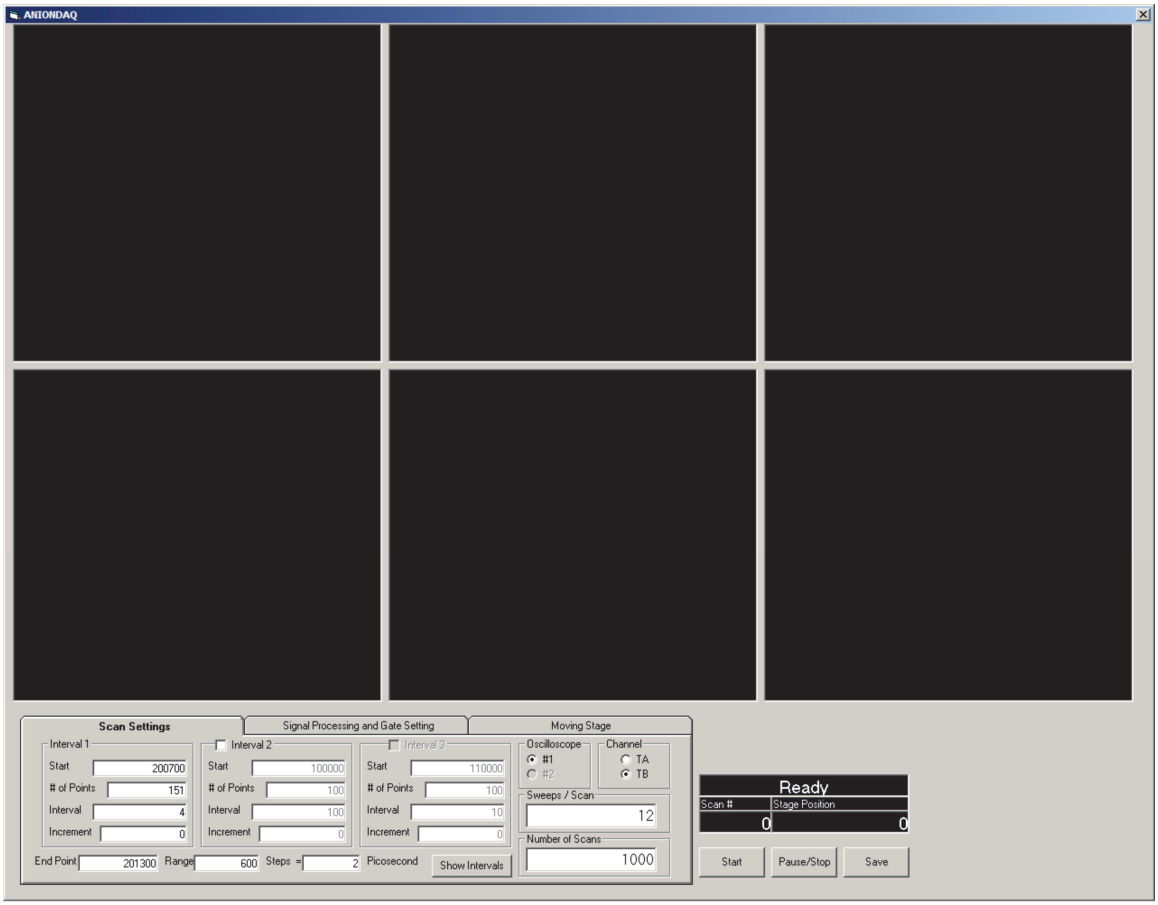

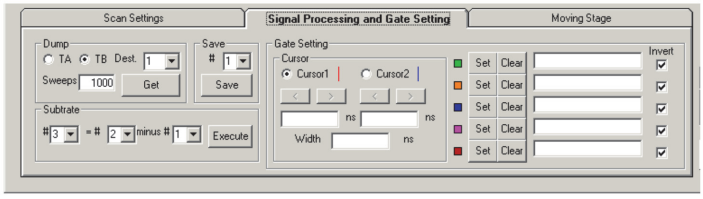

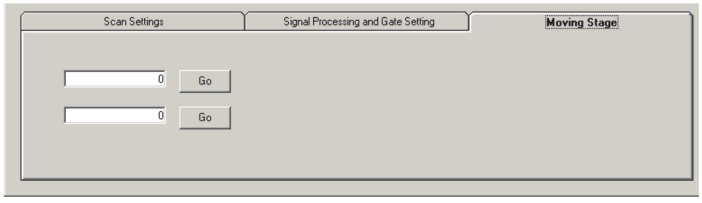

frmPauseStop

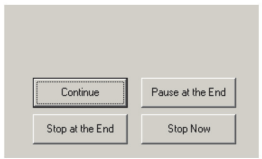

Main Form: Form1.frm

```
Attribute VB_Name = "Main"
Attribute VB_GlobalNameSpace = False
Attribute VB_Creatable = False
Attribute VB_PredeclaredId = True
Attribute VB_Exposed = False
Dim Start As Long, Start2 As Long, Start3 As Long, Int1 As Long, Inc1
As Long,
Int2 As Long, Inc2 As Long, Int3 As Long, Inc3 As Long
Dim NoPts1 As Integer, NoPts2 As Integer, NoPts3 As Integer, Nopts As
Integer
Dim flgGraphScope(5) As Boolean
Dim flgCursor1Set As Boolean, flgCursor2Set As Boolean
Dim flgGateSet(4) As Boolean
Dim flgDumped(1) As Boolean
Dim TotalPts As Integer
Dim CursorPosition As Integer, CursorWidth As Integer
Dim Cursor1Index As Integer, Cursor2Index As Integer
Dim GatePosition(4) As Integer, GateWidth(4) As Integer
Dim TraceVolt(5, 10000) As Single
Dim Xpts(1000) As Long
Dim TraceSum(500, 10000) As Double, TraceAvg(500, 10000) As Double
Dim TraceCurrent(500, 1000) As Single
Dim GateIntSum(4, 500) As Double, GateIntAvg(4, 500) As Double
Dim NoOfScans As Integer, NoofSweeps As Integer

Private Sub chkInt2_Click()
  frmInt2.Enabled = chkInt2.value
  txtInt2Start.Enabled = chkInt2.value
  txtInt2NoPts.Enabled = chkInt2.value
  txtInt2Int.Enabled = chkInt2.value
  txtInt2Inc.Enabled = chkInt2.value
  chkInt3.Enabled = chkInt2.value
  frmInt3.Enabled = chkInt2.value * chkInt3.value
  txtInt3Start.Enabled = chkInt2.value * chkInt3.value
  txtInt3NoPts.Enabled = chkInt2.value * chkInt3.value
  txtInt3Int.Enabled = chkInt2.value * chkInt3.value
  txtInt3Inc.Enabled = chkInt2.value * chkInt3.value
  Call UpdateInt
End Sub

Private Sub chkInt3_Click()
  frmInt3.Enabled = chkInt2.value
  txtInt3Start.Enabled = chkInt2.value
  txtInt3NoPts.Enabled = chkInt2.value
  txtInt3Int.Enabled = chkInt2.value
  txtInt3Inc.Enabled = chkInt2.value
  Call UpdateInt
End Sub

Sub UpdateInt()
  Dim EndPt As Long
  Start = CLng(txtInt1Start.Text)
  NoPts1 = CInt(txtInt1NoPts.Text)
  Int1 = CLng(txtInt1Int.Text)
```

```
  Inc1 = CLng(txtInt1Inc.Text)
  Start2 = Start + Int1 * (NoPts1 - 1) + Inc1 * (NoPts1 - 2) *
(NoPts1 - 1) /2
  NoPts2 = CInt(txtInt2NoPts.Text)
  Int2 = CLng(txtInt2Int.Text)
  Inc2 = CLng(txtInt2Inc.Text)
  Start3 = Start2 + Int2 * NoPts2 + Inc2 * (NoPts2 - 1) * NoPts2 / 2
  NoPts3 = CInt(txtInt3NoPts.Text)
  Int3 = CLng(txtInt3Int.Text)
  Inc3 = CLng(txtInt3Inc.Text)
  EndPt = Start2
  Nopts = NoPts1

  If frmInt2.Enabled = True Then
    EndPt = Start3
    Nopts = NoPts1 + NoPts2

    If frmInt3.Enabled = True Then
      EndPt = Start3 + Int3 * NoPts3 + Inc3 * (NoPts3 - 1) * NoPts3 /
2
      Nopts = NoPts1 + NoPts2 + NoPts3
    End If
  End If

  txtEndPt.Text = EndPt
  txtRange.Text = EndPt - Start
  txtRangePs.Text = Int((EndPt - Start) / 3) / 100
  If Start < 0 Or Start > 500000 Then Call ResetInt
  If NoPts1 < 2 Or NoPts1 > 1000 Then Call ResetInt
  If Int1 < 0 Or Int1 > 500000 Then Call ResetInt
  If Inc1 < -Int1 Or Inc1 > 500000 Then Call ResetInt
  If Int1 + (NoPts1 - 1) * Inc1 <= 0 Then Call ResetInt
  If Start + Int1 * (NoPts1 - 1) > 500000 Then Call ResetInt

  If chkInt2.value = vbChecked Then
    txtInt2Start.Text = Start2
    If Start2 < 0 Or Start2 > 500000 Then Call ResetInt
    If NoPts2 < 2 Or NoPts2 > 1000 Then Call ResetInt
    If Int2 < 0 Or Int2 > 500000 Then Call ResetInt
    If Inc2 < -Int2 Or Inc2 > 500000 Then Call ResetInt
    If Int2 + (NoPts1 - 2) * Inc2 <= 0 Then Call ResetInt
    If Start2 + Int2 * (NoPts2 - 1) > 500000 Then Call ResetInt
  End If

  If chkInt3.value = vbChecked Then
    txtInt3Start.Text = Start3
    If Start3 < 0 Or Start3 > 500000 Then Call ResetInt
    If NoPts3 < 2 Or NoPts3 > 1000 Then Call ResetInt
    If Int3 < 0 Or Int3 > 500000 Then Call ResetInt
    If Inc3 < -Int3 Or Inc3 > 500000 Then Call ResetInt
    If Int3 + (NoPts1 - 3) * Inc3 <= 0 Then Call ResetInt
    If Start3 + Int3 * (NoPts3 - 1) > 500000 Then Call ResetInt
  End If
End Sub

Private Sub cmdCursor1Left_Click()
```

```
  If Cursor1Index > 0 Then
    Cursor1Index = Cursor1Index - 1

    For i = 0 To 5
      lineGatePos1(i).X1 = Cursor1Index
      lineGatePos1(i).X2 = Cursor1Index
    Next i

    txtCursorPos1.Text = CLng(LecroyTB(Cursor1Index) * 1000000000#)

    If flgCursor2Set = True Then
      txtCursorWidth.Text = CLng(Abs(LecroyTB(Cursor2Index) -
LecroyTB(Cursor1Index)) * 1000000000#)
    End If
  End If
End Sub

Private Sub cmdCursor1Right_Click()
  If Cursor1Index < LecroyHPts - 1 Then
    Cursor1Index = Cursor1Index + 1

    For i = 0 To 5
       lineGatePos1(i).X1 = Cursor1Index
       lineGatePos1(i).X2 = Cursor1Index
    Next i

    txtCursorPos1.Text = CLng(LecroyTB(Cursor1Index) * 1000000000#)

    If flgCursor2Set = True Then
      txtCursorWidth.Text = CLng(Abs(LecroyTB(Cursor2Index) -
LecroyTB(Cursor1Index)) * 1000000000#)
    End If
  End If
End Sub

Private Sub cmdCursor2Left_Click()
  If Cursor2Index > 0 Then
    Cursor2Index = Cursor2Index - 1

    For i = 0 To 5
      lineGatePos2(i).X1 = Cursor2Index
      lineGatePos2(i).X2 = Cursor2Index
    Next i

    txtCursorPos2.Text = CLng(LecroyTB(Cursor2Index) * 1000000000#)

    If flgCursor1Set = True Then
      txtCursorWidth.Text = CLng(Abs(LecroyTB(Cursor2Index) -
      LecroyTB(Cursor1Index)) * 1000000000#)
    End If
  End If
End Sub

Private Sub cmdCursor2Right_Click()
  If Cursor2Index < LecroyHPts - 1 Then
    Cursor2Index = Cursor2Index + 1
```

```
    For i = 0 To 5
      lineGatePos2(i).X1 = Cursor2Index
      lineGatePos2(i).X2 = Cursor2Index
    Next i

    txtCursorPos2.Text = CLng(LecroyTB(Cursor2Index) * 1000000000#)

    If flgCursor1Set = True Then
      txtCursorWidth.Text = CLng(Abs(LecroyTB(Cursor2Index) -
LecroyTB(Cursor1Index)) * 1000000000#)
    End If
  End If
End Sub

Private Sub cmdDAQStart_Click()
  Dim GateIntValue(4, 500) As Double
  Dim GateIntMax(4) As Double, GateIntMin(4) As Double
  Dim TraceFilename As String, TraceFilenameNoScan As
String,TraceFilenameTD As String
  Erase TraceSum
  Erase TraceAvg
  Erase GateIntSum
  Erase GateIntAvg
  Erase GateIntValue
  flgPause = False
  flgPauseAtEnd = False
  flgStopAtEnd = False
  flgStopNow = False
  lblStatus.Caption = "Running"
  cdiSave.filename = ""
  Call cdiSave.ShowSave

  If cdiSave.filename <> "" Then
    Open cdiSave.filename For Output As #1
    Print #1, "Gate Settings:"

    For i = 0 To 4
      Print #1, "Gate#"; CStr(i + 1); ":"; txtGateSetting(i).Text
    Next i

    Close #1
    Call GenerateXArray
    Call Unidex_Init
    Call LecroyInit
    lineGatePos1(0).Visible = False
    lineGatePos2(0).Visible = False

    For i = 0 To 4
      picGraph(i + 1).Cls
      lineGatePos1(i + 1).Visible = False
      lineGatePos2(i + 1).Visible = False

      For j = 0 To 4
        shapeGate(6 * j + i + 1).Visible = False
      Next j
```

```
      If flgGateSet(i) = True Then
        Call GraphTransientInit(picGraph(i + 1), Xpts(0), Xpts(Nopts -
1), -0.01, 0.01)
        DoEvents
      End If
    Next i

    NoOfScans = CInt(txtNoOfScans.Text)
    NoofSweeps = CInt(txtSweeps.Text)
    Open "DelayTime.txt" For Output As #1

    For i = 0 To Nopts - 1
      Print #1, Xpts(i)
    Next i

    Close #1
    Open "TimeBase.txt" For Output As #1

    For i = 0 To LecroyHPts - 1
      Print #1, LecroyTB(i)
    Next i

    Close #1

    If optScanScopeChTA.value = True Then
      Call LecroyGetTraceInit(0, NoofSweeps)
    Else
      Call LecroyGetTraceInit(1, NoofSweeps)
    End If

    For i = 0 To NoOfScans - 1
      lblScanNo.Caption = i + 1

      For j = 0 To Nopts - 1

        If i Mod 2 = 0 Then
          jj = j
        Else
          jj = Nopts - 1 - j
        End If

        Call Unidex_Go(Xpts(jj))
        lblStagePos.Caption = Xpts(jj)
        If i < 999 Then TraceFilenameNoScan = "S0" & CStr(i + 1)
        If i < 99 Then TraceFilenameNoScan = "S00" & CStr(i + 1)
        If i < 9 Then TraceFilenameNoScan = "S000" & CStr(i + 1)
        If jj < 999 Then TraceFilenameTD = "TD0" & CStr(jj + 1)
        If jj < 99 Then TraceFilenameTD = "TD00" & CStr(jj + 1)
        If jj < 9 Then TraceFilenameTD = "TD000" & CStr(jj + 1)
        TraceFilename = TraceFilenameTD & TraceFilenameNoScan & ".tsc"

        If optScanScopeChTA.value = True Then
          Call LecroyGetTrace(TraceFilename)
        Else
          Call LecroyGetTrace(TraceFilename)
```

```
        End If

        Call LeCroyFileConvert(TraceFilename)
        Call picGraphScopeInit(picGraph(0), LecroyHPts)
        flgGraphScope(0) = True
        Call picGraphScopeDrawTrace(picGraph(0), LecroyVDisp(),
LecroyHPts, &HFFFFFF)
        DoEvents

        For k = 0 To 4
          For m = 0 To LecroyHPts - 1
            If flgGateSet(k) = True Then
              If m >= GatePosition(k) And m <= GatePosition(k) +
GateWidth(k) - 1 Then
                GateIntValue(k, jj) = GateIntValue(k, jj) +
LecroyVolt(m)
              End If
            End If
          Next m

          GateIntValue(k, jj) = GateIntValue(k, jj) / (GateWidth(k) +
1)
          If chkInv(k).value = Checked Then GateIntValue(k, jj) =
-GateIntValue(k, jj)
        Next k

        For k = 0 To 4
          If flgGateSet(k) = True Then
            picGraph(k + 1).Circle (Xpts(jj), GateIntValue(k, jj)),
            picGraph(k + 1).ScaleWidth / 200, vbYellow
            DoEvents
          End If
        Next k

        If flgPause = True Then
          frmPauseStop.Show
          frmPauseStop.Visible = True

          Do Until flgPause = False
            DoEvents
          Loop

          cmdPauseStop.Enabled = True
        End If

        If flgStopNow = True Then
          Exit For
        End If

        For k = 0 To LecroyHPts - 1
          TraceCurrent(jj, k) = LecroyVolt(k)
        Next k
      Next j

      For j = 0 To 4
        GateIntMax(j) = -9999
```

```
        GateIntMin(j) = 9999
      Next j

      For j = 0 To Nopts - 1
        For k = 0 To LecroyHPts - 1
          TraceSum(j, k) = TraceSum(j, k) + TraceCurrent(j, k)
          TraceAvg(j, k) = TraceSum(j, k) / (i + 1)
        Next k

        For k = 0 To 4
          If flgGateSet(k) = True Then
            GateIntSum(k, j) = GateIntSum(k, j) + GateIntValue(k,
j)
            GateIntAvg(k, j) = GateIntSum(k, j) / (i + 1)
            If GateIntAvg(k, j) > GateIntMax(k) Then GateIntMax(k)
= GateIntAvg(k, j)
            If GateIntAvg(k, j) < GateIntMin(k) Then GateIntMin(k)
= GateIntAvg(k, j)
          End If
        Next k
      Next j

      For j = 0 To 4
        If flgGateSet(j) = True Then
          If GateIntMax(j) <> GateIntMin(j) Then
            Call GraphTransientInit(picGraph(j + 1), Xpts(0),
Xpts(Nopts - 1), GateIntMin(j) - (GateIntMax(j) - GateIntMin(j)) *
0.1, GateIntMax(j) + (GateIntMax(j) - GateIntMin(j)) * 0.1)
            DoEvents
          End If

          For m = 0 To Nopts - 2
            picGraph(j + 1).Line (Xpts(m), GateIntAvg(j,m))-(Xpts(m +
1), GateIntAvg(j, m + 1)), shapeGate(6 * j).FillColor
          Next m
        End If
      Next j

      DoEvents

      If flgPauseAtEnd = True Then
        cmdPauseStop.Enabled = True
        cmdPauseStop.Caption = "Continue"
        lblStatus.Caption = "Paused"

       Do Until flgPauseAtEnd = False
          DoEvents
       Loop

       lblStatus.Caption = "Running"
     End If

     If flgStopAtEnd = True Then Exit For
     If flgStopNow = True Then Exit For
     If i = NoOfScans - 1 Then lblStatus.Caption = "Completed"
    Next i
```

```
  End If
End Sub

Private Sub cmdDumpGet_Click()
  Dim TargetGraph As Integer
  TargetGraph = CInt(combDumpDest.Text) - 1

  If flgDumped(0) = False Then
    Call LecroyGetTraceInit(0, 2)
    Call LecroyGetTrace("TMP.TMP")
    Kill "TMP.TMP"
    Call LecroyWait(10)
  End If

  If flgDumped(1) = False Then
    Call LecroyGetTraceInit(1, 2)
    Call LecroyGetTrace("TMP.TMP")
    Kill "TMP.TMP"
    Call LecroyWait(10)
  End If

  If optDumpSrcTA.value = True Then
    Call LecroyGetTraceInit(0, CInt(txtDumpSweeps.Text))
    Call LecroyGetTrace("\lecroy.trc")
  Else
    Call LecroyGetTraceInit(1, CInt(txtDumpSweeps.Text))
    Call LecroyGetTrace("\lecroy.trc")
  End If

  Call LeCroyFileConvert("\lecroy.trc")
  Kill ("\lecroy.trc")
  Call picGraphScopeInit(picGraph(TargetGraph), LecroyHPts)
flgGraphScope(TargetGraph) = True
  Call picGraphScopeDrawTrace(picGraph(TargetGraph), LecroyVDisp(),
LecroyHPts, &HFFFFFF)

  For i = 0 To LecroyHPts - 1
    TraceVolt(TargetGraph, i) = LecroyVolt(i)
  Next i

  If flgCursor1Set = True Then
    lineGatePos1(TargetGraph).Visible = True
    lineGatePos1(TargetGraph).X1 = Cursor1Index
    lineGatePos1(TargetGraph).X2 = Cursor1Index
  End If

  If flgCursor2Set = True Then
    lineGatePos2(TargetGraph).Visible = True
    lineGatePos2(TargetGraph).X1 = Cursor2Index
    lineGatePos2(TargetGraph).X2 = Cursor2Index
  End If

  For i = 0 To 4
    If flgGateSet(i) = True Then
      shapeGate(i * 6 + TargetGraph).Visible = True
      shapeGate(i * 6 + TargetGraph).Left = GatePosition(i)
```

```
      shapeGate(i * 6 + TargetGraph).Top = 32767
      shapeGate(i * 6 + TargetGraph).Width = GateWidth(i)
      shapeGate(i * 6 + TargetGraph).Height = 65535
    End If
  Next i
End Sub

Private Sub cmdGateClear_Click(Index As Integer)
  flgGateSet(Index) = False
  txtGateSetting(Index) = ""

  For i = 0 To 4
    shapeGate(Index * 6 + i).Visible = False
  Next i
End Sub

Private Sub cmdGateSet_Click(Index As Integer)
  If flgCursor1Set = True And flgCursor2Set = True Then
    If Cursor1Index < Cursor2Index Then
      GatePosition(Index) = Cursor1Index
    Else
      GatePosition(Index) = Cursor2Index
    End If

    GateWidth(Index) = Abs(Cursor2Index - Cursor1Index)
    txtGateSetting(Index).Text =
CStr(CLng(LecroyTB(GatePosition(Index)) * 1000000000#)) & "ns+" &
CStr(CLng(Abs(LecroyTB(Cursor1Index) - LecroyTB(Cursor2Index)) *
1000000000#)) & "ns"

    For i = 0 To 5
      shapeGate(Index * 6 + i).Visible = True
      shapeGate(Index * 6 + i).Left = GatePosition(Index)
      shapeGate(Index * 6 + i).Top = 32767
      shapeGate(Index * 6 + i).Width = GateWidth(Index)
      shapeGate(Index * 6 + i).Height = 65535
      lineGatePos1(i).Visible = False
      lineGatePos2(i).Visible = False
      flgCursor1Set = False
      flgCursor2Set = False
      cmdCursor1Left.Enabled = False
      cmdCursor1Right.Enabled = False
      cmdCursor2Left.Enabled = False
      cmdCursor2Right.Enabled = False
      txtCursorPos1.Text = ""
      txtCursorPos2.Text = ""
      txtCursorWidth.Text = ""
    Next i

    flgGateSet(Index) = True
  End If
End Sub

Private Sub cmdGoSP1_Click()
  Call Unidex_Go(CLng(txtSP1.Text))
End Sub
```

```
Private Sub cmdGoSP2_Click()
  Call Unidex_Go(CLng(txtSP2.Text))
End Sub

Private Sub cmdPauseStop_Click()
  If flgPauseAtEnd = True Then
    flgPauseAtEnd = False
    cmdPauseStop.Caption = "Pause/Stop"
  Else
    flgPause = True
  End If
End Sub

Private Sub cmdTraceSave_Click()
  Dim TargetTrace As Integer
  TargetTrace = CInt(combSaveTrace.Text) - 1

  If flgGraphScope(TargetTrace) = True Then
    cdiSave.ShowSave

    If cdiSave.filename <> "" Then
      Open cdiSave.filename For Output As #1

      For i = 0 To LecroyHPts - 1
        Print #1, LecroyTB(i); Chr$(9);
        Print #1, TraceVolt(CInt(combSaveTrace.Text) - 1, i)
      Next i
    End If

    Close #1
  End If
End Sub

Private Sub cmdStart_Click()
  Call picGraphScopeInit(picGraph(0), LecroyHPts)

  For i = 0 To 4
    If flgGateSet(i) = True Then
      shapeGate(i * 6 + TargetGraph).Visible = True
      shapeGate(i * 6 + TargetGraph).Left = GatePosition(i)
      shapeGate(i * 6 + TargetGraph).Top = 32767
      shapeGate(i * 6 + TargetGraph).Width = GateWidth(i)
      shapeGate(i * 6 + TargetGraph).Height = 65535
    End If
  Next i
End Sub

Private Sub cmdSubstrate_Click()
  Dim SubSrc1 As Integer, SubSrc2 As Integer, SubTarget As Integer
  Dim Max As Single, Min As Single
  Dim SubTraceGraph(10000) As Long
  SubSrc1 = CInt(combSubIn1.Text) - 1
  SubSrc2 = CInt(combSubIn2.Text) - 1
  SubTarget = CInt(combSubTarget.Text) - 1
  If flgGraphScope(SubSrc1) = True And flgGraphScope(SubSrc2) = True
```

```
Then
    Max = -9999
    Min = 9999

    For i = 0 To LecroyHPts - 1
      TraceVolt(SubTarget, i) = TraceVolt(SubSrc1, i) -
      TraceVolt(SubSrc2, i)
      If TraceVolt(SubTarget, i) > Max Then Max = TraceVolt(SubTarget,
i)
      If TraceVolt(SubTarget, i) < Min Then Min = TraceVolt(SubTarget,
i)
    Next i

    If Max = Min Then
      Max = 1
      Min = -1
    End If

    For i = 0 To LecroyHPts - 1
      SubTraceGraph(i) = CInt(((TraceVolt(SubTarget, i) - Min) * 65534
/(Max - Min)) - 32767)
    Next i

    Call picGraphScopeInit(picGraph(SubTarget), LecroyHPts)
    Call picGraphScopeDrawTrace(picGraph(SubTarget), SubTraceGraph(),
LecroyHPts, &HFFFFFF)
    flgGraphScope(SubTarget) = True

    For i = 0 To 4
      If flgGateSet(i) = True Then
        shapeGate(i * 6 + SubTarget).Visible = True
        shapeGate(i * 6 + SubTarget).Left = GatePosition(i)
        shapeGate(i * 6 + SubTarget).Top = 32767
        shapeGate(i * 6 + SubTarget).Width = GateWidth(i)
        shapeGate(i * 6 + SubTarget).Height = 65535
      End If
    Next i
  End If
End Sub

Private Sub cmdTestInt_Click()
  Call GenerateXArray
  Call GraphTransientInit(picGraph(1), Xpts(0), Xpts(Nopts - 1), -5,
5)

  For i = 0 To Nopts - 1
    picGraph(1).Circle (Xpts(i), 0), (Xpts(Nopts - 1) - Xpts(0)) *
0.005, vbYellow
  Next i
End Sub

Private Sub cmdTransientSave_Click()
  Dim AvgTrcFilename As String
  Dim FilenameNoofScan As String

  For i = 0 To Nopts - 1
```

```
    If i < 999 Then TraceFilenameNoScan = "TRCx" & CStr(i + 1)
    If i < 99 Then TraceFilenameNoScan = "TRCx0" & CStr(i + 1)
    If i < 9 Then TraceFilenameNoScan = "TRCx00" & CStr(i + 1)
    FilenameNoofScan = "Sc" & CStr(lblScanNo.Caption)
    If NoOfScans < 999 Then FilenameNoofScan = "Sc0" &
CStr(lblScanNo.Caption)
    If NoOfScans < 99 Then FilenameNoofScan = "Sc00" &
CStr(lblScanNo.Caption)
    If NoOfScans < 9 Then FilenameNoofScan = "Sc000" &
CStr(lblScanNo.Caption)
    AvgTrcFilename = FilenameNoofScan & TraceFilenameNoScan & ".txt"
    Open AvgTrcFilename For Output As #1

    For j = 0 To LecroyHPts - 1
      Print #1, TraceAvg(i, j)
    Next j

    Close #1

  Next i

  For i = 0 To 4
    If flgGateSet(i) = True Then
      Open "TSN" & CStr(i + 1) & FilenameNoofScan & ".txt" For Output
As #1

      For j = 0 To Nopts - 1
        Print #1, Xpts(j), Chr$(9), GateIntAvg(i, j)
      Next j

      Close #1
    End If
  Next i
End Sub

Private Sub Form_Load()
  Call LecroyInit
  Call Unidex_Init
  DoEvents

  For i = 1 To 6
    combDumpDest.AddItem CStr(i)
    combSubIn1.AddItem CStr(i)
    combSubIn2.AddItem CStr(i)
    combSubTarget.AddItem CStr(i)
    combSaveTrace.AddItem CStr(i)
  Next i

  For i = 0 To 5
    flgGraphScope(i) = False
  Next i

  flgLine1 = False
End Sub

Private Sub picGraph_MouseDown(Index As Integer, Button As Integer,
```

```
Shift As Integer, X As Single, Y As Single)
  If flgGraphScope(Index) = True Then
    If optCursor1 Then
      If X < 0 Then X = 0
      If X > LecroyHPts - 1 Then X = LecroyHPts - 1
      Cursor1Index = CInt(X)
      flgCursor1Set = True
      cmdCursor1Left.Enabled = True
      cmdCursor1Right.Enabled = True
      txtCursorPos1.Text = CLng(LecroyTB(Cursor1Index) * 1000000000#)

      If flgCursor2Set = True Then
        txtCursorWidth.Text = CLng(Abs(LecroyTB(Cursor2Index) -
LecroyTB(Cursor1Index)) * 1000000000#)
      End If

      lineGatePos1(Index).Visible = True

      For i = 0 To 5
        If flgGraphScope(i) = True Then
          lineGatePos1(i).Visible = True
        End If

        lineGatePos1(i).X1 = Cursor1Index
        lineGatePos1(i).X2 = Cursor1Index
      Next i

    Else

      If X < 0 Then X = 0
      If X > LecroyHPts - 1 Then X = LecroyHPts - 1
      Cursor2Index = CInt(X)
      flgCursor2Set = True
      cmdCursor2Left.Enabled = True
      cmdCursor2Right.Enabled = True
      txtCursorPos2.Text = CLng(LecroyTB(Cursor2Index) * 1000000000#)

      If flgCursor1Set = True Then
        txtCursorWidth.Text = CLng(Abs(LecroyTB(Cursor2Index) -
LecroyTB(Cursor1Index)) * 1000000000#)
      End If

      For i = 0 To 5
        If flgGraphScope(i) = True Then
          lineGatePos2(i).Visible = True
        End If

        lineGatePos2(i).X1 = Cursor2Index
        lineGatePos2(i).X2 = Cursor2Index
      Next i
    End If
  End If
End Sub

Private Sub txtInt1Inc_LostFocus()
  Call UpdateInt
```

```
End Sub

Private Sub txtInt1Int_LostFocus()
  Call UpdateInt
End Sub

Private Sub txtInt1NoPts_LostFocus()
  Call UpdateInt
End Sub

Private Sub txtInt1Start_LostFocus()
  Call UpdateInt
End Sub

Private Sub txtInt2Inc_LostFocus()
  Call UpdateInt
End Sub

Private Sub txtInt2Int_LostFocus()
  Call UpdateInt
End Sub

Private Sub txtInt2NoPts_LostFocus()
  Call UpdateInt
End Sub

Private Sub txtInt2Start_LostFocus()
  Call UpdateInt
End Sub

Private Sub txtInt3Inc_LostFocus()
  Call UpdateInt
End Sub

Private Sub txtInt3Int_LostFocus()
  Call UpdateInt
End Sub

Private Sub txtInt3NoPts_LostFocus()
  Call UpdateInt
End Sub

Private Sub txtInt3Start_LostFocus()
  Call UpdateInt
End Sub

Sub GenerateXArray()
  Call UpdateInt

  For i = 0 To NoPts1 - 1
    Xpts(i) = Start + Int1 * i + Inc1 * i * (i - 1) / 2
  Next i

  TotalPts = NoPts1

  If frmInt2.Enabled = True Then
```

```
    For i = 0 To NoPts2 - 1
      Xpts(NoPts1 + i) = Start2 + Int2 * i + Inc2 * i * (i - 1) / 2
    Next i

    TotalPts = Nopts + NoPts2

    If frmInt3.Enabled = True Then
      For i = 0 To NoPts3 - 1
        Xpts(NoPts1 + NoPts2 + i) = Start3 + Int3 * i + Inc3 * i *
(i - 1) / 2
      Next i

      TotalPts = NoPts1 + NoPts2 + NoPts3
    End If
  End If
End Sub
```

Form: frmPauseStop.frm

```
Attribute VB_Name = "frmPauseStop"
Attribute VB_GlobalNameSpace = False
Attribute VB_Creatable = False
Attribute VB_PredeclaredId = True
Attribute VB_Exposed = False

Private Sub cmdContinue_Click()
  flgPauseAtEnd = False
  flgStopAtEnd = False
  flgStopNow = False
  flgPause = False
  Main.lblStatus.Caption = "Running"
  frmPauseStop.Hide
End Sub

Private Sub cmdPauseAtEnd_Click()
  flgPauseAtEnd = True
  flgStopAtEnd = False
  flgStopNow = False
  flgPause = False
  frmPauseStop.Hide
  Main.lblStatus.Caption = "Will Pause at the End"
End Sub

Private Sub cmdStopEnd_Click()
  Dim mboxrtn As Integer
  mboxrtn = MsgBox("Are You Sure to Stop at the End of This Run?",
vbYesNo, "Stop at the End of this Run?")

  If mboxrtn = vbYes Then
    flgPauseAtEnd = False
    flgStopAtEnd = True
    flgStopNow = False
    flgPause = False
    frmPauseStop.Hide
```

```
    Main.lblStatus.Caption = "Will Stop at the End"
  End If
End Sub

Private Sub cmdStopNow_Click()
  Dim mboxrtn As Integer
  mboxrtn = MsgBox("Are You Sure to Stop the Scan?", vbYesNo, "Stop
Now?")

  If mboxrtn = vbYes Then
    flgPauseAtEnd = False
    flgStopAtEnd = False
    flgStopNow = True
    flgPause = False
    frmPauseStop.Hide
    Main.lblStatus.Caption = "Stopped"
  End If
End Sub
Private Sub Form_Load()
Main.lblStatus.Caption = "Paused"
End Sub
```

Module: GlobalDec.bas

```
Attribute VB_Name = "GlobalDec"
Global flgPause As Boolean
Global flgPauseAtEnd As Boolean
Global flgStopAtEnd As Boolean
Global flgStopNow As Boolean
```

Module: Unidex100.bas

```
Attribute VB_Name = "Unidex100"
Declare Function GetTickCount Lib "kernel32" () As Long

Global U100 As Integer
Global IndiHome As Boolean
Global IndiDest As Boolean
Const UnidexDevNo = "DEV4"

Public Sub Wait(msec As Long) 'Perform a dalay in msec
  StartTime = GetTickCount() 'GetTickCount is a variable of WinAPI,
  it will return how long the computer startup in msec
  'Use infinite loop to check if the time is reached

  Do While GetTickCount() - StartTime < msec
  Loop
End Sub

Public Sub Unidex_Init()
  Call ibfind(UnidexDevNo, U100)
  Call ibclr(U100)
```

```
  Wait (100)
  Call Unidex_Home
  Call ibwrt(U100, "#CBABSL" & Chr$(13))
End Sub

Public Sub Unidex_Reset()
  Call ibclr(U100)
End Sub

Public Sub Unidex_Home()
  Dim sU100Rtn As String * 3
  Dim iU100Rtn As Integer

  Call Unidex_Go(0)
  Call ibwrt(U100, "#CBHM" & Chr$(13))
  IndiHome = False
  iU100Rtn = 0
  Wait (500)

  Do Until iU100Rtn Mod 128 >= 64
    Call ibwrt(U100, "#FCBD1" & Chr$(10))
    Wait (10)
    Call ibrd(U100, sU100Rtn)
    Wait (10)
    iU100Rtn = CInt(sU100Rtn)
  Loop

  IndiHome = True
End Sub

Public Sub Unidex_Go(Dest As Long)
  Dim sU100Rtn As String * 3
  Dim iU100Rtn As Integer

  If Dest >= 0 And Dest <= 500000 Then

    If Dest <> 0 Then IndiHome = False
    IndiDest = False
    Call ibwrt(U100, "#CBD(" & CStr(Dest) & ")" & Chr$(13))
    iU100Rtn = 0
    Wait (100)

    Do Until iU100Rtn Mod 128 >= 64
      Call ibwrt(U100, "#FCBD1" & Chr$(10))
      Wait (10)
      Call ibrd(U100, sU100Rtn)
      Wait (10)
      iU100Rtn = CInt(sU100Rtn)
    Loop

    IndiDest = True
  End If

End Sub
```

Module: LeCroy9361.bas

```
Attribute VB_Name = "LeCroy9361"
Private Declare Function GetTickCount Lib "kernel32" () As Long
Global LecroyTB(10000) As Double
Global LecroyVolt(10000) As Double
Global LecroyHPts As Integer
Global InitTickCount As Long


Function IEEE_64BIT_To_Double(InBinaryArray() As Byte, FirstByte As
Integer) As
Double
  Dim ByteIndex As Integer, BitIndex As Integer
  Dim ByteValue As Integer
  Dim BinaryList(63) As Integer
  Dim Exponent As Double, Siginificand As Double

  For ByteIndex = 0 To 7
    ByteValue = CInt(InBinaryArray(FirstByte + ByteIndex))

    For BitIndex = 0 To 7
      BinaryList(8 * (7 - ByteIndex) + BitIndex) = (ByteValue And 2 ^
BitIndex) \ 2 ^ BitIndex
    Next BitIndex

  Next ByteIndex

  Exponent = 0
  Siginificand = 1

  For i = 52 To 62
    Exponent = Exponent + BinaryList(i) * 2 ^ (i - 52)
  Next i

  For i = 0 To 51
    Siginificand = Siginificand + BinaryList(i) * 2 ^ (i - 52)
  Next i

  IEEE_64BIT_To_Double = (-1) ^ BinaryList(63) * 2 ^ (Exponent -
1023) *Siginificand

End Function

Function IEEE_32BIT_To_Single(InBinaryArray() As Byte, FirstByte As
Integer) As Single
  Dim ByteIndex As Integer, BitIndex As Integer
  Dim ByteValue As Integer
  Dim BinaryList(63) As Integer
  Dim Exponent As Double, Siginificand As Double

  For ByteIndex = 0 To 3
    ByteValue = CInt(InBinaryArray(FirstByte + ByteIndex))

    For BitIndex = 0 To 7
```

```
     BinaryList(8 * (3 - ByteIndex) + BitIndex) = (ByteValue And 2 ^
BitIndex) \ 2 ^ BitIndex

    Next BitIndex
  Next ByteIndex

  Exponent = 0
  Siginificand = 1

  For i = 23 To 30
    Exponent = Exponent + BinaryList(i) * 2 ^ (i - 23)
  Next i

  For i = 0 To 22
    Siginificand = Siginificand + BinaryList(i) * 2 ^ (i - 23)
  Next i

  IEEE_32BIT_To_Single = (-1) ^ BinaryList(31) * 2 ^ (Exponent - 127)
* Siginificand

End Function

Sub LeCroyFileConvert(inFile As String)
  Dim i As Integer
  Dim BinReading(5000) As Byte
  Dim LecroyHpoints As Integer
  Dim VGain As Single, VOffset As Single, HInt As Single
  Dim HOffset As Double
  Open inFile For Binary As #1

  Do Until EOF(1)
    Get #1, , BinReading(i)
    i = i + 1
  Loop

  Close #1

  VGain = IEEE_32BIT_To_Single(BinReading(), 156)
  VOffset = IEEE_32BIT_To_Single(BinReading(), 160)
  HInt = IEEE_32BIT_To_Single(BinReading(), 176)
  HOffset = IEEE_64BIT_To_Double(BinReading(), 180)

  ' Read Number of Points
  LecroyHPts = 0

  For i = 0 To 3
    LecroyHPts = LecroyHPts + 256 ^ (3 - i) * BinReading(116 + i)
  Next i

  For i = 0 To LecroyHPts - 1
    LecroyTB(i) = HOffset + HInt * i
    LecroyVolt(i) = (BinReading(346 + 2 * i) * 256 + BinReading(346 +
2 * i+ 1)) * VGain - VOffset
  Next i
```

```
End Sub

Sub Wait(msec As Long)
  InitTickCount = GetTickCount()

  Do While GetTickCount() - InitTickCount < msec
    DoEvents
  Loop

End Sub
```

Module: GraphScope.bas

```
Attribute VB_Name = "GraphScope"

Sub picGraphScopeInit(picGraphScope As PictureBox, Xpts As Integer)
  picGraphScope.Cls
  picGraphScope.ScaleLeft = -(Xpts - 1) * 0.05
  picGraphScope.ScaleWidth = (Xpts - 1) * 1.1
  picGraphScope.ScaleTop = 35000
  picGraphScope.ScaleHeight = -70000

  For i = 1 To 9
    picGraphScope.Line ((Xpts - 1) * i / 10, -32767)-((Xpts - 1) * i /
10,32767), &H333333
  Next i

  For i = -3 To 7
    picGraphScope.Line (0, 8191.75 * i)-((Xpts - 1), 8191.75 * i),
&H333333
  Next i

  For i = 1 To 49
    picGraphScope.Line ((Xpts - 1) * i / 50, -1000)-((Xpts - 1) * i /
50,1000), &H333333
  Next i

  For i = -19 To 19
    picGraphScope.Line ((Xpts - 1) * 0.51, 1638.35 * i)-((Xpts - 1) *
0.49,1638.35 * i), &H333333
  Next i

  picGraphScope.Line ((Xpts - 1) / 2, -32767)-((Xpts - 1) / 2,
32767),&HAAAAAA
  picGraphScope.Line (0, 0)-((Xpts - 1), 0), &HAAAAAA
  picGraphScope.Line (0, -32767)-(0, 32767), &HAAAAAA
  picGraphScope.Line ((Xpts - 1), -32767)-((Xpts - 1),
32767),&HAAAAAA
  picGraphScope.Line (0, -32767)-((Xpts - 1), -32767), &HAAAAAA
  picGraphScope.Line (0, 32767)-((Xpts - 1), 32767), &HAAAAAA
End Sub
```

```
Sub picGraphScopeDrawTrace(picGraphScope As PictureBox,
InputVoltRaw() As Long, Xpts As Integer, Color As Single)

  For i = 0 To Xpts - 2
    picGraphScope.Line (i, InputVoltRaw(i))-(i + 1, InputVoltRaw(i +
1)),Color
  Next i
End Sub
```

Module: GraphTransient.bas

```
Attribute VB_Name = "GraphTransient"
Sub GraphTransientInit(GraphTransPic As PictureBox, XStart As Long,
XEnd As Long, YMin As Variant, YMax As Variant)
  Dim Xdiv As Long
  Dim Ydiv As Double
  GraphTransPic.Cls
  GraphTransPic.ScaleTop = YMax + 0.05 * (YMax - YMin)
  GraphTransPic.ScaleHeight = -(YMax - YMin) * 1.2
  GraphTransPic.ScaleLeft = XStart - 0.05 * (XEnd - XStart)
  GraphTransPic.ScaleWidth = (XEnd - XStart) * 1.1
  GraphTransPic.Line (XStart, YMin)-(XEnd, YMin), &HFFFFFF
  GraphTransPic.Line (XStart, YMax)-(XEnd, YMax), &HFFFFFF
  GraphTransPic.Line (XStart, YMin)-(XStart, YMax), &HFFFFFF
  GraphTransPic.Line (XEnd, YMin)-(XEnd, YMax), &HFFFFFF
  Xdiv = 10 ^ (CLng(Log(XEnd - XStart) / Log(10)) - 1)
  If (XEnd - XStart) / Xdiv > 12 Then Xdiv = Xdiv * 2
  If (XEnd - XStart) / Xdiv < 5 Then Xdiv = Xdiv / 2

  For i = CLng(XStart / Xdiv) + 1 To CLng(XEnd / Xdiv)
    GraphTransPic.Line (i * Xdiv, YMin)-(i * Xdiv, YMax), &H555555
  Next i
  If YMax - YMin < 1 And YMax - YMin <> Int(YMax - YMin) Then
    Ydiv = 10 ^ (Int((Log(YMax - YMin) - 1) / Log(10)) - 1)
  Else
    Ydiv = 10 ^ (Int(Log(YMax - YMin) / Log(10)) - 1)
  End If

  If (YMax - YMin) / Ydiv > 20 Then Ydiv = Ydiv * Int((YMax - YMin) /
Ydiv /10) * 10
  If (YMax - YMin) / Ydiv > 15 Then Ydiv = Ydiv * 2
  If (YMax - YMin) / Ydiv < 5 Then Ydiv = Ydiv / 2
  If (YMax - YMin) / Ydiv < 5 Then Ydiv = Ydiv / 2
  If (YMax - YMin) / Ydiv < 5 Then Ydiv = Ydiv / 2

  For i = Int(YMin / Ydiv) + 1 To Int(YMax / Ydiv)
    GraphTransPic.Line (XStart, Ydiv * i)-(XEnd, Ydiv * i), &H555555
  Next i

  If YMax * YMin < 0 Then GraphTransPic.Line (XStart, 0)-(XEnd,
0),&HFFFFFF
  GraphTransPic.Line (XStart, YMin)-(XEnd, YMin), &HFFFFFF
  GraphTransPic.Line (XStart, YMax)-(XEnd, YMax), &HFFFFFF
  GraphTransPic.Line (XStart, YMin)-(XStart, YMax), &HFFFFFF
```

```
  GraphTransPic.Line (XEnd, YMin)-(XEnd, YMax), &HFFFFFF
  GraphTransPic.PSet (XStart, YMin - (YMax - YMin) * 0.01), &H0
  GraphTransPic.ForeColor = &HFFFFFF
  GraphTransPic.Print "XOrigin:"; XStart; " ; XDiv:"; Xdiv
  GraphTransPic.PSet (XStart, YMin - (YMax - YMin) * 0.06), &H0
  GraphTransPic.Print "YMin:"; YMin; " ; YDiv:"; Ydiv
End Sub
```